

**A Study of Optical Topography for Imaging Human Brain Functions:  
Evaluation of Activation Signals and Its Methodological Improvement**

*March 2006*

**Hiroki Sato**

# Contents

<i>Abstract</i>	<i>iv</i>
<b>1. Introduction</b>	<b>1</b>
1.1 Noninvasive imaging methods for human brain functions	1
1.2 Development of OT from NIRS	8
1.2.1 Principles of NIRS in Detecting Activation Signals	9
1.2.2 From NIRS to OT	13
1.3 Random factors causing fluctuations in the OT activation signals	19
<b>2. Within-Subject Reproducibility of Activation Signals</b>	<b>32</b>
2.1 Introduction	32
2.2 Methods	33
2.2.1 Subject	33
2.2.2 OT measurement	34
2.2.3 Task paradigm	35
2.2.4 Data analysis	36
2.3 Results and Discussion	40
2.3.1 General aspects of reproducibility	40
2.3.2 Reproducibility of spatial information	41
2.3.3 Reproducibility of signal amplitude	44
2.3.4 Reproducibility of temporal information	46
2.4 Conclusion	49
<b>3. Inter-Subject Generality of Activation Signals</b>	<b>51</b>
3.1 Introduction	51
3.2 Methods	51
3.2.1 Subjects	51
3.2.2 OT measurement	52

3.2.3 Task paradigm _____	52
3.2.4 Data analysis _____	53
<b>3.3 Results and Discussion _____</b>	<b>54</b>
3.3.1 Occurrence probability of typical activation pattern _____	54
3.3.2 Variability of activation pattern _____	61
<b>3.4 Conclusion _____</b>	<b>67</b>
<b><i>4. Reducing Fluctuations in the Background Functions by Devising Task-Paradigm _____</i></b>	<b><i>69</i></b>
<b>4.1 Introduction _____</b>	<b>69</b>
<b>4.2 Methods _____</b>	<b>71</b>
4.2.1 Subject _____	71
4.2.2 Auditory stimuli _____	71
4.2.3 Task paradigm _____	72
4.2.4 Experimental procedures _____	74
4.2.5 OT procedures _____	75
4.2.6 Data analyses _____	77
<b>4.3 Results and Discussion _____</b>	<b>79</b>
4.3.1 Task performance _____	79
4.3.2 Mapping the difference between the story and repeat tasks _____	80
4.3.3 Spatial registration _____	81
4.3.4 Hemodynamic differences between the story and repeat runs _____	83
4.3.5 Relationships between $\Delta C'_{oxy}$ and $\Delta C'_{deoxy}$ dynamics _____	85
4.3.6 Laterality _____	86
<b>4.4 Conclusion _____</b>	<b>90</b>
<b><i>5. Reducing System-related Noise by Wavelength Selection _____</i></b>	<b><i>92</i></b>
<b>5.1 Introduction _____</b>	<b>92</b>
<b>5.2 Methods _____</b>	<b>96</b>
5.2.1 Subjects and measurement paradigm _____	96
5.2.2 NIRS measurement _____	99
5.2.3 Data analysis _____	100
<b>5.3 Results and Discussion _____</b>	<b>101</b>
5.3.1 Detected power of reflected light _____	101

5.3.2 Signal time course _____	103
5.3.3 Activation-signal amplitude _____	107
5.3.4 Wavelength-dependence of spatial sensitivity _____	111
5.3.5 Noise levels in $\Delta C'_{\text{oxy}}$ and $\Delta C'_{\text{deoxy}}$ _____	114
5.3.6 Signal-to-noise ratio _____	116
5.4 Conclusion _____	119
<b>6. Conclusion</b> _____	<b>121</b>
6.1 Conclusions _____	121
6.2 Prospects _____	124
<b>Acknowledgements</b> _____	<b>128</b>
<b>References</b> _____	<b>130</b>
<b>Publication List</b> _____	<b>138</b>

## Abstract

Optical topography (OT) is a noninvasive modality that is used to image human brain functions. This technique is based on near-infrared spectroscopy (NIRS), and involves the measurement of two hemoglobin (Hb) signals ( $\Delta C'_{\text{oxy}}$  and  $\Delta C'_{\text{deoxy}}$ ). Although this technique has been validated under certain specific conditions based on simulation and phantom studies, a number of random factors may cause fluctuations in the activation signals during practical measurements in the human brain. This study evaluates the activation signals measured by OT under the present conditions and aims to reduce the effects of some random factors on the signals, thereby improving the existing OT system to a more practical and complete imaging method.

Chapter 1 presents an introduction to OT and outlines the random factors that could probably cause fluctuations in the activation signals under the present conditions.

Chapters 2 and 3 provide information on the reproducibility of the activation signals, which is considered as an overall signal that may include fluctuations caused by all the random factors. First, chapter 2 reports the within-subject

reproducibility of the activation signals during the imaging of sensorimotor activations in the same subject, 6 months after the initial session. This study demonstrates a high reproducibility of the fundamental activation pattern (a positive  $\Delta C'_{oxy}$  and a negative  $\Delta C'_{deoxy}$ ), the location of the activation area, and the temporal dynamics (time courses) of the activation signals; however, the signal amplitudes were not consistent between the two sessions. The result emphasizes that the time course of the activation signal is particularly useful for assessing activation. Second, chapter 3 reports the reproducibility (generality) of the fundamental activation pattern in 31 subjects by applying the same paradigm as described in chapter 2. In this case, 90% of the subjects with similar locations of the activation area showed a positive  $\Delta C'_{oxy}$ , thereby suggesting that a positive  $\Delta C'_{oxy}$  is the most useful common parameter for detecting activation signals in different subjects. In addition, the high reproducibility of the location of activation areas observed in these two studies demonstrates the efficacy of the 10–20 system in determining the locations of the probe positions.

Chapters 4 and 5 present studies describing possible solutions for the effects of some random factors. Chapter 4 describes a solution for the fluctuation caused due to background functions such as attention. The fluctuation that is caused due to background functions rather than due to the targeted function is a serious problem

because rest periods essentially serve as the baseline, although there is no inherent baseline state in the brain. In this study, a dichotic listening task that controlled the subjects' attention was used at every stage to detect an intact activation signal from the targeted cognitive process of the speech recognition. The results showed a localized activation signal that is consistent with the results from a previous cognitive study; this demonstrates the efficacy of a devising task-paradigm in reducing the fluctuation due to background functions in OT. Chapter 5 reports a study that examines the practical relevance of wavelength selection in reducing the system-related noise of activation signals. Although optimal wavelength pairs can be proposed on the basis of theoretical estimations, the wavelength range should be limited based on the actual optical properties of the subject's head. To identify the optimal wavelength for pairing with a wavelength of 830 nm, the activation signals were practically examined at the possible wavelengths of 678, 692, 750, and 782 nm. The results demonstrate that the 692- and 830-nm pair produces the highest common signal-to-noise ratio.

Finally, the findings obtained from studies reported in chapters 2–5 are summarized in chapter 6 as the conclusion. Moreover, I have proposed a novel approach for improving the OT system in order to render it more useful and effective.

# 1. Introduction

## 1.1 Noninvasive imaging methods for human brain functions

The recent development of noninvasive techniques for imaging brain functions has advanced our knowledge regarding human brain mechanisms and cognitive abilities. There are two main approaches for the noninvasive imaging of brain functions: One measures the primary electrical signals originating from neural activity, and the other measures the secondary metabolic/vascular signals induced by the neural activity.<sup>1</sup> Electroencephalography (EEG)<sup>2</sup> and magnetoencephalography (MEG)<sup>3, 4</sup> are the techniques that use the former approach, and functional magnetic resonance imaging (fMRI)<sup>5-7</sup> and optical topography (OT)<sup>8, 9</sup> based on near-infrared spectroscopy (NIRS) are representatives of the latter approach (Table 1.1). Each technique has different characteristics with regard to spatial and temporal resolutions (Fig. 1.1).

Electrophysiological methods such as EEG and MEG are used to measure the electromagnetic signals that originate from the summation of electrical events in individual cells. These methods have the significant advantage of good temporal resolution, but they typically suffer from poor spatial resolution.



Table 1.1 Measurements in noninvasive functional imaging methods

Imaging method	Measurement target and physiological parameters
EEG	Electrical signal originating from the summation of neural activities
MEG	Magnetic signal originating from the summation of neural activities (limited to signals from the sulci but not the gyri) <sup>4</sup>
fMRI (BOLD signal)	Intensity change in the magnetic resonance signal due to change in cerebral blood oxygenation (concentration change in deoxygenated hemoglobin) in a voxel (millimeter order) of the brain
OT (Hb signals)	Intensity change in the transparent lights due to changes in cerebral blood oxygenation (concentration changes in oxygenated and deoxygenated hemoglobin) in an area (between the source and detector; centimeter order) of the cerebral cortex

Although dipole estimation has been applied in both EEG and MEG analyses to determine the original site of activation, it may lead to a wrong conclusion because in practice, it is difficult to solve the inverse problems. In particular, the estimation of activation sources in the EEG signal is almost impossible because the electrical signal spreads attenuated by tissues such as the cerebrospinal fluid and skull that have different electrical conduction rates. Although the MEG signal has uniform transparency for the tissue layers and it is possible to achieve a spatial resolution of the millimeter order in a specific case,<sup>4</sup> the magnetic signal attenuates in inverse proportion to the square of the distance (depth); therefore, estimation of the activation source in a deep area is difficult. In addition, MEG cannot clarify the

spatial extent of an activation area, and it can measure signals only from the sulci but not the gyri.<sup>4</sup> Accordingly, it is difficult to correlate these signals with defined anatomical structures and may be inappropriate for functional imaging at present.

On the other hand, another group of imaging techniques measures the metabolic or vascular changes induced by the neural activity. At present, fMRI could be the most important method [positron emission tomography (PET) is not described here because it is an invasive technique]. After the fMRI method (which is sensitive to blood oxygenation level; blood oxygenation level-dependent signal: BOLD signal) was developed in 1990,<sup>5-7</sup> many fMRI studies have been conducted worldwide.

Although the technique measures more indirect signals (secondary signals induced by the neural activity), it offers significant advantages—better spatial resolution and good delineation of the spatial extent of the activation area. In particular, fMRI has an excellent spatial resolution of the millimeter order and can even produce anatomical images. A recent study succeeded in imaging ocular dominance columns with an in-plane resolution of  $0.47 \times 0.47$  mm.<sup>10</sup> Due to the excellent spatial resolution and anatomical information provided by fMRI, this technique has often been used as the standard method for functional studies.

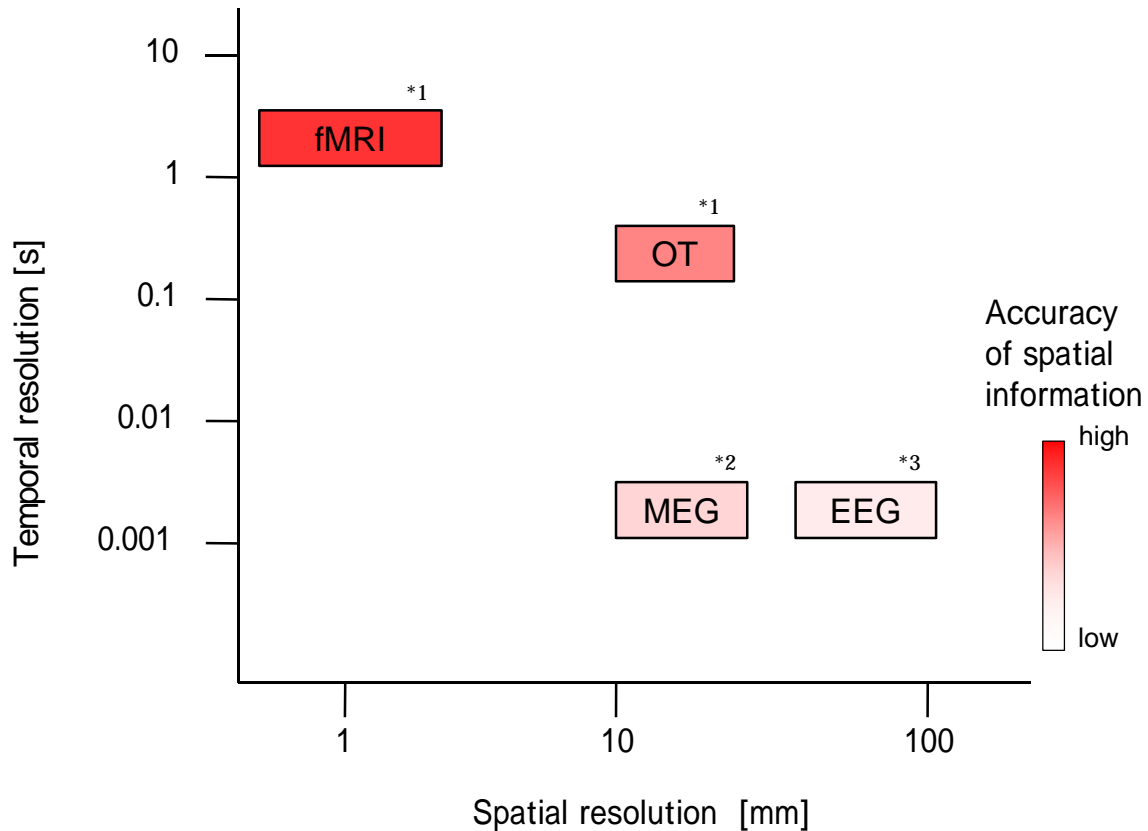


**Fig. 1.1** Rough estimation of the temporal and spatial resolutions in noninvasive functional imaging methods

- \*1 Sampling periods can be shorter depending on the measurement parameters, but the temporal resolution would be of the second order considering the speed of the vascular response accompanying the neural activity.
- \*2 Potential spatial resolution would be of the millimeter order if an inverse problem were solved in order to identify an activation source. However, reconstruction of the activation source is difficult due to some reasons (inability in estimating the size of the activation area, difficulty in detecting activation in a deep region, and practical inability of measuring the activation in a gyrus).<sup>4</sup>
- \*3 Estimation of the activation area is currently impossible using an EEG signal because the electrical signal is attenuated by tissues with different electrical conduction rates.<sup>2</sup>

OT is another imaging technique included in this group; it is a noninvasive modality for functional mapping with multiple measurement positions and was more recently developed from the NIRS technique.<sup>8, 9, 11, 12</sup> Two hemoglobin (Hb) signals originating from changes in the concentration of oxygenated hemoglobin (oxy-Hb) and deoxygenated hemoglobin (deoxy-Hb) in the cerebral cortex—oxy-Hb and deoxy-Hb signals—are measured by OT for imaging brain activation (see section 1.2 for more details). The measurement concept of OT is based on the common theory of fMRI, that is, regional cerebral blood flow (rCBF) and regional cerebral blood volume (rCBV) significantly increase as a result of the neural activity.<sup>1</sup> According to a study that examined the coupling between rCBF and cerebral metabolic rate of oxygen (CMRO<sub>2</sub>) by using PET, a stimulus-induced focal change in the rCBF (mean, 29%) exceeded the concomitant local increase in the CMRO<sub>2</sub> (mean, 5%).<sup>13</sup> This suggests that more oxygen is usually supplied to the activated region than is actually required. Accordingly, the oxy-Hb signal should increase and the deoxy-Hb signal should decrease in the veins and capillaries in the corresponding area of activation. In an fMRI study, activation is assessed by the BOLD signal, which varies according to changes in paramagnetic deoxy-Hb. Therefore, this oxygen metabolism in the activation region is the physiological basis of functional signals in both fMRI and OT measurements.

The two imaging methods—fMRI and OT—have been compared with respect to some features (Table 1.2). The most important advantage of fMRI over OT is the provision of excellent spatial resolution along with accurate anatomical information, as mentioned above. In addition, the presence of a standard analytical method (statistical parametric mapping: SPM; [www.fil.ion.ucl.ac.uk/spm](http://www.fil.ion.ucl.ac.uk/spm)) should contribute to the success of fMRI. On the other hand, OT also has several advantages over fMRI and other functional mapping techniques. First, OT imposes less physical constraints on the subject than fMRI. This enables the measurement of brain functions in a subject under normal conditions rather than experimental conditions. The safety of OT was confirmed by a direct experiment in which the temperature rise on the skin surface was measured.<sup>8, 14</sup> In conjunction with its high safety, this advantage enables the use of OT for imaging the brain functions of healthy infants.<sup>15, 16</sup> In addition, the portable compact system enables easy measurement of the brain function of patients confined to bed and healthy subjects in various environments.<sup>17-19</sup> Second, OT does not generate any measurement noise that could interfere with any auditory stimuli, whereas fMRI is accompanied by a loud scanning noise. This advantage of OT enables researchers to conduct studies using sound stimuli, particularly measurements of auditory function, under strictly controlled conditions. The lower expenditure associated with the use of OT than of

fMRI could also contribute to widening the application of OT. Moreover, the measurability of the two signals originating from oxy-Hb and deoxy-Hb in the cerebral cortex is helpful in elucidating the mechanism underlying the physiological changes produced by the neural activity. Thus, OT is expected to introduce a new dimension for imaging human brain functions, albeit with certain limitations such as restriction of the measurable area to the cortical surface and lower spatial resolution than that of fMRI.

This study aims to improve the OT system as a more useful and practical complete imaging method for human brain functions. The subsequent chapters (chapters 2–5) describe the evaluations of the activation signals (Hb signals in response to a stimulus or a task) and the attempts made to reduce the fluctuations caused by some random factors in order to achieve a more sensitive measurement of human brain functions (see section 1.3).

Table 1.2 Comparison of the characteristics of BOLD fMRI and OT

	<b>BOLD fMRI</b>	<b>OT</b>
<b>Subject's state</b>	<ul style="list-style-type: none"> <li>✓ Lies in the supine position</li> <li>✓ Head cannot be moved</li> <li>✓ Loud scanning noise</li> </ul>	<ul style="list-style-type: none"> <li>✓ No restrictions on position</li> <li>✓ Wears a probe cap with optical fibers (tolerance for some movements)</li> <li>✓ No measurement noise</li> </ul>
<b>Measurement system</b>	<ul style="list-style-type: none"> <li>✓ Large (requires an MRI room)</li> <li>✓ Costs: ¥ 300,000,000 ~</li> <li>✓ Recurring running cost (for helium)</li> </ul>	<ul style="list-style-type: none"> <li>✓ Compact and portable</li> <li>✓ Costs: ¥ 30,000,000 ~</li> <li>✓ No running cost</li> </ul>
<b>Spatial information</b>	<ul style="list-style-type: none"> <li>✓ Millimeter order with accurate anatomical image</li> </ul>	<ul style="list-style-type: none"> <li>✓ Centimeter order with no anatomical image</li> </ul>
<b>Temporal information</b>	<ul style="list-style-type: none"> <li>✓ Seconds order</li> </ul>	<ul style="list-style-type: none"> <li>✓ Seconds order (sampling period can be 100 ms)</li> </ul>
<b>Measurement target</b>	<ul style="list-style-type: none"> <li>✓ BOLD signals (paramagnetic deoxy-Hb signals)</li> </ul>	<ul style="list-style-type: none"> <li>✓ Hb signals (oxy-Hb and deoxy-Hb signals)</li> </ul>
<b>Analysis method</b>	<ul style="list-style-type: none"> <li>✓ Standard analytical method: SPM (statistical parametric mapping)</li> </ul>	<ul style="list-style-type: none"> <li>✓ No standard analytical method:</li> </ul>

## 1.2 Development of OT from NIRS

In this section of chapter 1, the technological principle of NIRS and OT used for measuring human brain activation is reviewed along with an introduction to the conventional OT system, which was commercially available between 1999 and 2001.

### 1.2.1 Principles of NIRS in Detecting Activation Signals

NIRS was first developed for monitoring cerebral oxygenation.<sup>20-25</sup> Its ability to measure the secondary metabolic signals induced by the neural activity was demonstrated later.<sup>26-30</sup> This thesis focuses on the OT method, which is used to measure the product of the optical path length and the concentration change in oxy-Hb (oxy-Hb signal:  $\Delta C'_{\text{oxy}}$ ) and deoxy-Hb (deoxy-Hb signal:  $\Delta C'_{\text{deoxy}}$ ) in the cerebral cortex in order to image brain activation. Since the OT system has been developed as a commercial product, its use has spread not only to the medical field but also to various other areas of research.

The basic principle of NIRS for functional measurements of the human brain is based on the modified Beer-Lambert law,<sup>31</sup> which expresses the relationship between light attenuation and the concentration of the absorber in a light-scattering medium such as the living body. The original Beer-Lambert law can be applied only to a non-scattering medium.

In the measurement technique adopted in this study, a combination of the modified Beer-Lambert law and dual-wavelength spectrophotometry has been used to measure the Hb signals (products of the effective optical path length and the changes in the concentrations of oxy-Hb and deoxy-Hb) that accompany brain activation.<sup>9</sup>



$$L \cdot \Delta C_{\text{oxy}} = \Delta C'_{\text{oxy}} = \frac{-\varepsilon_{\text{deoxy}}(\lambda_2) \cdot \Delta A_{(\lambda_1)} + \varepsilon_{\text{deoxy}}(\lambda_1) \cdot \Delta A_{(\lambda_2)}}{E}, \quad (1-1)$$

$$L \cdot \Delta C_{\text{deoxy}} = \Delta C'_{\text{deoxy}} = \frac{\varepsilon_{\text{oxy}}(\lambda_2) \cdot \Delta A_{(\lambda_1)} - \varepsilon_{\text{oxy}}(\lambda_1) \cdot \Delta A_{(\lambda_2)}}{E}, \quad (1-2)$$

where

$$E = \varepsilon_{\text{deoxy}}(\lambda_1) \cdot \varepsilon_{\text{oxy}}(\lambda_2) - \varepsilon_{\text{deoxy}}(\lambda_2) \cdot \varepsilon_{\text{oxy}}(\lambda_1). \quad (1-3)$$

The Hb signals ( $\Delta C'_{\text{oxy}}$  and  $\Delta C'_{\text{deoxy}}$ ) are expressed as the product of the concentration changes ( $\Delta C_{\text{oxy}}$  and  $\Delta C_{\text{deoxy}}$ ) and the indefinite optical path length in the activation region ( $L$ ), where  $\Delta A$ ,  $\varepsilon_{\text{oxy}}$ , and  $\varepsilon_{\text{deoxy}}$  indicate the logarithm of the intensity changes, the absorption coefficient of oxy-Hb, and that of deoxy-Hb, respectively, for two wavelengths ( $\lambda_1$  and  $\lambda_2$ ). Note that it is necessary to assume that the path length ( $L$ ) is constant for every wavelength because the accurate estimation of  $L$  is almost impossible with this technique. While methods have been suggested for obtaining the product of the absolute concentration changes and the mean optical path length that can be estimated using time-resolved measurement,<sup>24, 31, 32</sup> it is inappropriate to use the mean path length as an alternative to the effective path length ( $L$ ) in the activation region.<sup>33, 34</sup> Therefore, the product of the effective optical path length and the concentration changes in oxy-Hb and deoxy-Hb ( $\Delta C'_{\text{oxy}}$

and  $\Delta C'_{\text{deoxy}}$ ) are used as the Hb signals. If the wavelength dependence of  $L$  exists, the cross talk effect<sup>35, 36</sup> occurs and makes the independent measurements of multiple chromophores difficult. However, the cross talk effect can be negligible when measuring changes only in the oxy-Hb and deoxy-Hb signals.<sup>35, 36</sup> Further discussion regarding the optical path length and cross talk is offered in chapters 5.

For noninvasive optical measurements of the living body, lights with appropriate wavelengths and high permeability are required. The feasibility of noninvasive monitoring by using the near-infrared (NIR) region was demonstrated in the mammalian brain because skin and bony tissue were found to be relatively translucent to NIR light.<sup>20</sup> For the measurements of human brain function, NIR wavelengths that are symmetrical about the point where the optical absorptions of oxy-Hb and deoxy-Hb are equal (approximately 800 nm) have usually been selected as  $\lambda_1$  and  $\lambda_2$  (e.g., 780 and 830 nm; Fig. 1.2). The mixed-wavelength NIR light can penetrate the human head as shown in Fig. 1.3. By detecting the intensity changes in the transparent light from the detection position situated 30 mm away from the irradiation position, the values of  $\Delta C'_{\text{oxy}}$  and  $\Delta C'_{\text{deoxy}}$  in the cerebral cortex can be measured. In the measurement area, the midpoint between the irradiation and detection positions has the highest sensitivity for changes in the concentration of absorbers.<sup>37, 38</sup>

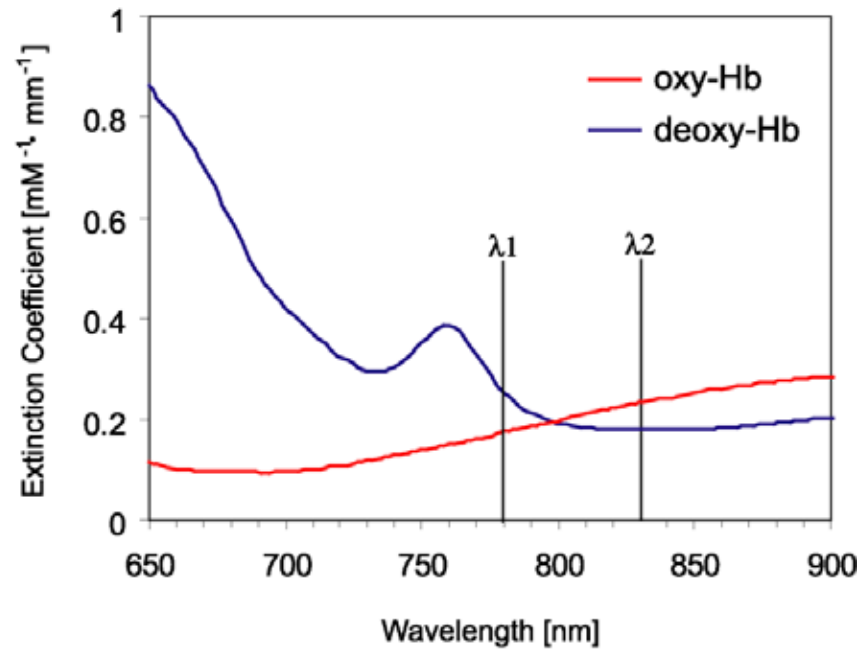


**Fig. 1.2** Absorption spectra of oxy- and deoxy-Hb and wavelengths ( $\lambda_1$ : 780 nm and  $\lambda_2$ : 830 nm) usually used for noninvasive measurements of human cortical function.

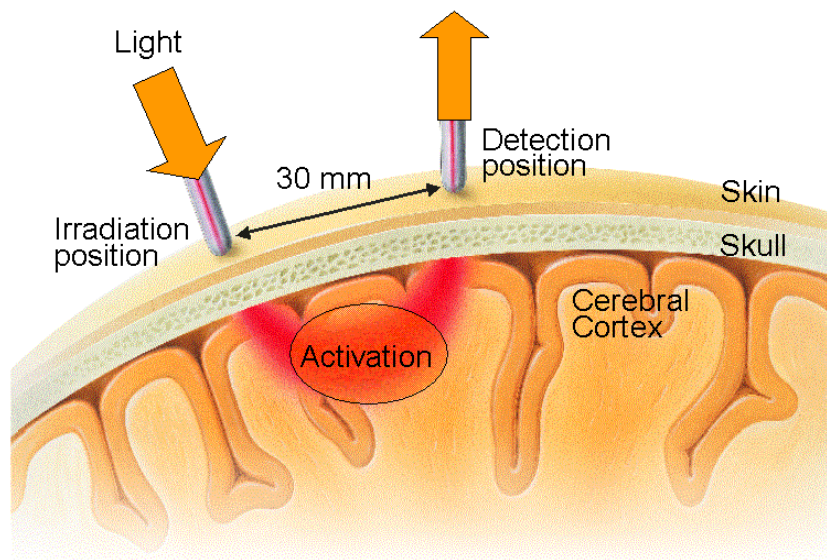


**Fig. 1.3** Schematic diagram of the measurement principle with respect to the anatomical structure of the human head.

### 1.2.2 From NIRS to OT

OT is a new extension of NIRS that is used to acquire a topographical image.<sup>8, 9, 12, 39, 40</sup> The earlier NIRS studies measured the spectroscopic reflection and scattering from a single region using a light emitter and a detector.<sup>26, 28-30</sup> The technological development from NIRS to OT is conceptually similar to that from nuclear magnetic resonance (NMR) spectroscopy to MRI.

OT measures the temporal changes in  $\Delta C'_{\text{oxy}}$  and  $\Delta C'_{\text{deoxy}}$  simultaneously from multiple regions by independently modulating the intensities of each radiated laser beam, that is, by frequency encoding of spatial information.<sup>8, 9, 11, 12, 39</sup> A block diagram of an OT system is shown in Fig. 1.4. The system uses two wavelengths of 780 nm and 830 nm as  $\lambda_1$  and  $\lambda_2$ , respectively, for the irradiation light, and each light source (LD: laser diodes) is modulated at a different frequency (1.0–8.7 kHz) to encode the irradiation positions and wavelengths. The scattered light is detected from the detection positions situated approximately 30 mm away from the irradiation positions by using an avalanche photodiode (APD). The dual-wavelength signals are decoded by using lock-in amplifiers using the reference signals from oscillators. Both irradiation and detection lights are propagated through optical fibers. In this paper, the portion of irradiating or detecting light that was in contact

with the head skin has been referred to as the probe.

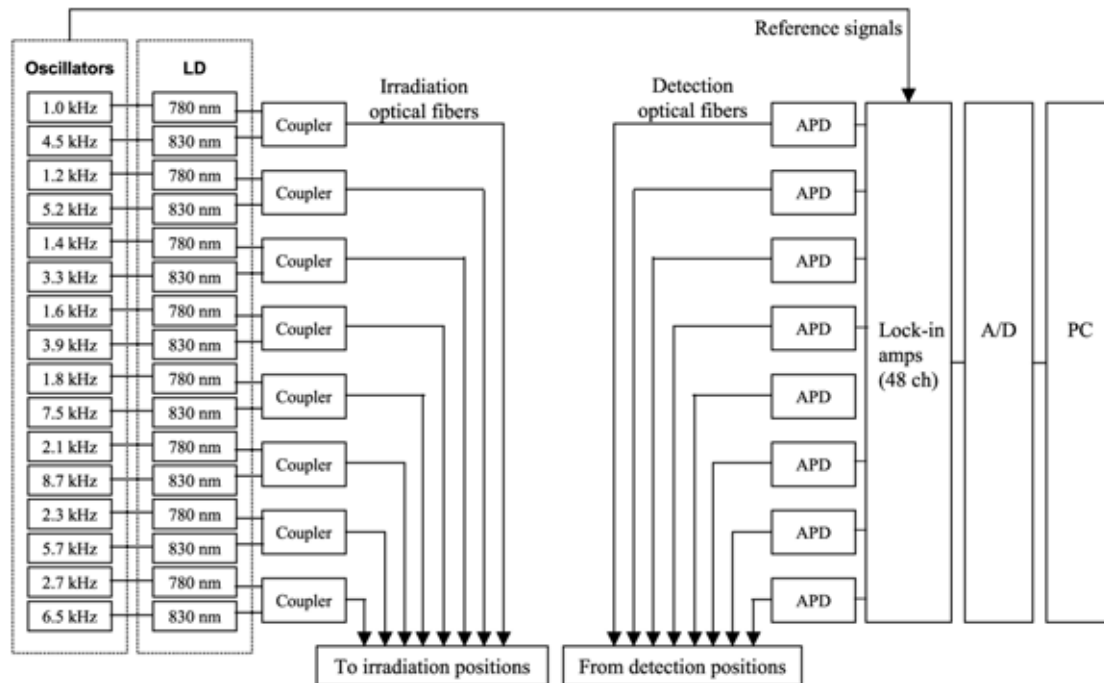


**Fig. 1.4** Block diagram of an OT system.<sup>8, 39</sup> LD: laser diode, APD: avalanche photo diode, A/D: analog/digital converter.

An example of the fiber arrangement for measuring 24 positions is shown in Fig. 1.5; this arrangement has 10 irradiation positions and 8 detection positions. The distance between the irradiation and detection positions is set to 30 mm in order to maximize the contribution of signals from the cerebral cortex located at a depth of approximately 15 mm from the scalp. The midpoint of the irradiation-detection (source-detector: S-D) distance is regarded as the measurement position because

here, the OT system is most sensitive to changes in chromophore concentration.<sup>37, 38</sup>

Although the minimum distance between the measurement positions in this system is 21 mm, a new method of arranging the optical fibers has been developed to improve the spatial resolution.<sup>41</sup>

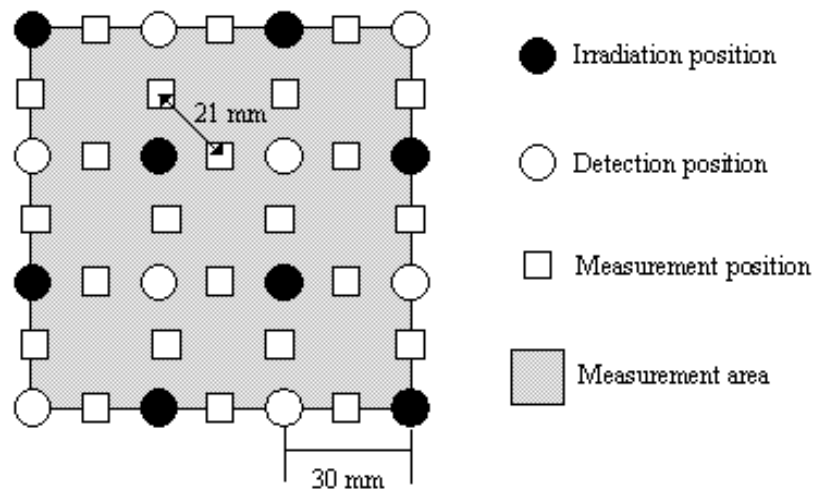


**Fig. 1.5** A representative arrangement of irradiation, detection, and measurement positions.<sup>8, 39</sup> The distance between the irradiation (source) and detection (detector) positions is set to 30 mm, and the minimum distance between the measurement positions is 21 mm when regarding the midpoint of the source-detector (S-D) distance as the measurement position. The gray shaded area shows the complete measurement area as defined by the source and detector positions.

The above-mentioned values were the main specifications of the OT system commercially available between 1999 and 2002 (Fig. 1.6). During measurements, the examiners fix a plastic probe holder on an optional position on the subject's head.

The system irradiates lights (LD: laser diodes) of two wavelengths—780 nm and 830 nm—(power of 1–2 mW for each wavelength) on multiple positions on the head. The scattered light rays are detected from the detection positions situated approximately 30 mm from the irradiation positions by using an APD. To measure any brain function, the examiners should provide appropriate sensory stimuli or cognitive tasks to the subjects. Finally, the Hb signals are plotted on time-course graphs and color maps using the unit mM·mm. The activation signal has usually been assessed by the appearance of a positive  $\Delta C'_{oxy}$  and a negative  $\Delta C'_{deoxy}$ ; however, no standard analysis methods have been proposed as yet.



**Fig. 1.6** The commercially available OT system (ETG-100, Hitachi Medical Corporation, Japan). The photograph has been provided by Hitachi Medical Corporation.

The fundamental capability of the OT system for measuring brain activation has been studied through simulation studies<sup>42</sup> and phantom studies.<sup>38-41</sup> First, Maki et al. used the Monte Carlo method to confirm the feasibility of the linear-signal processing (NIRS measurement algorithm used in OT; see section 1.2.1) based on the modified Beer-Lambert law.<sup>42</sup> The simulation of photon scattering for the reflection measurement in OT demonstrated the linear relationship between the measured absorbance change and the regional absorption change in the position corresponding to the cerebral cortex.<sup>42</sup> This result proved that the measurement algorithm based on the modified Beer-Lambert law could be used for OT on the assumption that scattering and background absorption are spatially homogeneous in the tissue. In addition, Yamashita et al. showed that an absorber (10 × 10 × 10 mm) painted black can be imaged at a depth of 15–30 mm in a tissue-simulating liquid model (a rectangular transparent plastic container filled with a 10% (vol/vol) solution of milk in water) using almost the same system as OT.<sup>40</sup> They also arranged a spherical absorber (diameter 10 mm) rotating in a cylindrical transparent plastic container filled with the same liquid mentioned above and demonstrated that the OT system could obtain dynamic topographic images of the moving absorber with a temporal resolution of 0.5 s in a measurement area of 90 × 90 mm.<sup>39</sup> This suggests that the OT system can detect topographic and dynamic images of the brain activity in the



cerebral cortex located at a depth of 15–25 mm below the scalp. Moreover, Yamamoto et al. examined the spatial sensitivity of topographic images by using a tissue-simulating solid model (phantom).<sup>38, 41</sup> The model was composed of an epoxy resin containing powdered titanium oxide<sup>43</sup> and consisted of the body and two parts (parts A and B). The two parts could be interchanged in the same position of the body; only part B had the activation area (absorber) with a different absorption coefficient to simulate the brain activation (the activation area was a cylinder with a diameter of 10 mm and a height of 10 mm), while part A had the same absorption coefficient as the body. Topographic activation images were obtained by the OT system by comparing the image of part A with that of part B. The results showed that the location of the activation area on the topographic images was consistent with the actual location of the absorber within a 3-mm margin of error in various locations of the probes relative to the absorber. This demonstrated that the OT system can be used to identify the activation position, but it also showed that the size of the activation area (area of the full width at half maximum of the signal distribution) varies depending on the relative position of the probes to the activation simulating absorber. To improve the spatial resolution of the topographic images, a new arrangement of optical fibers has been proposed.<sup>38, 41</sup> A few studies have also confirmed the feasibility of OT for imaging human brain activation in actual

measurements.<sup>9, 42</sup> However, they measured only the motor functions involved in a finger-tapping task in a maximum of five subjects and did not perform a qualitative evaluation of the activation signal pattern; furthermore, they did not observe clear activation in one of the five subjects.

### 1.3 Random factors causing fluctuations in the OT activation signals

The OT system has been mainly validated by studies that involved imaging an absorber in a scattering medium under restricted conditions, as mentioned above. However, some significant problems remain to be solved prior to implementing OT in practice because it is used to measure the brain activation in living human subjects, and the activation could vary not only among individuals but also within the same individual. In fact, consistent activation signals are not obtained occasionally due to certain reasons, including both system specification and methodological problems. In this study, some candidate factors were excluded from the possible random factors causing fluctuations in the activation signals. I have tried to solve them and to improve the OT system as a complete measurement system for more sensitive imaging of human brain functions.

In measurements of human brain functions, some random factors are unavoidable; this is common with most imaging methods.<sup>44</sup> The possible random factors causing the fluctuations in the OT activation signals are listed along with some system-related factors (Table 1.3).

**Table 1.3 Possible random and system-related factors causing fluctuations in the activation signals in OT measurements.**

Random factors 1	Random factors 2	System-related factors
Random factors (biological noise from a subject)	Random factors (interaction noise between the system and a subject)	System-related factors (system noise)
<ul style="list-style-type: none"> <li>➤ Variability of neural activity</li> <li>➤ Variability in the process of metabolic/vascular responses</li> <li>➤ Background functions</li> <li>➤ Attention level</li> <li>➤ Spontaneous oscillation</li> <li>➤ Systemic physiological change</li> </ul>	<ul style="list-style-type: none"> <li>➤ Probe positions (probe and head)</li> <li>➤ Optical properties of the human head (light and head tissue)</li> <li>➤ Attachment of probes (probe and head)</li> <li>➤ Body movement (probe and head)</li> </ul>	<ul style="list-style-type: none"> <li>➤ Irradiation power of light</li> <li>➤ Arrangement of measurement positions</li> <li>➤ Sampling period</li> <li>➤ Device performance</li> <li>➤ Measurement algorithm</li> <li>➤ Light wavelengths</li> </ul>

In practice, the effects of system-related factors, defined as the system noise, are determined based on the safety criterion and the device performance. For example, the irradiation power of lights is restricted for safety reasons although high

power irradiation would naturally result in high sensitivity. Besides, the consistency of light irradiation and detector performance, including the sampling period, are clearly defined by the device performance. Most of these system-related factors, including the measurement algorithm and light wavelengths, have been estimated and confirmed to be applicable to imaging brain activation by simulation and phantom studies based on the spectroscopic approach,<sup>38-42</sup> as introduced in the previous section. Note that the fundamental effects of the measurement algorithm and light wavelengths on the Hb signals could be systematically estimated under certain specific measurement conditions. A random factor, namely, the optical properties of the human head (random factor 2), will be discussed in relation to system-related noise depending on the measurement algorithm and light wavelengths (chapter 5).

In contrast to the system-related factors that can be controlled in every measurement, the estimation of uncontrollable random factors is difficult; therefore, the latter have not been examined adequately. The random factors are classified into two groups (Table 1.3) and will be explained next.

First, there are various biological noises that emanate from a subject (random factors 1). One of the factors is the variability of the neural activity itself. Even the

brain has autonomous fluctuations and does not always produce the same response to the same stimuli.<sup>45</sup> Moreover, variability may be present in the process that results in metabolic/vascular responses being induced by the neural activity.<sup>46</sup> The relationship between the neural activity and hemodynamic changes, which leads to changes in both the BOLD signal and Hb signals, has remained unsolved and is a challenging issue in the field of neuroscience. These two factors together are defined as the variability of physiological activation pattern in this thesis. The representative physiological activation patterns are considered to be an increase in the oxy-Hb signal and a decrease in the deoxy-Hb signal, which correspond to a positive  $\Delta C'_{\text{oxy}}$ <sup>1, 9, 30, 47, 48</sup> and a negative  $\Delta C'_{\text{deoxy}}$ <sup>1, 49</sup> value in the Hb signals (OT studies) and an increase in the BOLD signal intensity (fMRI studies). However, contrary to the general understanding, a negative  $\Delta C'_{\text{oxy}}$  value together with a positive  $\Delta C'_{\text{deoxy}}$  value in NIRS studies<sup>1, 28, 50</sup> and a decrease in the BOLD signal in fMRI studies<sup>51, 52</sup> have been reported. Although there might be various physiological activation patterns, they have not been classified, and their occurrence probabilities and the mechanism underlying these patterns still remain unknown.

Next, fluctuations due to background functions rather than the targeted function can be a significant random factor. This is a fundamental issue for most of the functional imaging methods because using rest periods as baseline conditions is

obligatory for measuring the activation signal in these methods. Conventionally, researchers have used the rest period with no task being performed as a zero-activity condition as compared to the task/stimulation period; however, recent reports have cautioned that there is no inherent baseline state in the brain; instead unconstrained cognitive activity is present.<sup>52, 53</sup> Accordingly, the fluctuations from background functions in the rest period can be a significant biological random factor, which should be considered here. In addition, the attention level is considered one of the background functions that cause fluctuations in the activation signals. Here, the attention level is defined as a kind of intention to perform the task and can be estimated by behavioral task performance. This effect has been reported in some functional studies. For example, a previous study reported that compared with performing actions without paying attention, focusing attention on the same movements increased the activity in the prefrontal, premotor, and parietal cortices.<sup>54</sup>

Other biological noises are the spontaneous oscillations and systemic physiological changes. Spontaneous oscillations in cerebral oxygenation have been reported in adults<sup>55</sup> and infants<sup>56</sup> during OT (NIRS) measurements. Although low-frequency ( $0.1 \text{ s}^{-1}$ ) and very-low-frequency oscillations ( $0.04 \text{ s}^{-1}$ ) are occasionally altered in proportion to the magnitude of functional activation, the effects on the activation signals can be avoided through the evaluation of the activation signals by

averaging several activation periods.<sup>55</sup> On the other hand, the effect of background systemic physiological processes such as heart rate and blood pressure on the activation signals has not yet been clarified. Studies pertaining to these systemic physiological processes are in progress.<sup>57</sup>

These random factors consisting of biological noises are common to other imaging methods such as EEG, MEG, and fMRI although the type of effect would differ depending on the measurement target (e.g., electrical signal or metabolic/vascular signal). Time-dependent (over successive measurements) differences are bound to occur within the same individual as well as among different individuals.

Second, there are various random factors consisting of the interaction noise between the system and a subject (random factors 2). These factors, except body movement, are relatively specific to each modality.

Among random factors 2, the first factor is the indefinite probe positions in relation to the brain and is related to the main disadvantage of OT as compared to fMRI (no anatomical image is produced in OT). The practical problem lies in the inability to determine the positions for probe placement on the head; this results in different measurement areas between different subjects and within the same subject.

The absence of standard positions for the placement of probes on the head is also a problem. In addition, the activation area cannot be matched with actual anatomical information through OT alone without using MRI although accurate spatial information is important in functional imaging methods.

The second factor in this group is the variability in the optical properties of the human head. It is impossible to clarify these properties in living subjects although those of various tissue samples have been studied.<sup>58</sup> The interaction between the optical property and light can affect the Hb signals in relation to the light wavelengths and measurement algorithm, which are classified under system-related factors. It should be noted that the fundamental effects of the measurement algorithm and light wavelengths on the Hb signals could be systematically estimated only if the optical properties of the human head are evident. In other words, the simulation and phantom studies could estimate the measurability of OT under some specific condition of measurements.

The next factor in this group is the attachment of probes. This can vary according to the method of probe fixation and the absorbance by the subject's hair. This factor might affect the system-related factor of device performance; however, this as well the next factor—body movement—is not discussed in this thesis. Body movement produces a significant noise and is common to both MEG and fMRI



because their measurement coordinates are fixed in the system, while in EEG and OT, the coordinates are fixed onto the subject's head. A quantitative evaluation of the effect of body movement on Hb signals is necessary, but OT can be relatively tolerant to some body movements.

In conclusion, although OT has been validated under some specific conditions mainly through simulation and phantom studies,<sup>9, 38-42</sup> a number of random factors may cause fluctuations in the activation signals in practical measurements of human brain functions (Table 1.3). Chapters 2–5 of this thesis report the next four studies that are related to some random factors; the studies are aimed at improving the OT system as a complete imaging method of human brain functions.

First, the reproducibility of OT activation signals (Hb signals in response to a stimulus or a task) in the sensorimotor cortex is examined (in chapters 2 and 3). The sensorimotor area is activated by the finger-tapping task (task paradigm); this task has been used in many functional studies, including not only OT<sup>9, 42, 47</sup> but also fMRI<sup>59, 60</sup> and PET.<sup>61, 62</sup> Note that the activation signal mentioned here is an overall signal that includes the fluctuations caused by all random factors in the conventional OT (Table 1.3). Therefore, it may be important to evaluate the reproducibility of the activation signals measured by OT in the present state in order

to examine the tolerance of these random factors; this is based on the assumption that the activation signal is exactly reproduced in the absence of random factors. Moreover, by identifying the characteristics of activation signals having a high reproducibility, it would be possible to find useful parameters for detecting activation signals effectively.

In the study reported in chapter 2, the within-subject reproducibility of the activation signals is evaluated during the imaging of sensorimotor activations in the same subject 6 months after the original session. Here, the reproducibility of a positive  $\Delta C'_{\text{oxy}}$  and a negative  $\Delta C'_{\text{deoxy}}$  in response to activation, the location of activation area, and the temporal dynamics (time courses) of activation signals are evaluated in the same subject.

In chapter 3, the reproducibility (generality) and variability of activation patterns, such as a positive  $\Delta C'_{\text{oxy}}$  and a negative  $\Delta C'_{\text{deoxy}}$ , are studied in 31 subjects by employing the same paradigm that is described in chapter 2. It is important to examine the fundamental reproducibility among a number of subjects because a larger number of random factors are considered to exist in the comparison of different subjects than in the within-subject comparison.

These studies, described in chapters 2 and 3, also examine the attempts to reduce a random factor—variability of probe positions. Here, the 10-20 electrode

system of the International Federation (the 10-20 system)<sup>63, 64</sup> has been used to determine the locations of probe positions on the head. The 10-20 system, used in the placement of electrodes for EEG recordings, is based on standard external landmarks on the skull (Fig. 1.7).

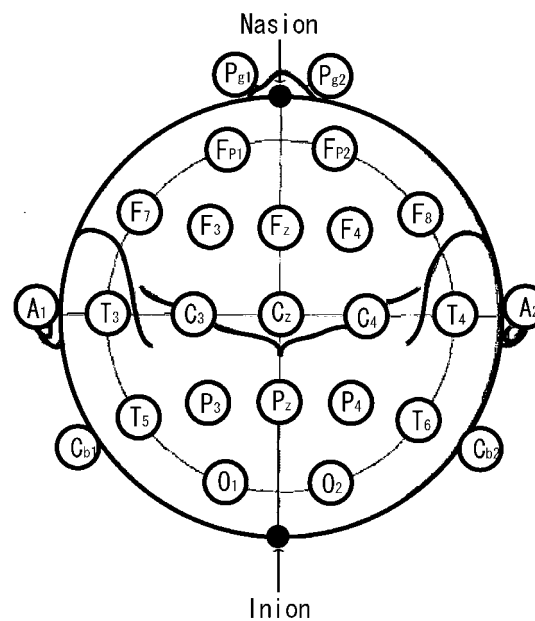


**Fig. 1.7** A single plane projection of the head with all the standard positions and the locations of the main fissures. The outer circle is drawn at the level of the nasion and inion. The inner circle represents the temporal line of electrodes. This figure provides a useful template for indicating the placement of electrodes during routine recordings in EEG measurements (reedited from the reference 64).

The 10-20 system is considered useful for determining the locations of the probe positions in OT because some MRI examinations showed a high agreement between

the 10-20 position and a specific anatomical area.<sup>65-67</sup> However, the effectiveness of the 10-20 system for functional imaging in OT has not yet been examined. Therefore, I examined the effectiveness of the reproducibility of the location of activation in the Hb signal map, both within the same subject and between subjects.

After evaluating the tolerance of the random factors and exploring the tolerant characteristics (highly reproducible parameters) of activation signals in the conventional OT measurements, possible solutions for the effects of some random factors are examined (described in chapters 4 and 5).

A study reported in chapter 4 examines the efficacy of a devising-task paradigm for reducing the activity (fluctuations) originating from background functions (random factor 1) such as the attention level. The task paradigm is defined as the design of tasks and/or stimuli to control the subject's state and the time sequence of the presentation. The basic concept is that minimizing the differences in background functions, for example, attention, between the task and rest periods is useful for measuring the delicate activation signals produced by the reduced fluctuations in the Hb signals. The activation signal produced in response to speech recognition is selected for this measurement because it has been confirmed that the small language components of speech recognition, such as word recognition and sentence comprehension, are represented in slightly different cortical areas.<sup>68</sup>

Accordingly, it would be appropriate to test the detection ability for delicate activation signals. The well-designed task paradigms have gradually been applied in fMRI studies; the effect of the devising-task paradigm in OT has not yet been demonstrated.

In a study reported in chapter 5, the practicality of wavelength selection for reducing the system-related noise is examined. Wavelength selection, which is one of the system-related factors, is concerned with the optical properties of the head (random factor 2: interaction noise between the system and a subject) in relation to the measurement algorithm. One light wavelength should be shorter than the conventional wavelength (780 nm) used in the theoretical estimation of system-related factors (measurement algorithm), but the wavelength range should be limited based on the actual optical properties of subject's head. Therefore, the possible wavelengths of 678, 692, 750, and 782 nm are examined for pairing with the wavelength of 830 nm in the practical NIRS measurements of activation signals in four different cortical areas among four subjects. To identify the optimal wavelengths for various cortical areas and subjects, activation signals in several cortical areas and subjects were examined.

Finally, the findings obtained from studies reported in chapters 2–5 are summarized in the conclusion (chapter 6) from the viewpoint of the effects of random

factors (Table 1.3) on the activation signals. In addition, based on the above-mentioned findings, I propose a future direction of improving the OT system in order to render it more useful and effective.

## 2. Within-Subject Reproducibility of Activation Signals

### 2.1 Introduction

In the work reported in this chapter, the within-subject reproducibility of the activation signals was examined. Note that the activation signal here is an overall signal that includes the fluctuations caused by all random factors (Table 1.3).

Therefore, it is useful to evaluate the reproducibility of the activation signals measured by OT in the present state for the examination of the tolerance of these random factors; this is based on the assumption that the activation signal is exactly reproduced in the absence of random factors. Moreover, by identifying the characteristics of activation signals having a high reproducibility, it would be possible to find useful parameters for detecting activation signals effectively.

Sensorimotor cortex activation by a simple finger-tapping task was selected to examine the reproducibility of activation signals because it has already been validated by a number of functional studies using PET,<sup>61, 62</sup> fMRI,<sup>59, 60</sup> and OT.<sup>9, 47</sup> Although the reproducibility of activation signals in PET and fMRI for sensorimotor-activation has already been examined,<sup>44, 69, 70</sup> there are few reports relating to the within-subject reproducibility of Hb signals in OT or NIRS measured

at different times. To minimize the effects of habituation and learning, which may affect some random factors, such as attention level, about six months was allowed to elapse between each subject's first and second experimental sessions and the subject was not asked to perform the experimental task during the six months period. Other conditions were also controlled for each subject (e.g., the same examiner and the same experiment place and time of day).

Here, the reproducibility of the increase or decrease in Hb signals in response to activation, the location of activation area, and the temporal dynamics (time courses) of activation signals are evaluated in the same subject. In addition, this study attempted to reduce a random factor—variability of probe positions—by applying the 10-20 system<sup>63, 64</sup> to determination of the locations of probe positions on the head.

## 2.2 Methods

### 2.2.1 Subject

Seven healthy adults (two men and five women between 28 and 44 years old; mean age = 35) participated in the experiment. Each gave written informed consent after the nature of the experimental procedures was explained before the



experiments. Six of the subjects showed right-handedness, and none reported a history of neurological disorder.

### 2.2.2 OT measurement

An OT system (ETG-100: Hitachi Medical Corporation, Japan), which can take measurements at 24 positions, was used. The system delivers light beams with 780- and 830-nm wavelengths through an optical fiber to the same position simultaneously. The scattered light was detected every 100 ms by using an avalanche photodiode (APD) 30 mm from the incident position through optical fibers. The average power of each light source was 1.5 mW, and each source was modulated at a different frequency to encode irradiated positions and wavelengths. Ten irradiated positions and eight detection positions were arranged to make 24 measurement positions (Fig.2.1).

The measurement positions were determined manually for each subject and were based on the 10–20 system.<sup>63, 64</sup> We measured 60×60-mm areas in the left and right parietal areas centered on C<sub>3</sub> and C<sub>4</sub> (Fig.2.1). The 60×60 mm square was defined as the measurement area for each hemisphere based on the arrangement of optical fibers (irradiation and detection positions). The centers of the bilateral measurement areas were considered to correspond to each primary sensorimotor

area based on previous studies examining the relation between locations of the

10–20 system and the underlying cortical areas.<sup>65-67</sup>

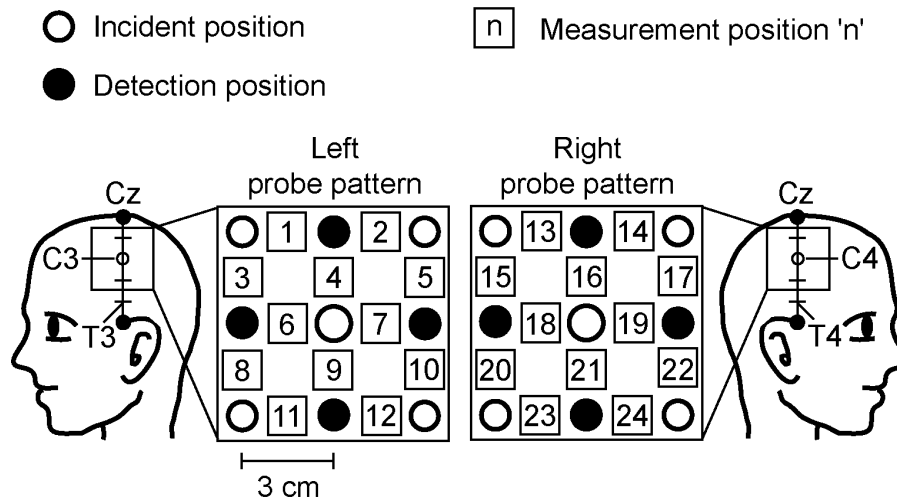


**Fig. 2.1** Arrangement of measurement positions in probe patterns over left and right sensorimotor areas centered on locations C3 and C4, respectively.

### 2.2.3 Task paradigm

The two experimental sessions for each subject were separated by about six months— $167 \pm 11$  days (mean  $\pm$  SD)—and two finger-tapping trials were conducted in each session (one with the left hand and one with the right hand) (Fig. 2.2). In each trial, the fingers of one hand were repeatedly placed on the tip of the thumb in the following order: forefinger – second finger – third finger – little finger – third finger – second finger – forefinger. The subjects were asked to repeat the tapping sequence at 3 Hz synchronized to the term “Finger tapping” blinking on a CRT monitor. Each

task period lasted for 30 s and was followed by 30 s of rest (rest period). Each trial consisted of six rest periods and five task periods (Fig. 2.2).

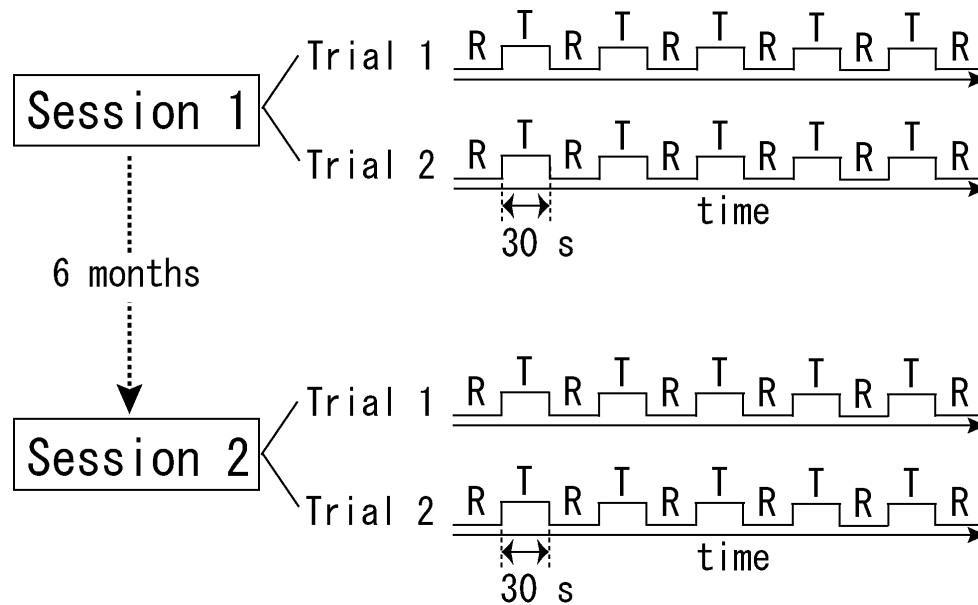


**Fig. 2.2 Schematic diagram of measurement sequence (session and trial). R: rest period, T: task (finger-tapping) period. A finger-tapping task using either left or right hand was conducted in each trial. The order of trials, right-hand or left-hand, was counterbalanced among subjects, and the order was fixed in the second session for each subject.**

#### 2.2.4 Data analysis

The data for each trial was divided into five 55-s “blocks”. A block consisted of 5 s of the rest period before a task (pre-task rest period), the 30-s task period, and 20 s of the rest period after the task (post-task rest period), as illustrated in Fig. 2.3.

The data collected for each block, i.e., the detected temporal attenuation changes at

each wavelength, were baseline-corrected using the data for the pre- and post-task rest periods. The Hb signals ( $\Delta C'_{\text{oxy}}$  and  $\Delta C'_{\text{deoxy}}$ ) were calculated by applying the modified Beer-Lambert Law as explained in chapter 1.2.

The activation signals were statistically assessed. Assuming that the time courses of activation signals varied among the subjects, a 25-s activation period was defined for each subject (see Fig. 2.3). A within-subject averaged time course over the five blocks was used to select the 25-s activation period with the maximum absolute mean change for each Hb signal. The 25-s activation period was allowed to shift from the initial 5 s after task onset to starting 15 s after task onset; the earliest period was from 5 s after task onset to task completion, and the latest period was from 15 s after task onset to 10 s after task completion.

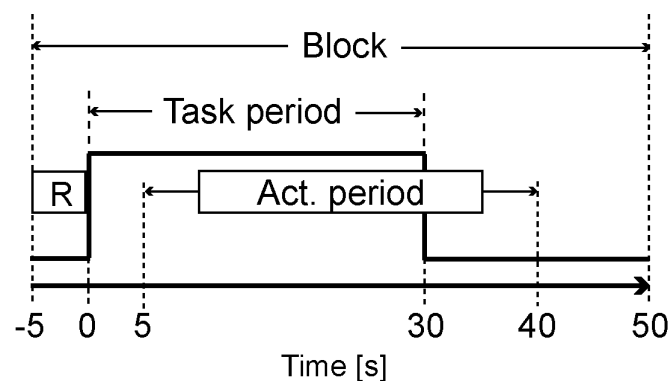


**Fig. 2.3 Schematic diagram of analysis parameters for a block. Mean values during 5 s of rest period before task (R) and 25 s of activation period were used for statistical analysis. Note that activation period can shift from 5 s after task onset to 10 s after task completion, depending on the maximum absolute value for each case.**

Using the mean changes in Hb signals during the pre-task period and those during the activation period for each block, we calculated the  $t$ -value (paired  $t$ -test) between the mean hemoglobin changes in the pre-task rest periods of five blocks and those in the activation periods of the same five blocks. The  $t$ -test is a common statistical method for assessing whether there is any statistical difference between the means of two groups (Fig. 2.4). The formula for the  $t$ -test is a ratio. The numerator of the ratio is merely the difference between the two means or averages. The denominator is a measure of the variability or dispersion of the scores. This formula is essentially another example of the signal-to-noise metaphor in research. That is, the difference between the means is the signal and the measure of variability is the noise that may render the accurate evaluation of the group difference difficult. In this thesis, the  $t$ -test is used for comparisons between two values, mainly for comparing the signal change in the activation period with that in the rest period.

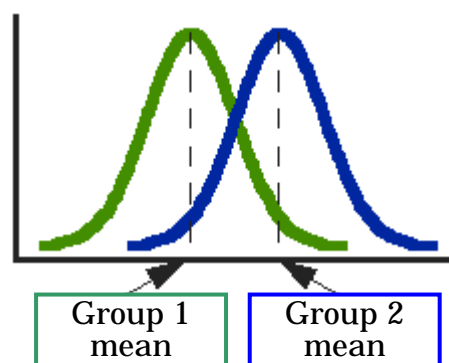


**Fig. 2.4** Conceptual image of the distributions of the two groups to be compared.

Measurement positions with significant  $t$ -values (two-tailed  $t$ -test,  $p < 0.1$ ) were identified as activation points by using the independent threshold ( $p < 0.1$ ) for each Hb signals ( $\Delta C'_{oxy}$  and  $\Delta C'_{deoxy}$ ). This statistical analysis was designed to determine the consistency (reproducibility within a session) of changes for the five activation periods. With this analysis, a system noise is not detected as an activation because its statistical value does not reach the threshold unless similar changes arise in every (or almost every) activation period. In addition, using activation periods 25 s long reduces the possibility of misidentifying an increase or decrease due to spontaneous oscillations of 0.1 Hz.<sup>55</sup> Moreover, a  $t$ -test using the mean value in the pre-task rest period (5 s) and that in the activation period (25 s) for each block reduces the effect of high-frequency system noise. Using the data for the activation points, the reproducibility of spatial information, signal amplitude, and temporal information between sessions was examined for each subject. The spatial information was represented by the activation center of the activation area. The coordinates of the activation center ( $x_c, y_c$ ) were defined as

$$x_c = \frac{\sum_i x_i a_i}{\sum_i a_i}, \quad y_c = \frac{\sum_i y_i a_i}{\sum_i a_i}, \quad (2-1)$$

where  $(x_i, y_i)$  denotes the coordinates of the  $i$ th activation point, and  $a_i$  is the signal amplitude at the  $i$ th activation point. Note that the measurement positions with no

significant changes were not used in calculating the activation center. The reproducibility of spatial information was examined by using the distance between the activation centers identified in the two sessions. The mean signal amplitudes during the activation periods and the time courses of the Hb signals ( $\Delta C'_{\text{oxy}}$  and  $\Delta C'_{\text{deoxy}}$ ) were used as the respective reproducibility indices for amplitude information and temporal information.

For various comparisons in this thesis, an ANOVA (analysis of variance) is employed in cases where the  $t$ -test is not applicable. ANOVA, occasionally referred to as the  $F$  test, is closely related to the  $t$ -test that is explained above. The major difference between the tests is that the  $t$ -test measures the difference between the means of two groups, whereas an ANOVA tests the difference between the means of two or more groups. The advantage of using ANOVA rather than multiple  $t$ -tests is that it reduces the probability of a type I error. Making multiple comparisons increases the likelihood of finding something by chance—making a type I error.

## 2.3 Results and Discussion

### *2.3.1 General aspects of reproducibility*

In the first session, every subject showed a positive  $\Delta C'_{\text{oxy}}$ , and a negative

$\Delta C'_{\text{deoxy}}$  in the hemisphere contralateral to the tapping hand. Besides, the same patterns in both  $\Delta C'_{\text{oxy}}$  and  $\Delta C'_{\text{deoxy}}$  were reproduced in the second session for every subject. This suggests that both the  $\Delta C'_{\text{oxy}}$  and  $\Delta C'_{\text{deoxy}}$  signals can reproduce the fundamental features (positive or negative) in each subject. The reproducibility was further examined using the 14 data sets (two hemispheres  $\times$  7 subjects) for  $\Delta C'_{\text{oxy}}$  and  $\Delta C'_{\text{deoxy}}$ .

### 2.3.2 Reproducibility of spatial information

Fig. 2.5 shows representative activation maps for the left-hand finger tapping for the two sessions of a subject. For both sessions, similar patterns of activation (positive  $\Delta C'_{\text{oxy}}$  and negative  $\Delta C'_{\text{deoxy}}$ ) were observed in the hemisphere contralateral to the tapping hand. In comparing the activation locations between the two sessions, the activation center was reproduced within 16.0 mm ( $\Delta C'_{\text{oxy}}$ ) and 18.6 mm ( $\Delta C'_{\text{deoxy}}$ ) on average (Table 2.1). A one-way ANOVA showed no significant effect of the kind of Hb signals on the activation center distances between sessions ( $F(1,26) = 0.34, p = 0.57$ ), which indicates that there is no difference between oxy-Hb and deoxy-Hb signals in the spatial reproducibility.



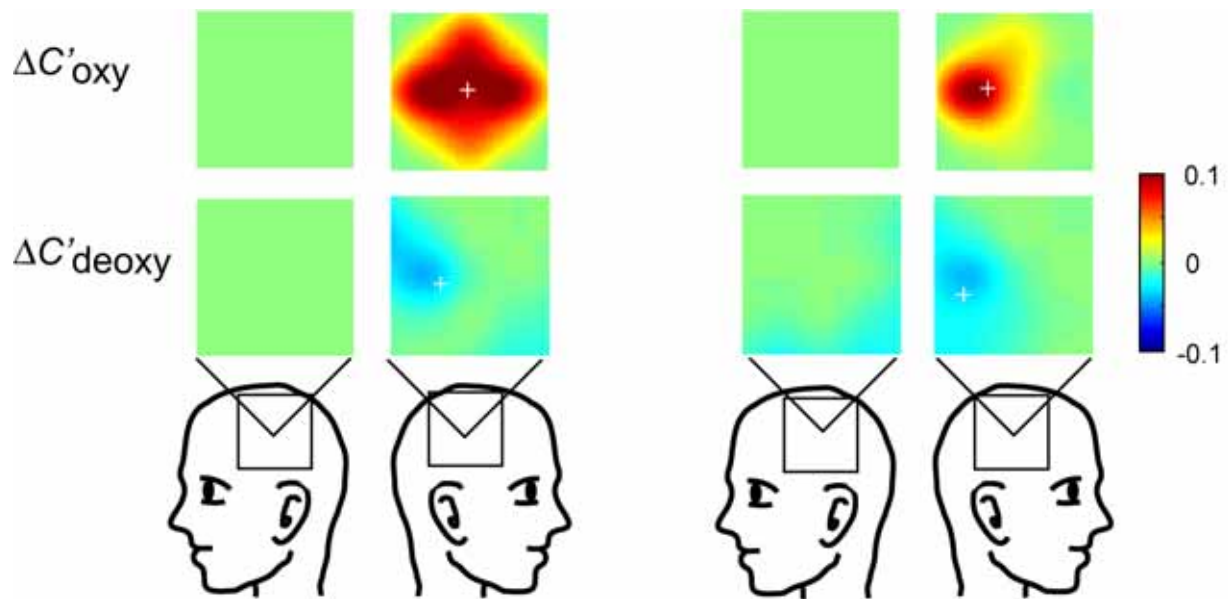


**Fig. 2.5** Representative activation maps in two sessions during the left-hand finger-tapping period. Limited positions with significant changes (activation points) are shown in color with linear interpolation, and other measurement positions with no significant change are equally zeroed. Note that the activation centers (“+”) were calculated using the raw coordinates of activation points weighted by the signal amplitude (distance between measurement positions > 21 mm).

**Table 2.1** Mean distance of activation centers between the two sessions.

	$\Delta C_{\text{oxy}}$	$\Delta C_{\text{deoxy}}$
Mean distance $\pm$ SD (mm)	$16.0 \pm 12.1$	$18.6 \pm 12.0$

Each subject showed similar activation-map spatial patterns between sessions. For each Hb signal, the activation center locations determined in the two experimental sessions were reproduced within 20 mm (Table 2.1), which is

comparable to the minimum distance between measurement positions in the current OT (21 mm). The high reproducibility of activation centers over time is consistent with the findings of a previous PET study<sup>70</sup> that showed consistent anatomical locations of motor activation after six months, and of an fMRI study<sup>44</sup> that also showed small distances between the activation centers determined in experimental sessions separated by 30, 49, and 60 days. Although these previous studies showed inter-session gaps of millimeter order, their results are not comparable with our OT results because of the difference in analytical methods and the spatial resolutions of those methods. For example, the previous fMRI study used  $1.17 \times 1.17 \times 1$ -mm voxels when identifying the coordinates of the maximum peak in the activation area as the activation center,<sup>44</sup> while the current OT used measurement positions separated by 21 mm when identifying the activation center.

In addition, it should be noted that that the spatial difference between sessions included unavoidable errors caused by a random factor, probe positions (the manual method for probe setting). The error in the probe positions was roughly estimated by 10-times repeated setting of the probe holder for one subject and marking of the measurement position each time. As a result, the difference among the repeated settings was about  $4.8 \pm 3.0$  (mean $\pm$ SD) mm. This small difference can result in a maximum shift of the activation center of 21 mm (the distance between

measurement positions) depending on the relationship between the location of the activation area and the probe positions.<sup>38, 71</sup> Consequently, the spatial reproducibility of the current OT system is less than 20 mm after six months within subject, including both physiological shifts and fluctuations caused by some random factors. A more accurate method to place the measurement probes, and a probe arrangement with higher-density measurement positions<sup>41, 71</sup> is needed to distinguish the actual physiological shift of the activation centers from fluctuations caused by some random factors.

### 2.3.3 Reproducibility of signal amplitude

Mean absolute values of  $\Delta C'_{oxy}$  and  $\Delta C'_{deoxy}$  in the activation period were given as the signal amplitude for each Hb signal. Averaged across subjects, they were  $0.095 \pm 0.045$  (mean $\pm$ SD) mM·mm for  $\Delta C'_{oxy}$  and  $0.044 \pm 0.018$  mM·mm for  $\Delta C'_{deoxy}$ . An ANOVA indicated a main effect of the kind of Hb on the signal amplitude ( $F(1,54)=32.5$ ,  $p < 0.0001$ ). This result is consistent with a previous study which showed that the activation-signal amplitudes for  $\Delta C'_{deoxy}$  are usually less than half those for  $\Delta C'_{oxy}$ .<sup>12</sup>

The signal amplitudes of  $\Delta C'_{oxy}$  and  $\Delta C'_{deoxy}$  were compared between sessions for each subject (Fig. 2.6). The signal amplitude was variable within each subject

and no consistent tendency was found across subjects. An ANOVA indicated no significant effects for sessions ( $\Delta C'_{\text{oxy}}$ :  $F(1,26) = 1.75$ ,  $p = 0.19$ ;  $\Delta C'_{\text{deoxy}}$ :  $F(1,26) = 1.04$ ,  $p = 0.32$ ), although the amplitude of the  $\Delta C'_{\text{oxy}}$  tended to be slightly lower in the second session (Fig 2.5). In percentage terms, the signal amplitudes varied: on average,  $-18\% \pm 31\%$  (mean  $\pm$  SD) for  $\Delta C'_{\text{oxy}}$  and  $-1\% \pm 60\%$  for  $\Delta C'_{\text{deoxy}}$ .

These results suggest variability of the signal amplitude in OT measurement, which could reflect fluctuations caused by some random factors. One possible random factor caused the fluctuation is the baseline differences, which are mainly caused by the background functions and spontaneous oscillation. The attention level is considered one of the background functions that cause fluctuations in the activation signals. For example, a previous study showed the attention level, one of the background functions, could increase the activity in some cortical area during the same movement task.<sup>54</sup> In addition, the existence of spontaneous oscillation in the hemoglobin oxygenation state has been shown by OT studies of adults<sup>55</sup> and infants,<sup>56</sup> and a difference in the baseline state could affect the activation amplitude, as suggested in previous fMRI and PET studies.<sup>52, 53</sup> Another random factor is probe positions, that is, small differences in measurement positions. As described above, the probe position can vary about 4.8 mm on average due to manual setting. The difference in measurement positions could affect the signal amplitude, since the

current method has uneven spatial sensitivity due to the relationship between the activation area (location and size) and the probe positions.<sup>71</sup> Although the tendency of a lower  $\Delta C'_{oxy}$  in the second session might indicate a habituation effect similar to the one shown in a previous fMRI study,<sup>44</sup> where habituation effects for sensorimotor activation were observed between two sessions separated by five hours and by one or two months, it would be difficult to estimate the activation level by using the signal amplitude in the present OT systems.

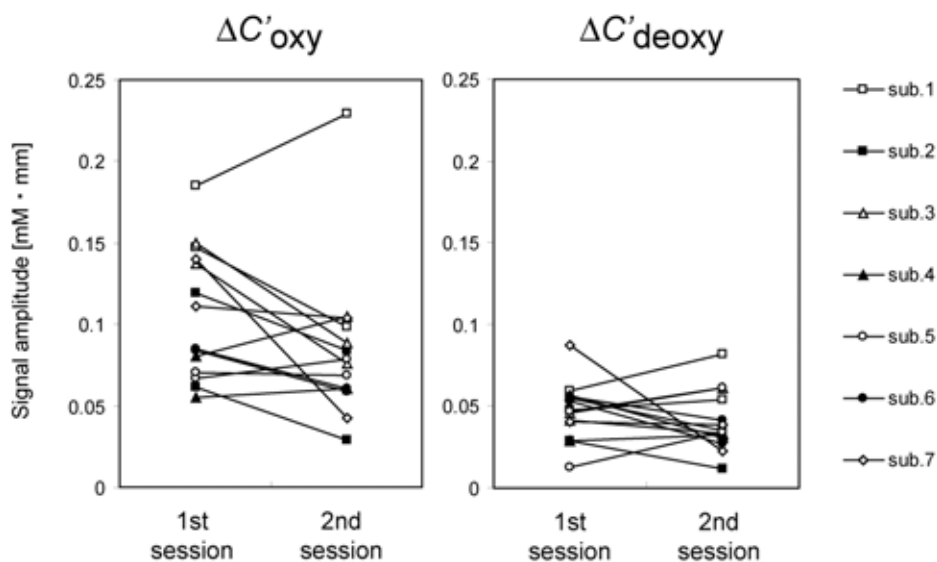


**Fig. 2.6** Signal amplitudes of each Hb signal for each subject in the two sessions.

#### 2.3.4 Reproducibility of temporal information

The reproducibility of temporal information was examined by comparing the time course of the activation signal between two sessions. Time courses for all

subjects are shown in Fig 2.7, and the mean between-sessions correlate coefficients for all subjects are listed in Table 2.2. Each subject showed time courses of similar shape in the two sessions, and the average correlation coefficient was high for each hemoglobin species.

Although no other NIRS studies have reported such a similar time course reproduced after more than a few days, the present findings could be important with regard to the development of a new OT application in a clinical area. Qualitative characteristics of the subject might be more clearly inferred from temporal information, such as the time course of the activation, than from spatial information and amplitude information that vary with some random factors. A recent study used the characteristics of the time course in  $\Delta C'_{oxy}$  to assess psychiatric patients with depression and schizophrenia.<sup>72</sup> Temporal information would indicate the temporal characteristics in the vascular response of neural activity, which in turn may relate to vascular elasticity. Consequently, examining the shape of time course in the same subject can be also useful for the evaluation of the subject's state, which will help longitudinal studies as well as monitoring rehabilitation effects.

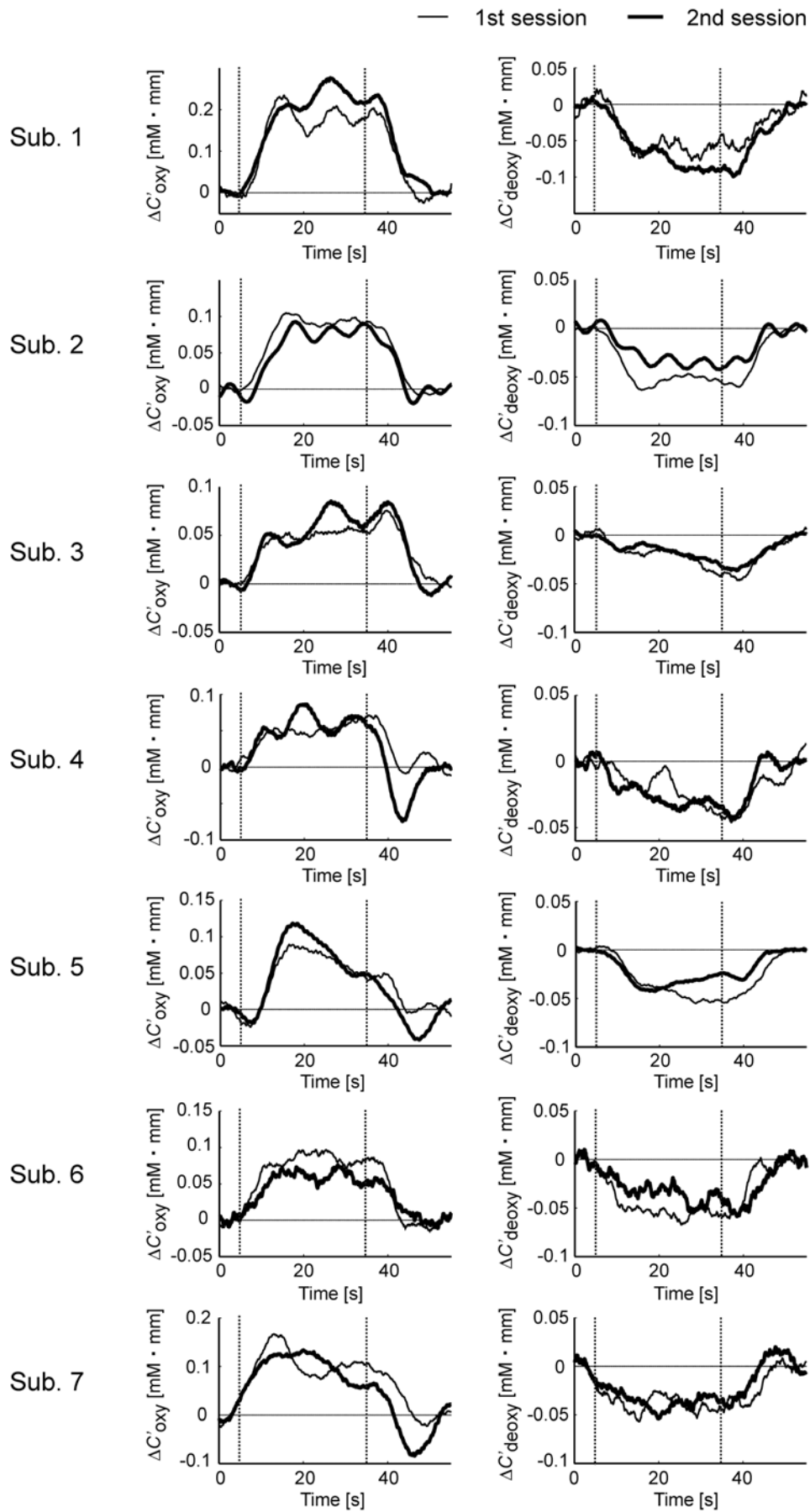


**Fig. 2.7 Comparison of time courses in two sessions for either hemisphere of each subject. Time courses of  $\Delta C_{oxy}$  and  $\Delta C_{deoxy}$  are shown in left column and right column, respectively. Measurement positions were 18 (1<sup>st</sup> session)/18 (2<sup>nd</sup> session) (see Fig. 2.5) for subjects 1, 3, 6, and 7, and 19/19 for subject 2, in left-hand finger-tapping session. Measurement positions were 9/10 and 6/9 for subjects 4 and 5, respectively, in right-hand finger-tapping session. Correlation coefficients (Pearson's product-moment correlation coefficient) of time courses were as follows: 0.955 ( $\Delta C_{oxy}$ ) and 0.911 ( $\Delta C_{deoxy}$ ) for Subject 1; 0.975 ( $\Delta C_{oxy}$ ) and 0.935 ( $\Delta C_{deoxy}$ ) for Subject 2; 0.950 ( $\Delta C_{oxy}$ ) and 0.956 ( $\Delta C_{deoxy}$ ) for Subject 3; and 0.814 ( $\Delta C_{oxy}$ ) and 0.740 ( $\Delta C_{deoxy}$ ) for Subject 4; 0.939 ( $\Delta C_{oxy}$ ) and 0.846 ( $\Delta C_{deoxy}$ ) for Subject 5; 0.951 ( $\Delta C_{oxy}$ ) and 0.785 ( $\Delta C_{deoxy}$ ) for Subject 6; and 0.835 ( $\Delta C_{oxy}$ ) and 0.812 ( $\Delta C_{deoxy}$ ) for Subject 7.**

**Table 2.2 Mean correlation coefficients between time courses of the two sessions.**

	$\Delta C'_{oxy}$	$\Delta C'_{deoxy}$
Mean correlation coefficient $\pm$ SD	$0.877 \pm 0.135$	$0.843 \pm 0.074$

## 2.4 Conclusion

This study examined the within-subject reproducibility of the activation signals during the imaging of sensorimotor activations in the same subject 6 months after the original session. In the first place, for all subjects the activations in positive  $\Delta C'_{oxy}$  and negative  $\Delta C'_{deoxy}$  were reproduced in the hemisphere contralateral to the



tapping hand. The results demonstrated the consistent fundamental pattern, a positive  $\Delta C'_{oxy}$  and a negative  $\Delta C'_{deoxy}$  for the activation signals. This result suggests that the positive  $\Delta C'_{oxy}$  is a useful parameter for detecting activation signals with tolerance to some random factors. Secondly, the activation center was reproduced within 20 mm on average across subjects, suggesting fair reproducibility comparable to the minimum distance between measurement points (2.1 cm) in OT. That is, it is possible to reproduce the activation center (spatial information) in within-subject OT imaging with an error of approximately 20 mm when the 10–20 system is used. The high reproducibility of the spatial information demonstrates the efficacy of the 10-20 system to determine the locations of probe positions within the same subject. Next, the signal amplitudes varied within subject between sessions even though no consistent tendency in the changes was found. Finally, signal time courses between the two sessions for each subject showed high correlation coefficients, which is the most significant finding in the present study. These results suggest the course of temporal information is particularly useful for detecting activation signals with the tolerant characteristic for random factors. The time-course temporal information would be valuable for examining qualitative characteristics both within and across subjects and will expand the applications of OT.

### 3. Inter-Subject Generality of Activation Signals

#### 3.1 Introduction

In chapter 3, the reproducibility (generality) of activation patterns, such as a positive  $\Delta C'_{oxy}$  and a negative  $\Delta C'_{deoxy}$ , is studied in 31 subjects by employing the same paradigm that is described in chapter 2. It is important to examine the fundamental reproducibility among a number of subjects because a larger number of random factors are considered to exist in the comparison of different subjects than in the within-subject comparison. This study also explore the efficacy of applying the 10-20 system<sup>63, 64</sup> to determination of the locations of probe positions in different subjects.

#### 3.2 Methods

##### 3.2.1 Subjects

Thirty-one healthy adults (21 men, 10 women; mean age  $34 \pm 8.9$ , range 23 to

56) gave written informed consent before the experiments. All the subjects showed right-handedness except one, and none reported a history of neurological disorders.

### *3.2.2 OT measurement*

The same OT system used in Chapter 2 was used. The measurement area was also determined in the same way in Chapter 2. The 6×6 cm square was defined as the measurement area for each hemisphere based on the arrangement of optical fibers (irradiation and detection positions). The probe patterns were positioned parallel to the line connecting Cz to T3 (left hemisphere) or T4 (right hemisphere). The centers of the bilateral measurement areas were considered to correspond to each primary sensorimotor area based on previous studies examining the relationship between locations of the 10–20 system and cortical area.<sup>65-67</sup>

### *3.2.3 Task paradigm*

The same finger-tapping task introduced in Chapter 2 was used to activate sensorimotor cortices. The subjects were asked to repeat the tapping sequence at 3-Hz timed to the rate of the term “Finger tapping” blinking on a CRT monitor for 30-s (activation) followed by 30-s of rest (baseline). There were a total of five activation/baseline cycles per session. Two sessions of finger tapping (one left-hand tapping and one right-hand tapping) were conducted per subject in a

counterbalanced order among subjects. During the measurements, the subject sat on a chair and was instructed to fix his or her gaze on the fixation point at the center of the screen and to concentrate on the task.

#### 3.2.4 Data analysis

The Hb signals ( $\Delta C'_{\text{oxy}}$  and  $\Delta C'_{\text{deoxy}}$ ) were measured in the same way as described in Chapter 2. The statistical analysis was also the same as explained in Chapter 2. The only difference was that directional changes (positive or negative) were not assumed for both  $\Delta C'_{\text{oxy}}$  and  $\Delta C'_{\text{deoxy}}$  in this work. Therefore, one 25-s activation period with maximum absolute value of the mean signal was selected for each hemoglobin species, and measurement positions with significant  $t$ -values (two-tailed  $t$ -test,  $p < 0.1$ ) were identified as activation positions. The decision threshold for a “one-tailed  $t$ -test,  $p < 0.05$ ” was used for activation estimation in assuming a change in one direction for each hemoglobin species (positive  $\Delta C'_{\text{oxy}}$  and negative  $\Delta C'_{\text{deoxy}}$ ) in Chapter 3. Note that “two-tailed  $t$ -test,  $p < 0.1$ ” used in this Chapter is practically the same as the threshold in Chapter 2.

### 3.3 Results and Discussion

#### 3.3.1 Occurrence probability of typical activation pattern

The occurrence probability of the typical activation pattern (positive  $\Delta C'_{oxy}$  and negative  $\Delta C'_{deoxy}$ ) was assessed for each measurement-position (Fig. 3.1).

Positive  $\Delta C'_{oxy}$  in the hemisphere contralateral to the tapping hand was observed with high probability. In addition, the measurement positions with high probabilities were around the center of the measurement area (left hemisphere: Positions 6 and 9; right hemisphere: Position 16). Contrary to that, negative  $\Delta C'_{deoxy}$  showed less probability although the activation centers were almost the same as that for  $\Delta C'_{oxy}$  (left hemisphere: Position 9; right hemisphere: Position 16). This result suggests that the positive  $\Delta C'_{oxy}$  is a useful parameter for detecting activation signals with tolerance to some random factors. In addition, the finding that the activation positions tended to be located around the center of the measurement area demonstrated the usefulness of the 10–20 system for determining the measurement positions in different subjects.

The mean signal amplitudes for subjects who showed the typical activation pattern are given in Table 3.1. The mean amplitudes for  $\Delta C'_{oxy}$  was 0.109 mM·mm, while that for  $\Delta C'_{deoxy}$  was about half (-0.048 mM·mm). The amplitudes sometimes varied widely among subjects, from small (Fig. 3.2 (a)) to large (Fig. 3.2 (b)).

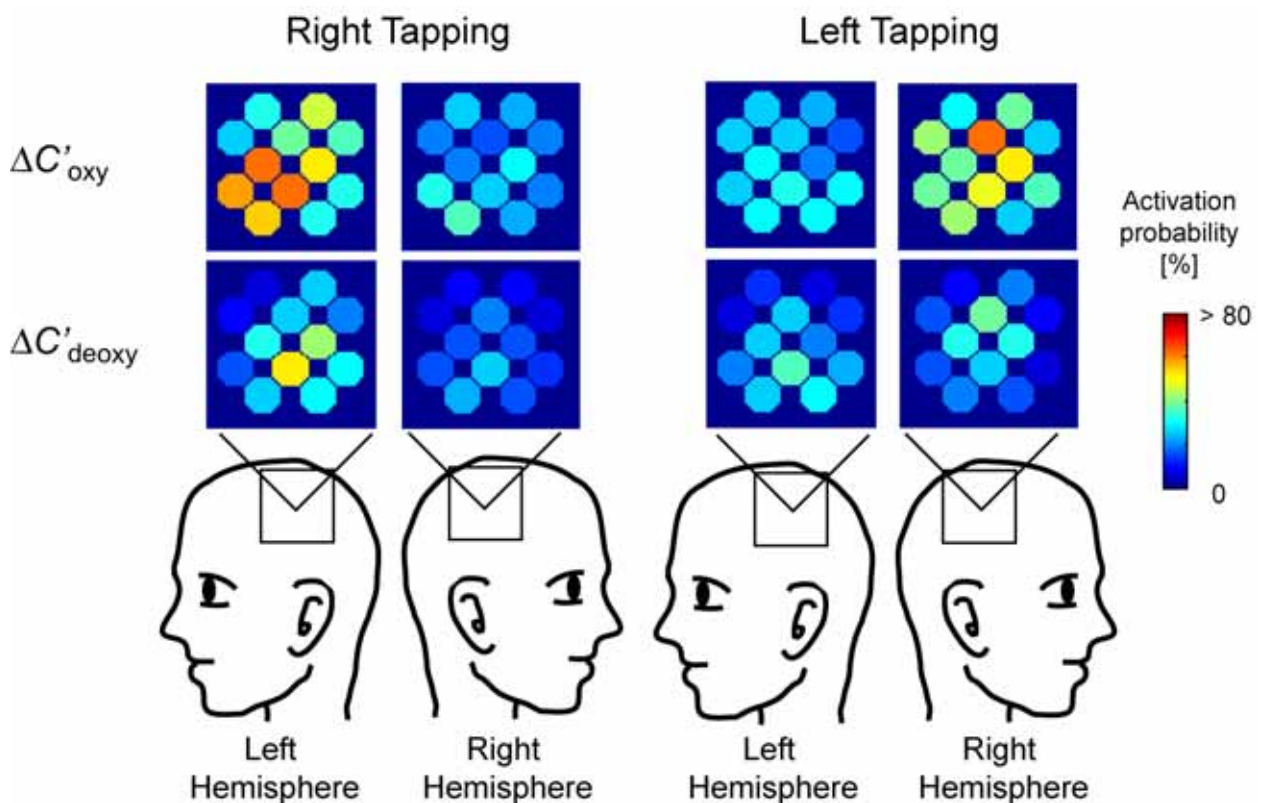


**Fig. 3.1** Color maps of occurrence probabilities of typical activation pattern (positive  $\Delta C'_{oxy}$  and negative  $\Delta C'_{deoxy}$ ) for each measurement position.

**Table 3.1** Mean signal amplitude of each hemoglobin species among subjects who showed typical activation pattern (positive  $\Delta C'_{oxy}$ , negative  $\Delta C'_{deoxy}$ ). An activation position with the highest signal amplitude within the contralateral hemisphere to the tapping hand for each subject was used.

	$\Delta C'_{oxy}$	$\Delta C'_{deoxy}$
Mean signal amplitude $\pm$ SD (mM $\cdot$ mm)	0.109 $\pm$ 0.063	-0.047 $\pm$ 0.026

Thus, the amplitude information in the activation signal is not very useful in evaluating the activation. Further, the study in chapter 2 reported less reproducibility of the amplitude information within a subject.

The numbers of subjects who showed a significant  $\Delta C'_{oxy}$  and  $\Delta C'_{deoxy}$  (either positive or negative) for the hemisphere contralateral to the tapping hand are shown in Table 3.2. The most common change was a positive  $\Delta C'_{oxy}$  (90%; left hemisphere 28/31, right hemisphere 28/31). Moreover, in 91% of the subjects showing this change, at least one of the four measurement-positions in the central area (left hemisphere: Positions 4, 6, 7, and 9; right hemisphere: Positions 16, 18, 19, and 21) was included. A negative  $\Delta C'_{deoxy}$  were less frequently observed ( $\Delta C'_{deoxy}$ : 76%, left hemisphere 24/31, right hemisphere 23/31). In 91% of the subjects showing a negative  $\Delta C'_{deoxy}$ , at least one of the four measurement positions in the central area was included. Although  $\Delta C'_{deoxy}$  was generally negative, 16% of the subjects showed a positive  $\Delta C'_{deoxy}$ ; a negative  $\Delta C'_{oxy}$  was observed for only one subject for the hemisphere contralateral to the tapping hand.

The physiological changes of the typical activation pattern (positive  $\Delta C'_{oxy}$  and negative  $\Delta C'_{deoxy}$ ) were consistent with accepted theory<sup>1, 49</sup> and previous NIRS studies.<sup>9, 47</sup> The occurrence probabilities in a previous study<sup>47</sup> were nearly consistent with the present results for both  $\Delta C'_{oxy}$  (about 89% in the previous study and 90% in

this study) and  $\Delta C'_{\text{deoxy}}$  (about 84% in the previous study and 76% in this study).

Moreover the combination of a positive  $\Delta C'_{\text{oxy}}$  and a negative  $\Delta C'_{\text{deoxy}}$  was observed in 73 and 71% of the cases for the previous and present study, respectively.

**Table 3.2 Number of subjects (out of 31) who showed a significant  $\Delta C'_{\text{oxy}}$  and  $\Delta C'_{\text{deoxy}}$  (two-tailed  $t$ -test,  $p < 0.1$ ).**

		Left hemisphere (right-hand tapping)	Right hemisphere (left-hand tapping)
$\Delta C'_{\text{oxy}}$	Positive	28 (25)*	28 (26)
	Negative	1(1)	1(0)
	Insignificant	2	2
$\Delta C'_{\text{deoxy}}$	Positive	3 (3)	7 (1)
	Negative	24 (21)	23 (22)
	Insignificant	4	1

\*Numbers in ( ) shows number of subjects having a significant change at measurement positions in the central area (left hemisphere: Positions 4, 6, 7, 9; right hemisphere: Positions 16, 18, 19, 21).

The present results showed that a negative  $\Delta C'_{\text{deoxy}}$  was observed less frequently in the activation center than positive  $\Delta C'_{\text{oxy}}$  (Fig. 3.1; left hemisphere: Position 9; right hemisphere: Position 16). This could be due to the smaller total number of  $\Delta C'_{\text{deoxy}}$  activation positions compared to the other hemoglobin species for each subject.



One possible reason for this is the effect of a random factor, systemic changes, on the responses of  $\Delta C'_{oxy}$ . It has been suggested that a finger-tapping task can lead to systemic changes in blood pressure and heart rate that affect measurements of  $\Delta C'_{oxy}$  in particular.<sup>73, 74</sup> The  $\Delta C'_{oxy}$  had a larger activation area, i.e., they were measured at more positions, while the activation area for  $\Delta C'_{deoxy}$  was more focused. While monitoring the systemic effects and using an analytical method that subtracts the effects from the signals would be ideal,<sup>73</sup> a more practical approach may be to design a task paradigm that does not induce systemic variance between the rest period and task period.

Although it was difficult to distinguish the systemic effects from the cortical response or other random effects in this study, the activation area for  $\Delta C'_{deoxy}$  may actually have been smaller than those for  $\Delta C'_{oxy}$  for most subjects. A previous study of simultaneous recordings of fMRI and NIRS signals suggests that  $\Delta C'_{deoxy}$  provides more specific information for focal cerebral responses than  $\Delta C'_{oxy}$ .<sup>75</sup> Moreover, another study of simultaneous recordings showed that an activation map using  $\Delta C'_{oxy}$  did not overlap maps using  $\Delta C'_{deoxy}$  and BOLD signals.<sup>50</sup> Further study of the spatial and temporal diversities between the two signals ( $\Delta C'_{oxy}$  and  $\Delta C'_{deoxy}$ ) is thus important. Higher spatial resolution, however, will be needed before OT can be used to analyze the activation centers accurately.

The probable positions of the highest activation were observed to differ between the left (Position 9) and right hemispheres (Position 16). This longitudinal asymmetry of the highest activation positions could probably be due to a random factor, namely, the probe position, which could be attributed to a methodological problem or an anatomical characteristic of the cerebral cortex. The methodological problem refers to the inaccuracy placement of the measurement probes since they were placed on the head manually, though the positions were determined using the 10-20 system. Development of a better method for accurate positioning is thus needed. In addition, the anatomical characteristic could influence the asymmetry due to the anatomical asymmetry of the cerebral cortex. According to a previous study,<sup>76</sup> the parietal and temporal cortices of the left hemisphere are larger than those of the right hemisphere in most subjects. As a result, even though the probes are placed symmetrically on the head surface, they may actually be shifted upwards in relation to the cerebral cortex. A placement error of only a few millimeters can mislead the peak activation position to the next measurement position when the investigated area is placed at the center of the measurement area surrounded by four measurement positions.<sup>41</sup> Even with this possible low spatial resolution, the finding that measurement positions with high activation probabilities were around the center of the measurement area (left hemisphere: Positions 4, 6, 7, and 9; right

hemisphere: Positions 16, 18, 19, and 21) suggests that the 10–20 system is useful in determining the measurement area for OT.

Examination of the activation probabilities in detail (Table 3.2) shows that a negative  $\Delta C'_{\text{deoxy}}$ , which can cause the typical BOLD signal pattern, was not as consistently observed (negative 76%, positive 16%) as a positive  $\Delta C'_{\text{oxy}}$  (positive 90%, negative 3%). This peculiar feature of  $\Delta C'_{\text{deoxy}}$ —the possibility of it being positive or negative—might be another reason for the less-focused activation in  $\Delta C'_{\text{deoxy}}$ . These results suggest that the  $\Delta C'_{\text{deoxy}}$  signal can occasionally vary not only in amplitude but also in direction, which conflicts with the common idea of BOLD fMRI.

The crosstalk effect due to the wavelength dependence of sensitivity<sup>35, 77</sup> might be one reason for the variability in  $\Delta C'_{\text{deoxy}}$ . However, practical identification of the optical path and the activation location is needed to estimate the effect of crosstalk accurately.

Another possibility is that the variability in  $\Delta C'_{\text{deoxy}}$  reflects some physiological phenomena relating to brain activation, since unusual behavior in the  $\Delta C'_{\text{deoxy}}$  or the BOLD signal has been previously reported.<sup>1, 51</sup> The variability of hemodynamic responses is normally considered to be dependent on several factors such as cerebral blood flow (CBF), cerebral blood volume (CBV), and oxygen consumption rate (CMRO<sub>2</sub>).<sup>50</sup> One previous study showed positive, negative, and

silent BOLD signals with a negative, positive, and subthreshold  $\Delta C'_{\text{deoxy}}$ , respectively, while  $\Delta C'_{\text{oxy}}$  showed various behaviors, by simultaneous measurement of fMRI and NIRS.<sup>50</sup> Another study demonstrated positive  $\Delta C'_{\text{oxy}}$  and  $\Delta C'_{\text{deoxy}}$  in the capillary area along with a negative  $\Delta C'_{\text{deoxy}}$  and positive  $\Delta C'_{\text{oxy}}$  in the large vein area.<sup>78</sup>

### 3.3.2 Variability of activation pattern

To determine the relationships between  $\Delta C'_{\text{oxy}}$  and  $\Delta C'_{\text{deoxy}}$  in greater details, the combination patterns were classified. The patterns and appearance frequencies are shown in Table 3.3.

The most common pattern (positive  $\Delta C'_{\text{oxy}}$  and negative  $\Delta C'_{\text{deoxy}}$ :  $\uparrow \downarrow$ ) was shown in 22 subjects (71%) for each hemisphere. In addition, positive  $\Delta C'_{\text{oxy}}$  with subthreshold  $\Delta C'_{\text{deoxy}}$  ( $\uparrow -$ ) was observed in three and one subjects (total 6%) for the left and right hemispheres, respectively.

Another frequent pattern was the all-positive pattern ( $\uparrow \uparrow$ ), which was observed in three and five subjects (total 13%) for the left and right hemispheres, respectively. There were mainly two types of changes in this pattern; a general type showed a strong positive  $\Delta C'_{\text{oxy}}$  with a positive  $\Delta C'_{\text{deoxy}}$  (Fig. 3.2 (c)), and a singular type which showed a strong positive  $\Delta C'_{\text{oxy}}$  and  $\Delta C'_{\text{deoxy}}$  (Fig. 3.2 (d)).

A significant characteristic of all these patterns was a positive  $\Delta C'_{oxy}$ , which was observed in 90% of the cases. The 10% that did not show a positive  $\Delta C'_{oxy}$  were grouped into three patterns; the first is the pattern with a negative  $\Delta C'_{oxy}$  and a positive  $\Delta C'_{deoxy}$  in the right hemisphere during left tapping (Fig. 3.2 (f);  $\downarrow \uparrow$ ). In addition, the same subject showed only a negative  $\Delta C'_{oxy}$  in the left hemisphere during right-hand tapping ( $\downarrow -$ ), but a similar pattern of a negative  $\Delta C'_{oxy}$  and a positive  $\Delta C'_{deoxy}$  was observed in the right (ipsilateral) hemisphere. The changes for this subject were therefore classified as being the same pattern. Another is the pattern with a positive  $\Delta C'_{deoxy}$  only in the right hemisphere ( $- \uparrow$ ) while the subject showed all-positive pattern ( $\uparrow \uparrow$ ) in the left (ipsilateral) hemisphere (Fig. 3 (d)). The last is the pattern with a negative  $\Delta C'_{deoxy}$  only (Fig. 3.2 (e);  $- \downarrow$ ). This pattern was observed in two subjects (both hemispheres in one; one hemisphere in the other). Note that in every case of these three patterns there was a signal change in at least one of the hemispheres.

Table 3.3 Patterns of signal changes and their occurrence rate among 31 subjects.

Change pattern* <sup>1</sup>		Left Hemisphere (Right-hand tapping)	Right Hemisphere (Left-hand tapping)
$\Delta C'_{oxy}$	$\Delta C'_{deoxy}$		
↑	↑	3	5
↑	↓	22	22
↑	-	3	1
↓	↑	0	1 * <sup>2</sup>
↓	↓	0	0
↓	-	1 * <sup>2</sup>	0
-	↑	0	1 * <sup>3</sup>
-	↓	2 * <sup>4</sup>	1 * <sup>4</sup>
-	-	0	0
Total		31	31

\*<sup>1</sup> ↑ positive, ↓ negative, - subthreshold change. The changes were assessed using a two-tailed *t*-test ( $p < 0.1$ ). When both changes appeared for one condition, the change for more measurement positions was used; when both changes appeared for the same number of measurement positions, the change with the maximum *t*-value (absolute value) was used.

\*<sup>2</sup> A subject's pattern with a negative  $\Delta C'_{oxy}$  and a positive  $\Delta C'_{deoxy}$  in the right hemisphere during left tapping. In addition, this subject showed only a negative  $\Delta C'_{oxy}$  in the left hemisphere during right-hand tapping (↓ --), and a similar pattern of a negative  $\Delta C'_{oxy}$  and a positive  $\Delta C'_{deoxy}$  was observed in the right (ipsilateral) hemisphere.

\*<sup>3</sup> a positive  $\Delta C'_{deoxy}$  was found only in the right hemisphere (- ↑) while the subject showed all-positive pattern (↑ ↑) in the left (ipsilateral) hemisphere.

\*<sup>4</sup> Three cases including both hemispheres of one subject.  $\Delta C'_{deoxy}$  was consistently negative though  $\Delta C'_{oxy}$  tended to be noisy.

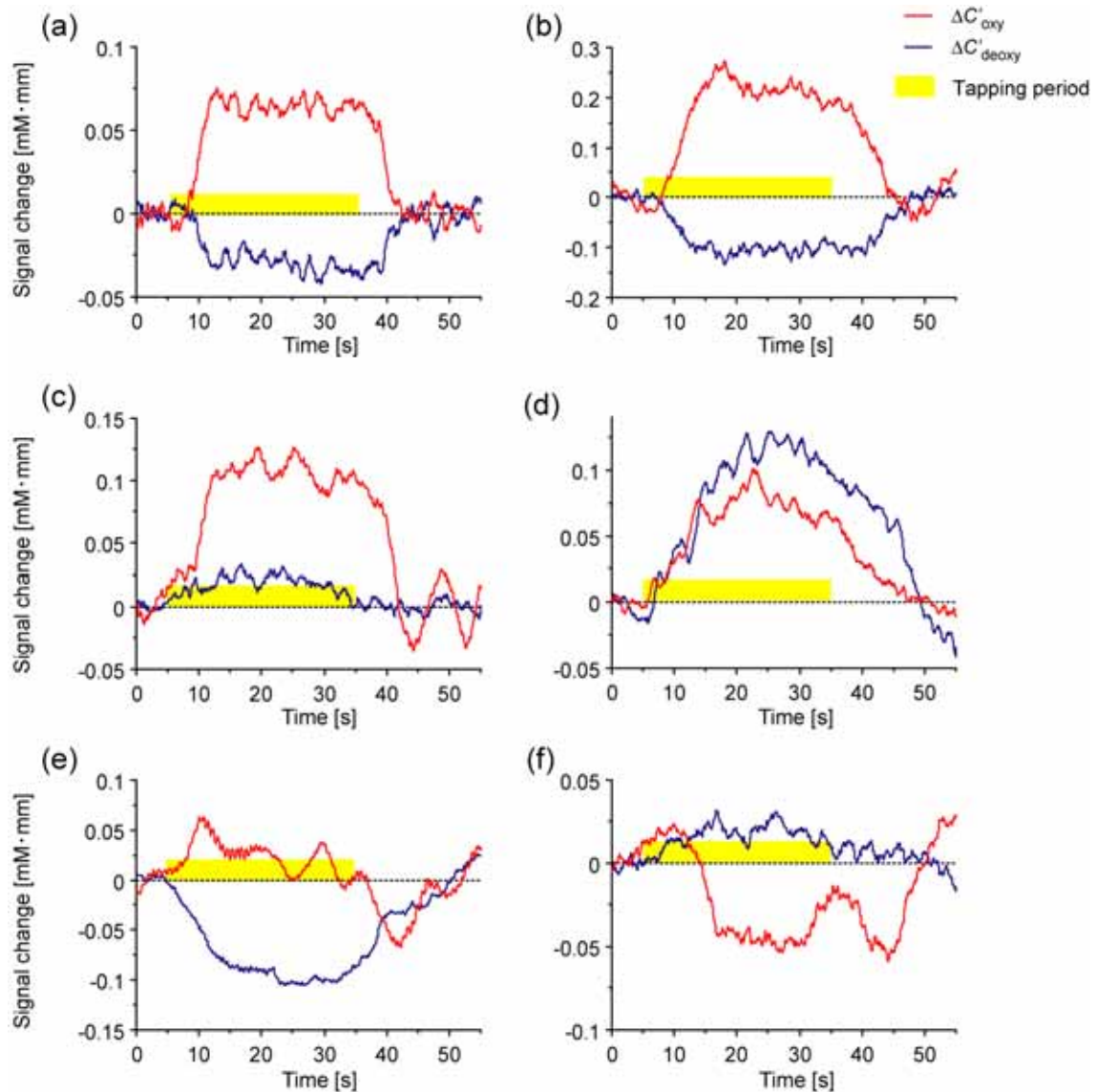


**Fig. 3.2** Representative time courses of  $\Delta C'_{oxy}$  and  $\Delta C'_{deoxy}$ . Typical activation pattern (positive  $\Delta C'_{oxy}$  and negative  $\Delta C'_{deoxy}$ ) is shown in (a) and (b); changes in (b) are larger than those in (a). An all-positive pattern (positive  $\Delta C'_{oxy}$  and  $\Delta C'_{deoxy}$ ) is shown in (c) and (d). Pattern in (d) was a rare case— $\Delta C'_{deoxy}$  was positive similar to  $\Delta C'_{oxy}$ . Two exceptional patterns are shown in (e) and (f). The pattern with only a negative  $\Delta C'_{deoxy}$ , (e), was observed in only two subjects. The pattern with a negative  $\Delta C'_{oxy}$  and a positive  $\Delta C'_{deoxy}$ , (f), was observed in only one subject.

The patterns with a positive  $\Delta C'_{oxy}$  and no positive  $\Delta C'_{deoxy}$  ( $\uparrow \downarrow$  and  $\uparrow -$  in Table 3.3) were classified into the same category, which was the most common pattern seen in this study. These patterns were observed in 25 and 23 subjects (77%) for the left and right hemispheres, respectively. As mentioned above, the variety of patterns for  $\Delta C'_{deoxy}$  could depend on CBF, CBV, and  $CMRO_2$ <sup>1, 49, 51</sup> and on the proportions of the capillary and large vein areas in the measurement region.<sup>78</sup> Simulation studies in which the proportions of these factors were changed might be useful in determining the physiological mechanisms leading to each pattern. In addition, the crosstalk effect due to anatomical characteristics or different S/N's in the  $\Delta C'_{deoxy}$  signal may have resulted in the pattern with subthreshold  $\Delta C'_{deoxy}$  ( $\uparrow -$ ).

The all-positive pattern ( $\uparrow \uparrow$  in Table 3.3), which was occasionally observed (13%), was also reported in a number of previous NIRS studies.<sup>27, 78, 79</sup> In one of the previous studies, this pattern occurred in capillary areas such as the inferior frontal gyrus (Broca's area), while the common pattern with a negative  $\Delta C'_{deoxy}$  occurred in large vein areas such as the superior temporal area.<sup>78</sup> If the variability of the hemodynamics depends on the distribution of the vascular system, there could be a large variability in the distributive condition of vessels among subjects even for the same cortical area.

Our observation on both the common pattern and the all-positive pattern in



the same cortical area during the same activation paradigm suggests that the variation in activation signals depends on the subject's anatomical characteristics and condition rather than the characteristics of the measurement area or the paradigm.

The patterns described above showing a positive  $\Delta C'_{oxy}$  were observed in 90% of the subjects. This suggests high reliability of  $\Delta C'_{oxy}$  as an activation signal whereas some previous studies used only  $\Delta C'_{total}$  (the sum of  $\Delta C'_{oxy}$  and  $\Delta C'_{deoxy}$ ) to identify cognitive-related activation.<sup>16, 80, 81</sup>

The other 10% are interpreted as follows: an atypical pattern with a positive  $\Delta C'_{deoxy}$  (Fig. 3.2 (f);  $\downarrow \uparrow$  and  $- \uparrow$  in Table 3.3) was observed in one subject. The combination pattern, which is similar to the deactivation in fMRI<sup>1, 50-52</sup> and PET,<sup>53, 82</sup> possibly appears when  $CMRO_2$  significantly increases during activation.<sup>50</sup>

Another is the pattern with a negative  $\Delta C'_{deoxy}$  only (Fig. 3.2 (e);  $- \downarrow$  in Table 3.3), which was observed in two subjects (both hemispheres in one; one hemisphere in the other). This pattern might result from less sensitivity for  $\Delta C'_{oxy}$ . While the  $\Delta C'_{oxy}$  signal tended to be positive more, the level did not reach the statistical threshold for these subjects. This is possibly due to greater noise in the  $\Delta C'_{oxy}$  signal than in the  $\Delta C'_{deoxy}$  one. Physiological noise, such as low frequency oscillations<sup>55</sup> or systemic changes,<sup>73, 74</sup> can have more effect on  $\Delta C'_{oxy}$  than on  $\Delta C'_{deoxy}$ . Although it

may be possible to subtract the systemic changes from Hb signals by using simultaneously recorded data for the arterial saturation and heart rate,<sup>73</sup> simultaneous measurements of these physiological signals with NIRS is difficult.

Another pattern was a positive  $\Delta C'_{\text{deoxy}}$  only in the right hemisphere ( $-\uparrow$  in Table 3.3) during left-hand tapping, while this subject showed an all-positive pattern ( $\uparrow\uparrow$ ) in the ipsilateral (left) hemisphere as well as during contralateral right-hand tapping (Fig. 3.2 (d)). While activation in both hemispheres during unilateral finger movement has been reported,<sup>83, 84</sup> predominant activation in the ipsilateral one rarely occurs in normal adults. Further examination with anatomical imaging will be necessary to explain this unusual lateralization.

### 3.4 Conclusion

The generality (variability) of the Hb signals induced by sensorimotor activation was studied in 31 healthy subjects by employing the same paradigm described in chapter 2. Activation patterns with a positive  $\Delta C'_{\text{oxy}}$  for the hemisphere contralateral to the tapping hand were observed with a high probability (90%), thereby suggesting that a positive  $\Delta C'_{\text{oxy}}$  is the most useful parameter for detecting

activation signals. In addition, the finding that the activation positions tended to be around the center of the measurement area demonstrated the usefulness of the 10–20 system in determining the measurement positions even in different subjects. That is, it is possible to reproduce the activation center (spatial information) in OT imaging for different subjects with an error of approximately 30 mm (the distance between adjoining measurement positions) when the 10–20 system is used.

On the other hand, a negative  $\Delta C'_{\text{deoxy}}$ , which can cause the typical BOLD signal pattern, was not observed consistently in this study (76%). In addition, various atypical activation patterns were observed in approximately 10% of the subjects. Clarifying the effects of random factors on the differences in activation signals will be important for both OT improvement and physiological studies.

## 4. Reducing Fluctuations in the Background Functions by Devising Task-Paradigm

### 4.1 Introduction

In this chapter, the efficacy of a devising-task paradigm for reducing the fluctuations (activity) originating from background functions (random factor 1) such as the attention level was examined. The task paradigm is defined as the design of tasks and/or stimuli to control the subject's state and the time sequence of the presentation. The basic concept is that minimizing the differences in background functions, for example, attention, between the task and rest periods is useful for measuring the delicate activation signals produced by the reduced fluctuations in the Hb signals.

As explained chapter 1.3, fluctuations due to background functions rather than the targeted function can be a significant random factor. This is a fundamental issue for most of the functional imaging methods because using rest periods as baseline conditions is obligatory for measuring the activation signal in these methods. Conventionally, researchers have used the rest period with no task being performed as a zero-activity condition as compared to the task/stimulation period;

however, recent reports have cautioned that there is no inherent baseline state in the brain; instead unconstrained cognitive activity is present.<sup>52, 53</sup> Accordingly, the fluctuations from background functions in the rest period can be a significant biological random factor, which should be considered here. In addition, the attention level is one of the background functions that cause fluctuations in the activation signals. Although the significance of controlling the subject state in the resting period has become common knowledge in cognitive science, this idea is not fully comprehended by OT researchers. Most of the previous functional studies using OT or NIRS focused on primary functions in the visual domain<sup>29, 30</sup> and the sensorimotor domain,<sup>9, 12, 47</sup> or the obscure cognitive functions of the frontal lobes,<sup>26, 28, 30</sup> not using any control task in the resting state.

In this study, a dichotic listening task that controlled the subjects' attention was used at every stage to detect an intact activation signal from the targeted cognitive process. The activation signal that is produced in response to speech recognition is selected for this measurement because it has been confirmed that small language components of speech recognition, such as word recognition and sentence comprehension, are represented in slightly different cortical areas.<sup>68</sup> Accordingly, it would be appropriate to test the detection ability for delicate activation signals. Well-designed task paradigms have been applied in fMRI studies

over the years; the effect of the devising-task paradigm in OT has not yet been demonstrated.

## 4.2 Methods

### *4.2.1 Subject*

Seven male native Japanese speakers (ages: 21 – 32) participated in the present study. They showed right-handedness (laterality quotients: 81 – 100) by the Edinburgh inventory.<sup>85</sup> The subjects' consent was obtained in written form prior to the experiments. Approval for the human experiments was obtained from the institutional review board of the University of Tokyo, Graduate school of Arts and Sciences.

### *4.2.2 Auditory stimuli*

The auditory stimuli used in this study were speech sounds and non-speech sounds that were presented in speech-recognition tasks and a control task, respectively. All speech sounds were digitized (16 bit, 11025 Hz) using speech synthesis software (Oshaberi-mate, Fujitsu, Tokyo, Japan) that converts Japanese written text into sound waveforms. Sine wave tone and white noise used in the

control task were synthesized by sound-editing software (Sound Forge XP, Sonic Foundry, Inc.). Speech sounds and non-speech sounds were presented with a stereophonic headphone at the peak of 60-dB and 58-dB sound pressure levels, respectively.

#### *4.2.3 Task paradigm*

A dichotic listening paradigm was used for all tasks in this study. Dichotic listening is a psychological procedure, where two different sounds are presented to both the left and right ears (one sound to each ear) normally using a set of headphones. Subjects are generally requested to pay attention to either one or both (divided attention condition) of the sounds in the task. The task using this procedure is considered to be effective in controlling the subjects' attention. Target stimuli and non-target stimuli were simultaneously presented to different ears every 2 s, and a target was alternatively presented to either the left ear or the right ear at random intervals. The frequency of presentation of targets was balanced between the left and right ears. Subjects were asked to track targets and to press a button when a target was shifted to the other side.

In the control task, a tone (sine wave: 1000 Hz) and white noise (low-pass cut-off frequency: 1000 or 10000 Hz) were presented as targets and non-targets,

respectively (duration: 1000 ms). In order to confirm that subjects performed tasks by recognizing targets, a tone of different pitch (sine wave: 300 Hz) was presented as a non-target at a lower rate. These probe stimuli prevented subjects from performing the tasks by tracking non-targets only.

Two speech-recognition tasks were used: (1) a repeat task, in which the targets consisted of one repeated sentence, and (2) the story task, in which the targets were successive different sentences of a continuous story. In the repeat task, one sentence (duration: 1000 – 1530 ms, mean: 1270 ms) was repeated for a 36-s period, and different sentences were used in each period. Successive sentences for the story task were divided into phrases at natural break-points (duration: 590 – 1650 ms, mean: 1150 ms) for the presentation. In both tasks, a non-target was obtained by scrambling the sequence of syllables of the correspondent target. These jumbled stimuli conformed to the rules of Japanese phonetics but had no meaning. A sentence different from the target for the repeat task and contextually anomalous phrases for the story task were used as probe stimuli. These tasks, therefore, cannot be completed appropriately by just identifying speech sounds without paying attention to their meanings.

The essential differences among these tasks are listed in Table 4.1. In every task, some background functions such as sound listening, attention to perform the



task, and finger movement (button press) are controlled. Therefore, the activation signals due to speech recognition, including speech sound listening, word recognition, sentence comprehension, and context comprehension, between the story task and control task were expected to be comparable. Moreover, a more selective activation signal induced by the target function, i.e., sentence comprehension, can be extracted by comparing the story task and the repeat task.

**Table 4. 1 Expected components involved in the three tasks**

		Control task	Repeat task	Story task
Targeted function	Context comprehension			✓
Background functions	Sentence comprehension		✓	✓
	Word recognition		✓	✓
	Speech sound listening		✓	✓
	Sound listening	✓	✓	✓
	Attention	✓	✓	✓
	Finger movement (button press)	✓	✓	✓

#### 4.2.4 Experimental procedures

During the experiments, the subject sat in a chair with his eyes closed in a dark room. A pair of head shells with probe sockets was attached on both sides of the subject's head. In a single run with the repeat tasks (R), a 36-s period for the control

task and the repeat task alternated three times, with one more control period at the end of a run. A single run with the story tasks (S) had the same alternation.

Twelve runs were performed in the order of alternating S-R-R-S and R-S-S-R in one imaging session. Each subject was tested in at least two sessions. The first run of either S or R was counterbalanced by subsequent sessions.

After the experiment, a three-dimensional (3D) magnetic resonance (MR) image was taken of the subject to reconstruct a cortical surface image. Alfacalcidol beads (0.25  $\mu\text{g}$ ) buried in a head shell were used as MR markers, which can be identified on the MR image as spheres (diameter: 3 mm).

#### *4.2.5 OT procedures*

Two OT systems with the same calibration (ETG-100 and ETG-A1; Hitachi Medical Corporation, Tokyo, Japan) were used, one for each hemisphere.

Near-infrared laser diodes with two wavelengths (780 nm and 830 nm) were used as the light sources. The reflected lights were detected with avalanche photodiodes located 30 mm from an incident position. Using lock-in amplifiers, the detected signal was separated into individual light sources with each wavelength (Yamashita et al., 1999). The transmittance data  $\ln T(\lambda, t)$  for a wavelength ( $\lambda$ ) at measurement time ( $t$ ) was obtained for each run.

The position of each MR marker was a midpoint between an incident point and a detection point. Each measurement point was defined as an intersection of the cortical surface and a perpendicular line from a marker point (Maki et al., 1996). Twenty-two points in each hemisphere were simultaneously measured at minimum spatial intervals of 21 mm, and each point was sampled every 500 ms. The measured region in each hemisphere centered on the Sylvian fissure and covered an area of  $6 \times 12 \text{ cm}^2$  (Fig. 4.1).

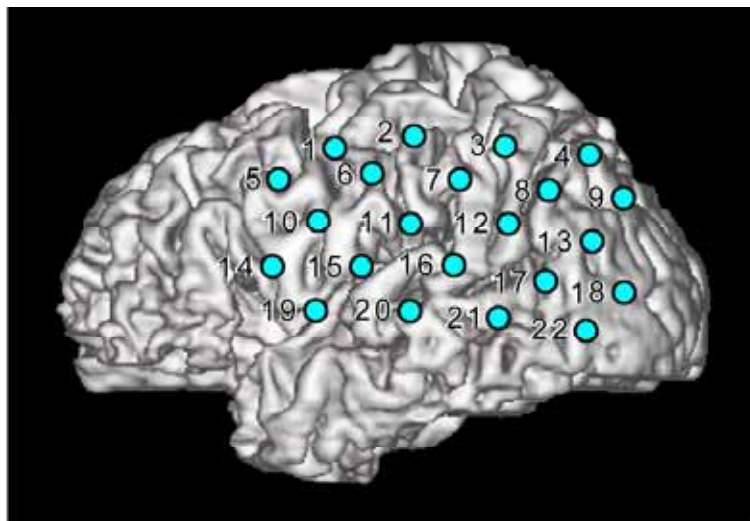


**Fig. 4.1** The measurement positions in the left hemisphere. The numbers represent index numbers for the measurement positions. The right hemisphere has the same arrangement of measurement points (1 at the superior-posterior corner). Cortical surface images were reconstructed from 3D MR images of a representative subject.

#### 4.2.6 Data analyses

Time-series data of  $\ln T(\lambda, t)$  in a single run were baseline-corrected with a curve of the third degree, which was fitted for time points during the control task (Fig. 4.2). Either intra-subject data or inter-subject data of multiple runs (R or S) were then averaged for each wavelength before calculating the Hb signals. In the case of calculating the hemodynamics in the story run (S) relative to that in the repeat run (R), averaged runs under the two conditions were directly compared. R or S was also compared with the baseline curve in a similar manner. Because the Hb signals are relative changes from the baseline in the latter case, a long-range fitting, which spans more than one cycle of control-stimulation-control, should be used to estimate a baseline level throughout a single run (Fig. 4.2). By comparing  $\ln T(\lambda, t)$  under two conditions, the Hb signals ( $\Delta C'_{\text{oxy}}$  and  $\Delta C'_{\text{deoxy}}$ ) were calculated.

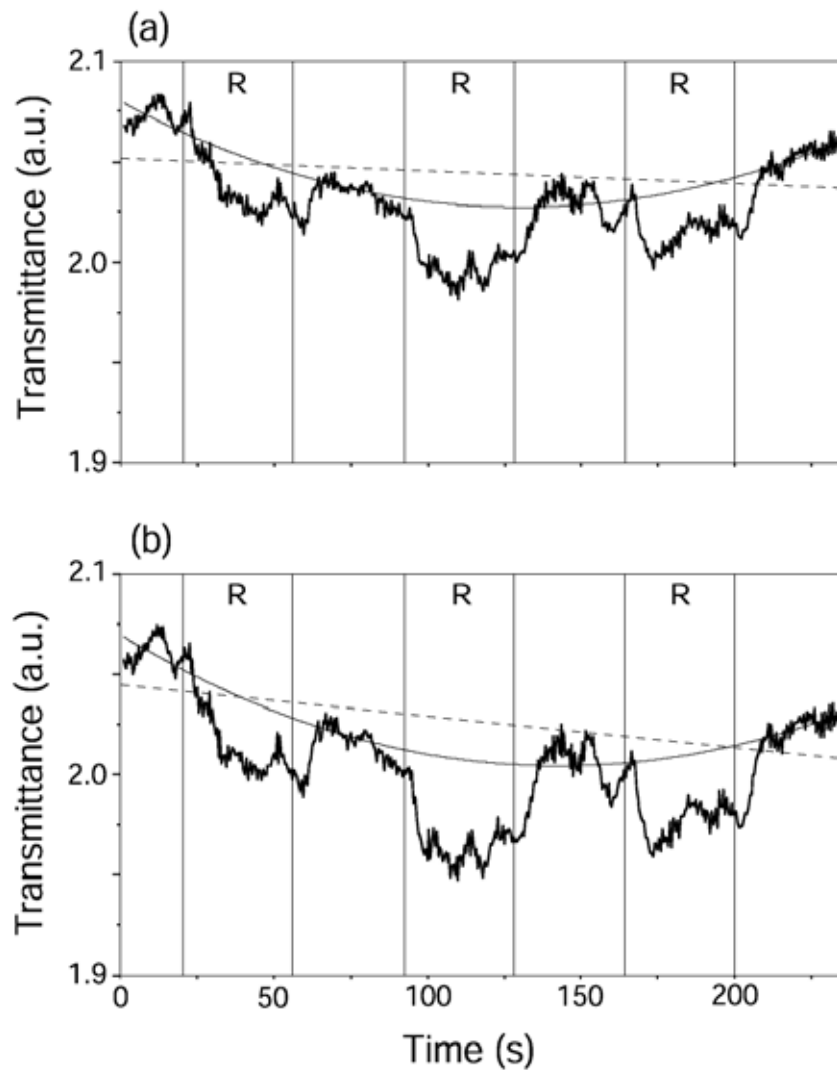


**Fig. 4.2** Representative time courses of transmittance data at Ch 16 for one subject. (a) Data for a wavelength of 780 nm. (b) Data for a wavelength of 830 nm. Thick solid lines show the averaged transmittance data  $\ln T(\lambda, t)$  for each wavelength ( $\lambda$ ) at time ( $t$ ) in an arbitrary unit (a.u.). Note the prominent signal changes, which synchronize with each onset and end of three periods of the repeat task (R). For baseline correction, the data are fitted for time points during the control task with a curve of the third degree (thin solid lines). The relative difference between data for the two wavelengths is not affected when only linear interpolation is applied (broken lines), but fitting with a third-degree curve was found to be better than linear fitting for a long-range fitting, which proved that the activation signal was reproduced for each task period.

The Hb signals were assumed to be delayed 6 s from the task periods in this study, and each shifted period of the story and repeat tasks was defined as an activation period. A correlation coefficient ( $r$ ) of hemoglobin time points with a box-car waveform (each period: 36 s, delay: 6 s) was calculated for each measurement point (Bandettini et al., 1993; Watanabe et al., 1998), and an  $r$ -map was created from the  $r$ -values. As a threshold for the  $r$ -values, 0.73 or  $-0.73$  was chosen for statistical significance ( $P = 0.05$ ). This level of significance was determined from an equation:

$$P = 2 \cdot Q(TH \cdot N^{1/2}), \quad (4-1)$$

where  $Q(u)$  represents the upper probability of normal distribution above  $u$ ,  $TH$  is a threshold of  $r$ , and  $N$  is the number of samples.  $N$  should be the number of independent samples, and here  $N = 7$  was assumed, which was the number of alternated periods in each run.

## 4.3 Results and Discussion

### 4.3.1 Task performance

The behavioral accuracy and reaction times are shown in Table 4.2. An ANOVA indicated no main effect of tasks in the total performance ( $F(2,18) = 2.7$ ,  $p$

> 0.05), or in the probe performance ( $F(2,18) = 3.3, p > 0.05$ ). On the other hand, there was a main effect of tasks in the reaction time ( $F(2,18) = 7.5, p < 0.005$ ).

Post-hoc tests (Fisher's PLSD) revealed a difference between control and repeat tasks ( $p < 0.05$ ), and a difference between control and story tasks ( $p < 0.005$ ). The

difference between the repeat and story tasks, however, was not significant ( $p > 0.1$ ).

These results suggest that the repeat and story tasks were equally balanced in terms of behavioral control for task difficulty.

**Table 4.2 Behavioral performances for tasks**

Task	Total accuracy (%)	Probe accuracy (%)	Reaction time (ms)
Control	97 ± 1.0	98 ± 0.8	660 ± 59
Repeat	97 ± 1.2	96 ± 1.3	870 ± 73
Story	93 ± 1.6	94 ± 1.1	990 ± 49

Note: Mean and standard errors are shown (N = 7).

#### 4.3.2 Mapping the difference between the story and repeat tasks

The  $r$ -map for the hemodynamics in the story run relative to that in the repeat run shows a focal activation in the left superior temporal cortex (Fig. 4.3). In these figures,  $r$ -maps for averaged data among subjects were superimposed on a representative cortical surface image of one subject. Two measurement positions at

16 and 21 showed significant activation in  $\Delta C'_{oxy}$  (Fig. 4.3 (a)). These two measurement points were on the superior and middle temporal gyri. Comparing the individual mean signals during the story and repeat tasks (at a plateau level, from 10 s after the onset to the end of the task period) of Position 16 and those of Position 21, ANOVA (subjects  $\times$  channels  $\times$  periods) indicated the main effect of channels ( $F(1,32) = 4.2, p < 0.05$ ) and no other main effects. The positive  $\Delta C'_{oxy}$  at Position 21 was significantly larger than that at Position 16. Moreover, the  $t$ -map in  $\Delta C'_{deoxy}$  (4.3 (b)) showed Position 21 as a significant activation point. These results showed that the activation in the story task relative to the repeat task was more prominent in the mid-lateral part (Position 21) of the left temporal cortex.

#### 4.3.3 Spatial registration

The measured areas were carefully assessed among subjects using their 3D MR images. Based on Talairach coordinates,<sup>86</sup> the positions of measurement points were determined for each subject. The largest distance in the positions of the same measurement point among subjects was less than 18 mm in both hemispheres. The activated measurement points shown in Fig. 4.1 were confirmed to be on the superior and middle temporal gyri in all subjects (Ch 16:  $x = -65 \pm 2.0, y = -36 \pm 6.3, z = 16 \pm 5.0$ ; Ch 21:  $x = -64 \pm 1.9, y = -48 \pm 6.5, z = 5.9 \pm 5.5$ ).



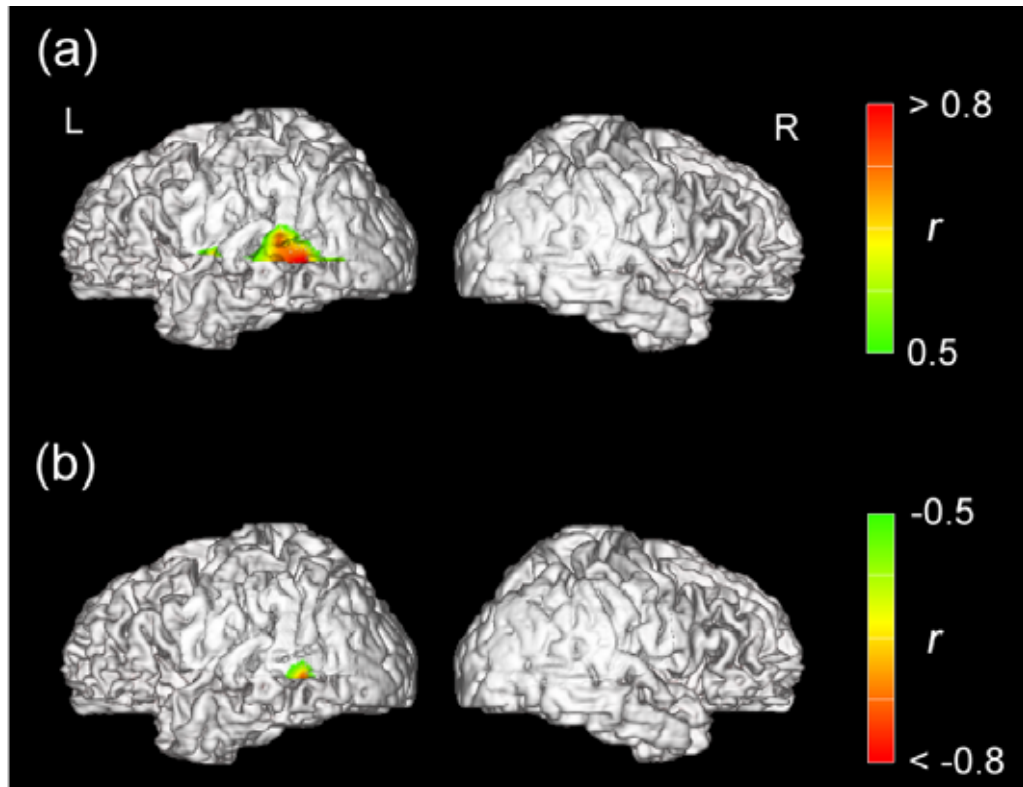


**Fig. 4.3 Superior temporal cortex activation in the story task. (a) The  $r$ -maps of  $\Delta C'_{oxy}$  in the story task relative to the repeat task. The  $r$ -values were calculated from averaged data among subjects. The cortical surface images were reconstructed from 3D MR images of the same subject as in Fig. 4.1. In each map,  $r$ -values are color-coded using the color scale on the right. 4Activation in the story task was found in the left superior temporal cortex. Two points at Positions 16 and 21 showed significant  $r$ -values in the area (Point 16:  $r = 0.73$ , Point 21:  $r = 0.84$ ). The  $r$ -maps for the right hemisphere showed no significant activation in this comparison ( $r < 0.5$ ). (b) The  $r$ -maps of  $\Delta C'_{deoxy}$  in the story task relative to the repeat task. Focal activation was found in the mid-lateral part of the left temporal cortex. The position at 21 showed a significant  $r$ -value ( $r = -0.73$ ). The  $r$ -maps for the right hemisphere showed no significant activation in this comparison ( $r > -0.5$ ).**

#### 4.3.4 Hemodynamic differences between the story and repeat runs

The hemodynamics in the story and repeat runs relative to the baseline were further examined. The temporal changes at Positions 16 and 21 are shown in Fig. 4.4. With a delay of 6 s, a positive  $\Delta C'_{\text{oxy}}$  synchronized with each onset of the story task, and after reaching a plateau,  $\Delta C'_{\text{oxy}}$  returned to the baseline level at the end of the task (Fig. 4.4 (a), (b)). Although a negative  $\Delta C'_{\text{deoxy}}$  also synchronized with each period of the story task,  $\Delta C'_{\text{deoxy}}$  did not exactly mirror the temporal dynamics of  $\Delta C'_{\text{oxy}}$ . Similar, but smaller, changes in both  $\Delta C'_{\text{oxy}}$  and  $\Delta C'_{\text{deoxy}}$  were observed in the repeat run (Fig. 4.4 (c), (d)). These results suggest that the hemodynamics reflects the processing of complex temporal and spectral features related to speech sounds.

These two measurement points (Positions 16 and 21) showed similar hemodynamics, which was confirmed by significant temporal correlations ( $p < 0.0001$ ) in the story task ( $\Delta C'_{\text{oxy}}$ : 0.97,  $\Delta C'_{\text{deoxy}}$ : 0.80) and in the repeat task ( $\Delta C'_{\text{oxy}}$ : 0.88,  $\Delta C'_{\text{deoxy}}$ : 0.65). Although Position 16 did not show significant activation for  $\Delta C'_{\text{deoxy}}$  in the direct comparison (Fig. 4.3 (b)), the hemodynamics at both measurement points were parallel when compared with the baseline.

After the two measurement positions were averaged, the individual mean hemodynamics in the activation periods were statistically compared between the story and repeat runs (Fig. 4.5). Both the positive  $\Delta C'_{\text{oxy}}$  and negative  $\Delta C'_{\text{deoxy}}$

during the story task were two times larger than those during the repeat task.

ANOVA (subjects  $\times$  tasks  $\times$  periods) was performed separately for  $\Delta C'_{\text{oxy}}$  and  $\Delta C'_{\text{deoxy}}$ .

This analysis indicated a significant main effect of tasks ( $\Delta C'_{\text{oxy}}$ :  $F(1,12) = 36$ ,

$\Delta C'_{\text{deoxy}}$ :  $F(1,12) = 36$ ,  $p < 0.0001$ ) without any interactions.

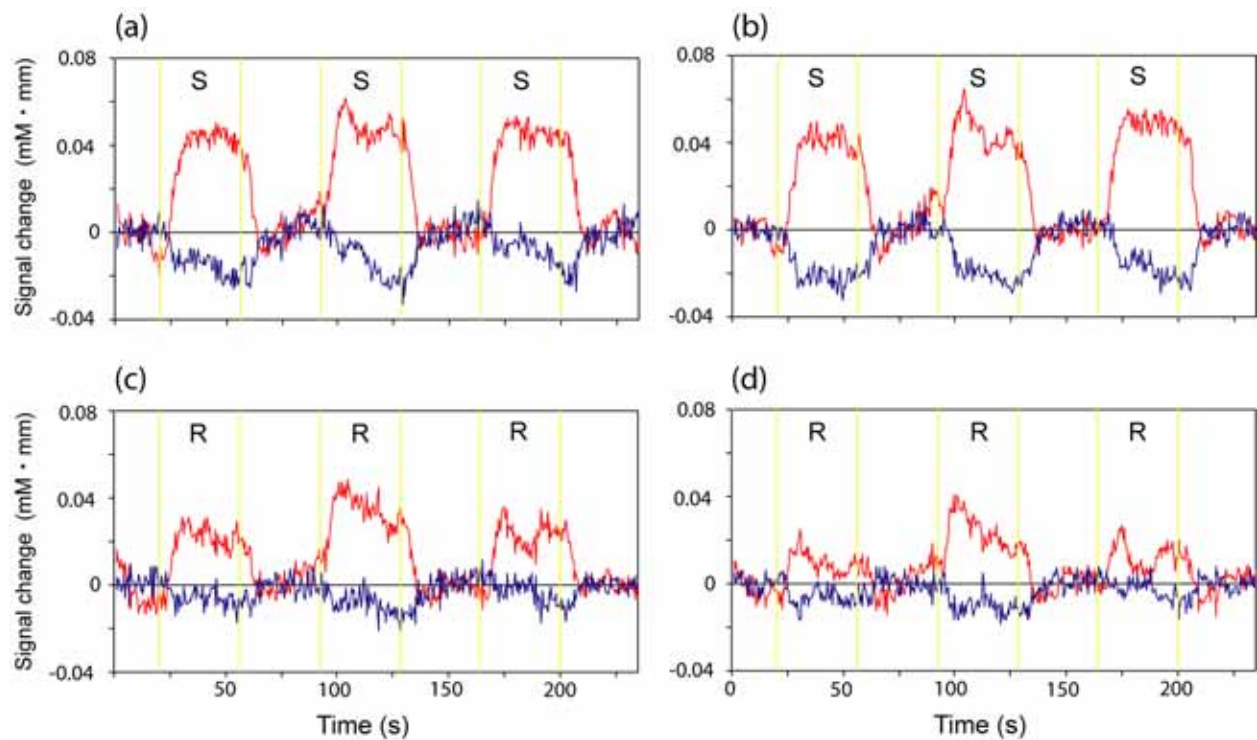


**Fig. 4.4 Hemodynamics in speech-recognition tasks relative to the control task. (a) The story run at Position 16. (b) The story run at Position 21. (c) The repeat run at Position 16. (d) The repeat run at Position 21. Red lines show the mostly positive  $\Delta C'_{\text{oxy}}$ , whereas blue lines show the mostly negative  $\Delta C'_{\text{deoxy}}$ . These temporal changes were calculated from averaged data among subjects. There are three periods of either the story task (S) or the repeat task (R) in each run.**

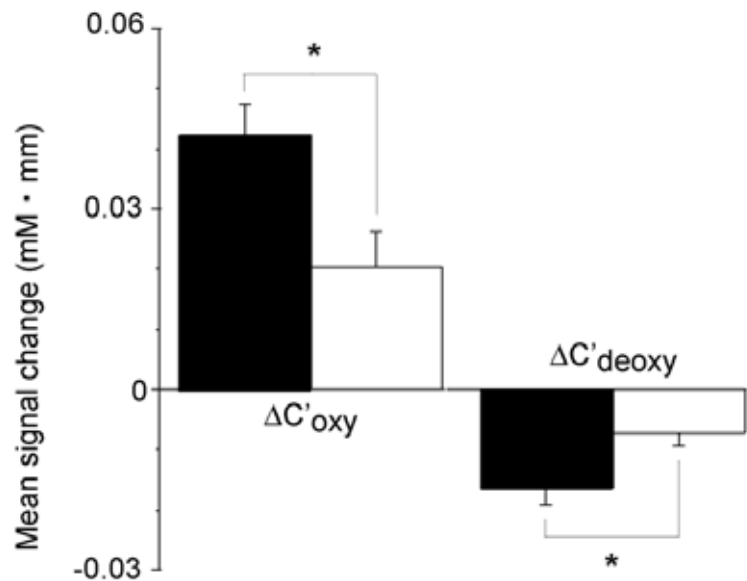


**Fig. 4.5 Mean signals in the activation periods relative to the baseline. Each sample is intra-subject averaged data of mean Hb signals during each activation period, averaging Position 16 and Position 21. Error bars indicate the standard errors (n = 21). The filled bars denote mean signal changes in the story task, and the open bars denote changes in the repeat task. According to post-hoc tests (Fisher's PLSD), the differences between the story and repeat tasks were significant in both  $\Delta C'_{oxy}$  and  $\Delta C'_{deoxy}$  (\* $P < 0.01$ ).**

#### 4.3.5 Relationships between $\Delta C'_{oxy}$ and $\Delta C'_{deoxy}$ dynamics

Two types of correlations between  $\Delta C'_{oxy}$  and  $\Delta C'_{deoxy}$  dynamics were further examined. First, mean of either  $\Delta C'_{oxy}$  or  $\Delta C'_{deoxy}$  in each activation period were compared among subjects (Position 16 and Position 21 averaged). The inter-subject correlation coefficient between mean  $\Delta C'_{oxy}$  and mean  $\Delta C'_{deoxy}$  was significantly negative in the story task ( $-0.71$ ,  $p = 0.0001$ ) and in the repeat task ( $-0.86$ ,  $p < 0.0001$ ). In both tasks, the more the  $\Delta C'_{oxy}$  signals increased, the more the  $\Delta C'_{deoxy}$

signals decreased. This result suggests that means of both  $\Delta C'_{oxy}$  and  $\Delta C'_{deoxy}$  are useful indices of task activation that can be used for functional mapping.

Secondly, each corresponding time point of  $\Delta C'_{oxy}$  and  $\Delta C'_{deoxy}$  was compared in the activation periods of the story run for inter-subject averaged data. As indicated above, the exact temporal dynamics of  $\Delta C'_{deoxy}$  did not mirror those of  $\Delta C'_{oxy}$ .

Accordingly, the temporal correlation coefficient between  $\Delta C'_{oxy}$  and  $\Delta C'_{deoxy}$  was not significant (0.11,  $p > 0.1$ , Position 16 and Position 21 averaged). These results indicate that the temporal information of  $\Delta C'_{oxy}$  and  $\Delta C'_{deoxy}$  may reflect different physiological processes whose temporal dynamics are dependent over the long term ( $\sim 30$  s) but are different in the short term ( $< 10$  s).

#### 4.3.6 Laterality

Hemispheric differences were examined by separately analyzing the temporal dynamics of  $\Delta C'_{oxy}$  in the story and repeat runs. The  $r$ -maps of  $\Delta C'_{oxy}$  in each task relative to the baseline are shown in Fig. 4.6. Activation area was found in the superior temporal cortex bilaterally in both comparisons. Measurement positions with significant  $r$ -values are listed in Table 4.3. Positions 16, 20, and 21 were located on the superior temporal cortex, and Positions 15 and 19 were found on the Sylvian fissure in almost all hemispheres. Some of these measurement points showed

activation in both hemispheres. It is clear that wider regions with more measurement points were activated in the story task than the repeat task in both hemispheres.

After the measurement points shown in Table 4.3 were averaged within each subject, the mean  $\Delta C'_{oxy}$  in each activation period were examined among subjects. ANOVA (subjects  $\times$  hemispheres  $\times$  tasks  $\times$  periods) indicated no main effect of hemispheres ( $F(1,44) = 0.10, p > 0.1$ ), but there was a significant interaction between hemispheres and tasks ( $F(1,44) = 5.5, p < 0.05$ ). Separate ANOVA for hemispheres indicated a main effect for tasks only in the left hemisphere (Left:  $F(1,12) = 12, p < 0.01$ , Right:  $F(1,12) = 0.68, P > 0.1$ ). This result is consistent with the  $r$ -map of direct comparison between the story and repeat runs (Fig. 4.3).

**Table 4.3 Comparison of measurement points with activation**

Hemisphere	Task	Measurement points with activation
Left	Story	15, 16, 19, 20, 21
	Repeat	16, 20
Right	Story	15, 16, 19, 20
	Repeat	15, 19, 20

**Note:** Numbers shown are the measurement positions whose  $r$ -values were above the threshold of  $r = 0.73$ . These  $r$ -values were obtained by using  $\Delta C'_{oxy}$  time courses, which were calculated from averaged data among subjects. These Position numbers correspond to positions in Fig. 4.1.

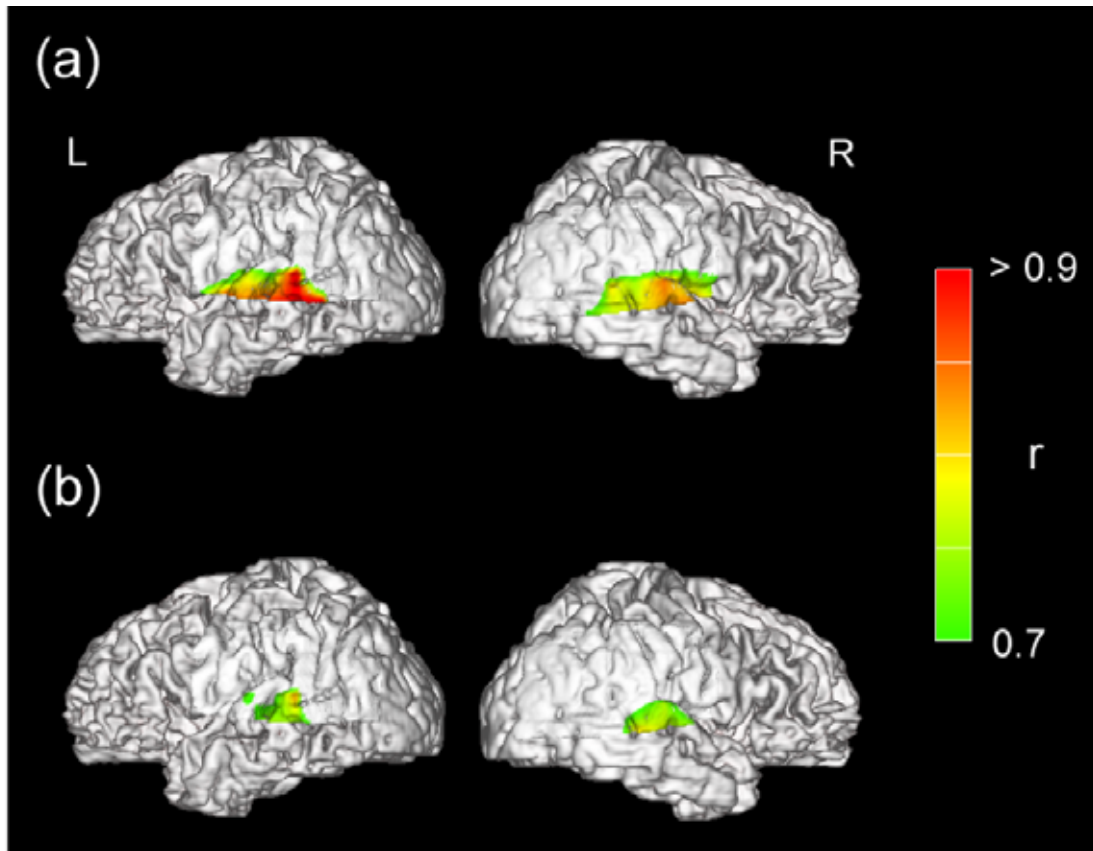


**Fig. 4.6 Superior temporal cortex activation in the story and repeat tasks. (a) The  $r$ -maps of  $\Delta C'_{oxy}$  in the story task relative to the control task. Averaged data among subjects were used to obtain the  $r$ -values. The  $r$ -maps were superimposed on the same brain images as in Fig. 4.1. The  $r$ -values are color-coded using the color scale shown in the figure. Although the superior temporal cortex was found to be activated in both hemispheres, the left hemisphere showed more prominent activation relative to the right hemisphere. (b) The  $r$ -maps of  $\Delta C'_{oxy}$  in the repeat task relative to the control task. In both hemispheres, similar activation was found in the superior temporal cortex. The activation in the repeat task was less prominent compared with that in the story task. Channels for the measurement points with significant  $r$ -values are listed in Table 4.3.**

There are two major findings in the present chapter. First, focal activation was found in the left superior temporal cortex, preferentially for the story task over the repeat task. Compared with the baseline, it was confirmed that a positive  $\Delta C'_{oxy}$  and a negative  $\Delta C'_{deoxy}$  synchronized with each period of the story run. These activation patterns were consistent with results of most of the previous NIRS studies.<sup>9, 12, 47, 87</sup> Although similar changes were observed in the repeat run, the signals in the repeat run were half those in the story run. Secondly, a correspondence and dissociation between  $\Delta C'_{oxy}$  and  $\Delta C'_{deoxy}$  dynamics were found. The mean  $\Delta C'_{oxy}$  and  $\Delta C'_{deoxy}$  signals in each activation period were negatively correlated, while the exact temporal dynamics of  $\Delta C'_{oxy}$  and  $\Delta C'_{deoxy}$  did not mirror each other.

Critical differences in cognitive factors between the story and repeat tasks would be the load of processing speech stimuli. Recognition of successive different sentences of a story demands more auditory, memory, and language information processing than the recognition of repeated sentences. The selective activation in the superior and middle temporal gyri reported here is consistent with the role of the primate temporal association area in memory storage and memory retrieval.<sup>88</sup> Further, this finding is consistent with a previous PET study that clearly showed an activation of the left superior and middle temporal gyri when subjects listened to



continuous speech in their native language.<sup>68</sup> Moreover, the left middle temporal gyrus was activated only in that story condition among other conditions such as distorted stories, matching with the prominent activation of Position 21 in the present study.

The current study clearly shows that the OT can be successfully applied to mapping the functional localization of delicate cognitive processes, as well as to measure the temporal dynamics of cognitive activity. Because there was a correspondence and dissociation between  $\Delta C'_{oxy}$  and  $\Delta C'_{deoxy}$  dynamics, it suggests that OT has the potential to provide novel information not previously obtained with other imaging techniques.

#### 4.4 Conclusion

This study examined a possible solution for a random factor of background functions by devising-task for controlling these background functions. In this case, the speech recognition task that controls some background functions, such as the subjects' attention, is used in every period to detect an intact activation signal from the targeted cognitive process. A comparison between the story task and the repeat

task showed selective activation in the superior and middle temporal gyri; this finding is consistent with the results of previous studies.<sup>68</sup>

This result demonstrates the efficacy and significance of devising task-paradigm for reducing the fluctuations resulting from background functions and detecting delicate activation signals in OT measurements.

## 5. Reducing System-related Noise by Wavelength Selection

### 5.1 Introduction

In this chapter, the practicality of wavelength selection for reducing the system-related noise is examined. Wavelength selection, which is one of the system-related factors, is concerned with the optical properties of the head (random factor 2: interaction noise between the system and a subject) in relation to the measurement algorithm.

In dual-wavelength analysis, equations (eqs. (1-1)-(1-3)) based on the modified Beer-Lambert law are used as described in Chapter 1.2. Here, The Hb signals ( $\Delta C'_{\text{oxy}}$  and  $\Delta C'_{\text{deoxy}}$ ) are expressed as the hemoglobin concentration changes ( $\Delta C_{\text{oxy}}$  and  $\Delta C_{\text{deoxy}}$ ) multiplied by the indefinite optical path-length in the activation region ( $L$ ). Wavelengths that are symmetric about the point where the optical absorptions of oxy Hb and deoxy Hb are equal (approximately 800 nm) are usually represented as  $\lambda_1$  and  $\lambda_2$  (e.g., 780 and 830 nm). However, optimal wavelengths have not yet been determined considering both the theoretical and practical aspects. The present study aims at improving the signal-to-noise ratio (S/N) by reducing the system-related noise for  $\Delta C'_{\text{oxy}}$  and  $\Delta C'_{\text{deoxy}}$  that express cortical activation by selecting an

appropriate wavelength pair for practical use.

According to the general error-propagation law, the noise levels in the Hb signals depend on the differences in the hemoglobin absorption coefficients between the two wavelengths.<sup>89</sup> The theoretical noise levels in  $\Delta C'_{\text{oxy}}$  and  $\Delta C'_{\text{deoxy}}$  depend on the wavelengths and can be expressed as

$$(\delta\Delta C'_{\text{oxy}(\lambda_1, \lambda_2)})^2 = \left(\frac{-\varepsilon_{\text{deoxy}(\lambda_2)}}{E}\right)^2 (\delta\Delta A_{(\lambda_1)})^2 + \left(\frac{\varepsilon_{\text{deoxy}(\lambda_1)}}{E}\right)^2 (\delta\Delta A_{(\lambda_2)})^2, \quad (5-1)$$

$$(\delta\Delta C'_{\text{deoxy}(\lambda_1, \lambda_2)})^2 = \left(\frac{\varepsilon_{\text{oxy}(\lambda_2)}}{E}\right)^2 (\delta\Delta A_{(\lambda_1)})^2 + \left(\frac{-\varepsilon_{\text{oxy}(\lambda_1)}}{E}\right)^2 (\delta\Delta A_{(\lambda_2)})^2, \quad (5-2)$$

where  $\delta\Delta C'_{\text{oxy}(\lambda_1, \lambda_2)}$  and  $\delta\Delta C'_{\text{deoxy}(\lambda_1, \lambda_2)}$  are the indirectly measured noise levels of  $\Delta C'_{\text{oxy}(\lambda_1, \lambda_2)}$  and  $\Delta C'_{\text{deoxy}(\lambda_1, \lambda_2)}$ , and  $\delta\Delta A_{(\lambda_1)}$  and  $\delta\Delta A_{(\lambda_2)}$  are the directly measured noise levels of  $\Delta A_{(\lambda_1)}$  and  $\Delta A_{(\lambda_2)}$ . Assuming that  $\delta\Delta A_{(\lambda_1)}$  and  $\delta\Delta A_{(\lambda_2)}$  are random and independent,  $\delta\Delta C'_{\text{oxy}(\lambda_1, \lambda_2)}$  and  $\delta\Delta C'_{\text{deoxy}(\lambda_1, \lambda_2)}$  are calculated using equations (5-1) and (5-2). On the assumption that  $\delta\Delta A_{(\lambda_1)}$  and  $\delta\Delta A_{(\lambda_2)}$  are the same, using a wavelength pair having a larger difference in the hemoglobin absorption between the two wavelengths should reduce system-related noise. For example, wavelengths shorter than 780 nm paired with 830 nm should provide less noise in measurements of  $\Delta C'_{\text{oxy}}$  and  $\Delta C'_{\text{deoxy}}$ .<sup>89</sup> Another study using a similar theory suggests that the 780- and 830-nm pairing is not optimal for oxygen-saturation-related measurements.<sup>90</sup>

However, the optimal range of wavelengths has not been determined and the effectiveness of these wavelengths for practical use is still unclear. A previous study<sup>89</sup> measured only motor function in the parietal lobe of one subject although optical properties are predicted to depend on the anatomical variances among subjects and areas. Although the results supported the theoretical prediction that using two wavelengths having larger differences in the absorption coefficients of hemoglobin reduces measurement noise, they did not clarify the method's practicality. On the other hand, another study<sup>90</sup> conducted simultaneous measurements with multiple wavelengths of 675, 691, 752, 780, 788, 830, and 840 nm. The study, however, did not compare actual noise levels among wavelength pairs although it concluded that pairing 690 or 760 nm with 830 nm is better than pairing 780 nm with 830 nm for measuring oxygenation changes.

Experimental examination of the Hb signal dynamics resulting from the use of an optimal wavelength (approximately 650-750 nm) paired with 830 nm is necessary to determine the practicality of this method because simulation studies cannot verify every possible model. In particular, the practicality of each wavelength should be investigated by measuring the variation in the detected light power, which depends on the transparency of the wavelength in tissue. Moreover, the dependencies of the activation-signal profile and S/N on the wavelengths should be

examined to verify that these wavelengths measure the hemodynamics induced by the same cortical activation.

In this study, the cortical activations in four areas (frontal, occipital, parietal, and temporal) were measured and simultaneously recorded. Five possible wavelengths (678, 692, 750, 782, and 830 nm) were used to determine an optimal wavelength among 678, 692, 750, and 782 nm for pairing with 830 nm in order to reduce the system noise in practical measurements. Note that the wavelengths that are suggested for use are limited to two because it is not possible to achieve a low system noise in this method by using more than two wavelengths. One of the reasons for this is that the directly measured noise levels such as  $\delta\Delta A_{(\lambda,1)}$  and  $\delta\Delta A_{(\lambda,2)}$  in equations (5-1) and (5-2), would increase according to the number of wavelengths. Moreover, the irradiation power of each wavelength should be lower if a greater number of wavelengths are used because the total irradiation power of the light is restricted based on the safety criterion. This naturally results in increased noise levels in the directly measured optical signals.

## 5.2 Methods

### *5.2.1 Subjects and measurement paradigm*

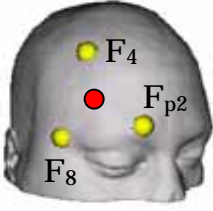
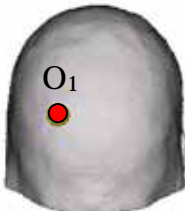
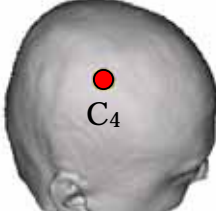
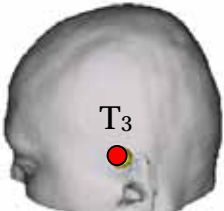
Four subjects (two men, two women; ages 25-45) gave informed consent to participate in this study. All subjects showed right-handedness by the Edinburgh inventory.<sup>85</sup>

Four stimulation paradigms were given to each subject for measurement of the four cortical areas (Table. 5.1). To measure frontal cortex activation, mental arithmetic tasks were used. Some mental tasks including the mental arithmetic task were used to activate the frontal cortex in previous NIRS studies.<sup>27, 28</sup> During the task, a number from 1 to 9 was randomly presented every 1500 ms, and the subjects were instructed to mentally calculate the running total and to whisper the answer with minimal jaw movement at the end of each string that comprised 10 numbers. For the occipital cortex measurements, rectangular black-and-red checkerboard stimuli with the squares reversing between black and red at a frequency of 8 Hz were presented. The occipital activation during the checker-board stimulation was previously reported in an OT study.<sup>91</sup> The subjects were instructed to focus their attention on the fixation cross at the center. The parietal cortices were activated using a finger-tapping task—the fingers of the left hand were placed on the tip of the

thumb in serial order (forefinger – second finger – third finger – little finger – third finger – second finger – forefinger). The subjects were asked to repeat the tapping sequence as rapidly as possible during the time ‘Tapping’ was presented on a CRT monitor. Certain previous studies have shown the involvement of sensorimotor activation in the parietal lobe in a finger-tapping task.<sup>9, 47</sup> Auditory-language stimuli (speech sounds) were used for the temporal area measurements. The efficacy of speech sounds in inducing temporal cortex activation was demonstrated in the study described in chapter 4. The subject wore headphones and was instructed to carefully listen to a Japanese story presented through the headphones while looking at the fixation cross on the monitor. In each measurement paradigm, a 15-s stimulation period and a 30-s rest period were alternated ten times after a 30-s rest period. All the visual stimuli were displayed on a CRT monitor placed 70 cm from the subject’s eyes in a dark room. During the measurements, the subject sat in a chair and was instructed to fix his or her gaze on the cross at the center of monitor and to concentrate on each task.



**Table 5.1 Task/Stimulation paradigms and the measurement positions for the four cortical areas**

	Measurement area			
	Frontal cortex	Occipital cortex	Parietal cortex	Temporal cortex
Task/Stimulus	Mental-arithmetic task <sup>27, 28</sup>	Checkerboard stimulus <sup>91</sup>	Finger-tapping task <sup>9, 47</sup>	Speech-sounds listening task (see chapter 4)
Targeted function	Working memory	Visual perception	Sensorimotor function	Speech recognition
Measurement position according to the 10-20 system <sup>63, 64</sup>				

The measurement positions are shown by the [MünsterT2T-Converter\(3DVersion\)](http://wwwneuro03.uni-muenster.de/ger/t2tconv/conv3d.html) (<http://wwwneuro03.uni-muenster.de/ger/t2tconv/conv3d.html>).

The measurement positions were determined for each subject based on the preliminary experiments using OT (ETG-100: Hitachi Medical Corporation, Japan) using the 780- and 830-nm pairing. The positions showing significant activation in the frontal areas were around the middle of the  $F_{P2}$ ,  $F_4$ , and  $F_8$  locations in the 10-20 system (Table 5.1). The measurement positions in the occipital, parietal, and temporal areas were determined to be around the  $O_1$ ,  $C_4$ , and  $T_3$  locations, respectively (Table 5.1). In general, the locations in the international 10-20 system have an appropriate relationship with cortical anatomy.<sup>65, 67</sup>

## 5.2.2 NIRS measurement

A measurement system with five laser diodes operating at different wavelengths (678, 692, 750, 782, and 830 nm) was used (Fig. 5.1). The five waves were guided into an optical fiber to irradiate the same point simultaneously. The continuous mixed-light was irradiated on the subjects' head, and the reflected light was detected every 100 ms using an avalanche photodiode (APD) located 30 mm from the incident position. Optical fibers (diameter of 1 mm) were used for both the irradiating and detecting lights. The average power of each light source was 0.93 mW, and each source was modulated at a different frequency (1.0 - 2.7 kHz) to enable separation using a lock-in amplifier after detection.

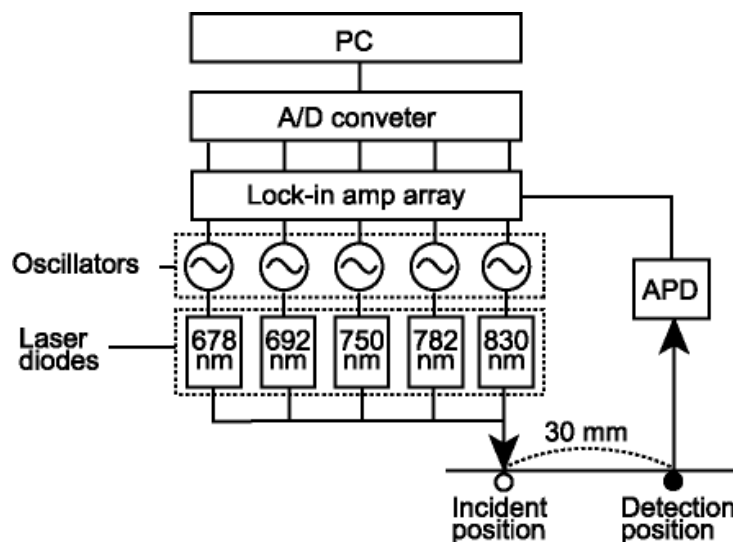


Fig. 5.1 Diagram of measurement system. APD: avalanche photodiode

### 5.2.3 Data analysis

The detected temporal data for the attenuation change at each wavelength were separated into blocks consisting of a 5-s pre-stimulation period during the resting state, a 15-s stimulation period during the stimulation, and a 25-s post-stimulation period during the rest state. The data were baseline-corrected using the data for the 5-s pre-stimulation period and the data for the final 10-s of the post-stimulation period. After eliminating the blocks with artifacts caused by obvious motions such as a cough or sneeze, more than eight blocks were left for each area and subject. The  $\Delta C'_{\text{oxy}}(\lambda_1, \lambda_2)$  and  $\Delta C'_{\text{deoxy}}(\lambda_1, \lambda_2)$  were derived in the same way as described in Chapter 2.1 from the attenuation data of two wavelengths ( $\Delta A_{(\lambda_1)}$  and  $\Delta A_{(\lambda_2)}$ ), one of which was fixed at 830 nm and paired with one of the four other wavelengths. The  $\Delta C'_{\text{oxy}}$  and  $\Delta C'_{\text{deoxy}}$  for the 782- and 830-nm pair (the 782-nm pairing) were compared with those for the 678-, 692-, and 750-nm pairing in each area.

Activation signals were statistically assessed and selected. Assuming that the hemodynamics induced by the stimuli were delayed 6 s from the stimuli onset, the shifted period of the stimulation was defined as the activation period. The mean  $\Delta C'_{\text{oxy}}$  ( $\Delta C'_{\text{deoxy}}$ ) during the pre-stimulation period and those during the activation period were calculated for each block. Based on the  $t$ -value (paired  $t$ -test) between

the mean  $\Delta C'_{\text{oxy}}$  ( $\Delta C'_{\text{deoxy}}$ ) in the pre-stimulation periods and those in the activation periods, data with significant  $t$ -values (two-tailed  $t$ -test,  $p < 0.1$ ) were selected for further analysis using the activation signal. After the selection, the mean  $\Delta C'_{\text{oxy}}$  ( $\Delta C'_{\text{deoxy}}$ ) in the activation periods were used to examine the signal amplitude and signal-to-noise ratio (S/N). The S/N was calculated by dividing the signal amplitude with the noise amplitude.

The noise amplitude in the  $\Delta C'_{\text{oxy}}$  ( $\Delta C'_{\text{deoxy}}$ ) was determined using attenuation data for the first pre-stimulation period of 20 s before the original data was separated into blocks. The  $\Delta C'_{\text{oxy}}$  and  $\Delta C'_{\text{deoxy}}$  were derived from the attenuation data after it was baseline-corrected using a line. The noise amplitude was defined as the standard deviation in the  $\Delta C'_{\text{oxy}}$  and  $\Delta C'_{\text{deoxy}}$  after applying a high-pass 1.5-Hz filter. A filtering threshold was set so as to extract the pure system noise, eliminating the effect of spontaneous low-frequency fluctuations and physiological signals such as respiration and pulse signals.

## 5.3 Results and Discussion

### 5.3.1 Detected power of reflected light

The detected power of the original reflected light (830 nm) is shown in Fig.

5.2 for each cortical area. The power detected in the frontal area differed greatly from those in the other areas, probably because the subjects had no hair covering the frontal area. The power detected in the temporal area was higher than in the occipital and parietal areas, possibly due to differences in the root-of-hair density and cranium thickness.

As shown in Fig. 5.3, the relative detected power was weaker the shorter the wavelength, except for the frontal area. Compared with the detected power for 830 nm, those for 678, 692, and 750 nm were 36%, 44%, and 59% on average, respectively. The power detected in each area differed depended on the wavelength, suggesting the need for spectroscopic study of human hair.

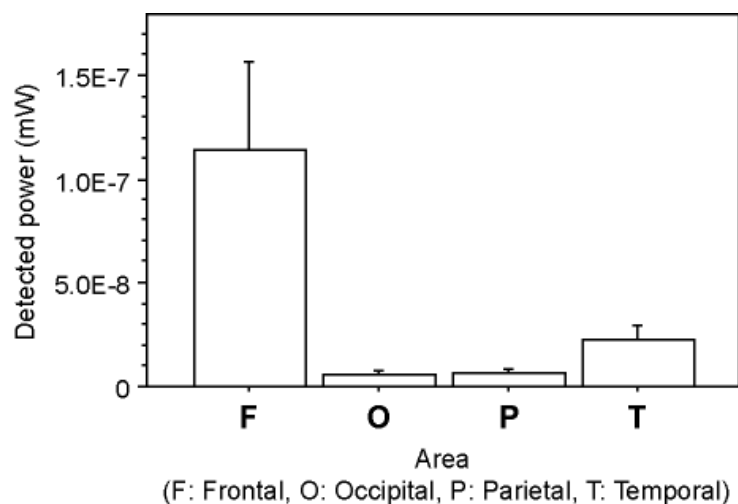


**Fig. 5.2 Mean detected power (830 nm) in four cortical areas, calculated using recorded voltage, and corrected for detector's wavelength sensitivity and amplifier gain. Error bars indicate standard error.**

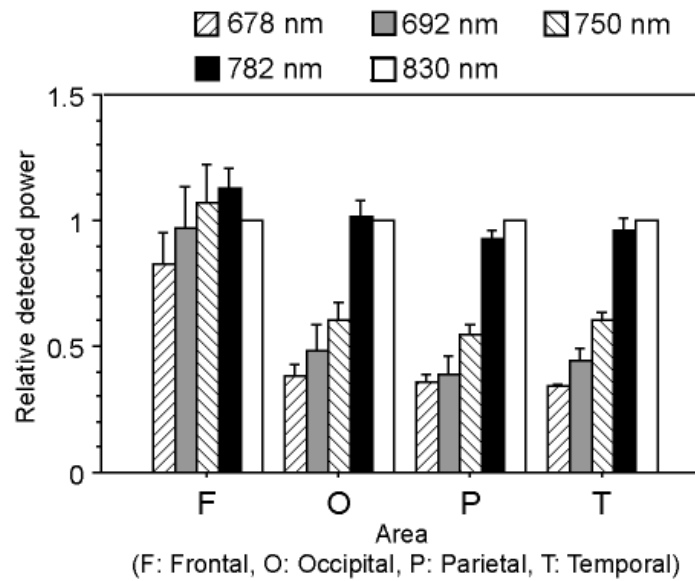


**Fig. 5.3** Relative detected power of five wavelengths for each area corrected for detector's wavelength sensitivity and amplifier gain, and normalized by data for 830 nm. Error bars indicate standard error.

### 5.3.2 Signal time course

The block-averaged results for each cortical area for each wavelength pair for a representative subject are shown in Fig. 5.4. The shapes of the time courses obtained with the different wavelength pairs were similar for each area. As in previous Chapters, a positive  $\Delta C'_{oxy}$  and negative  $\Delta C'_{deoxy}$  were observed during the task period in the occipital, parietal, and temporal areas. However, both of  $\Delta C'_{oxy}$  and  $\Delta C'_{deoxy}$  were positive in the frontal area. This result suggests that the fundamental variability (positive or negative) in  $\Delta C'_{deoxy}$  was not due to the wavelength selection because every wavelength-pair showed a similar tendency, while the cause of variable  $\Delta C'_{deoxy}$ , as discussed in Chapter 3, is still under debate.

The  $t$ -tests for all subjects except one indicated significant activation for both  $\Delta C'_{oxy}$  and  $\Delta C'_{deoxy}$  in every cortical area. The exceptional subject showed subthreshold  $\Delta C'_{deoxy}$  only in the parietal and occipital areas. One reason for the exception might be the possibility of variation in the  $\Delta C'_{deoxy}$ ,<sup>50, 78</sup> and another possibility is a poor S/N for  $\Delta C'_{deoxy}$  in both areas (Table 5.2). The activation-signal amplitudes for  $\Delta C'_{deoxy}$  are usually less than half those for oxy-Hb.<sup>12</sup>

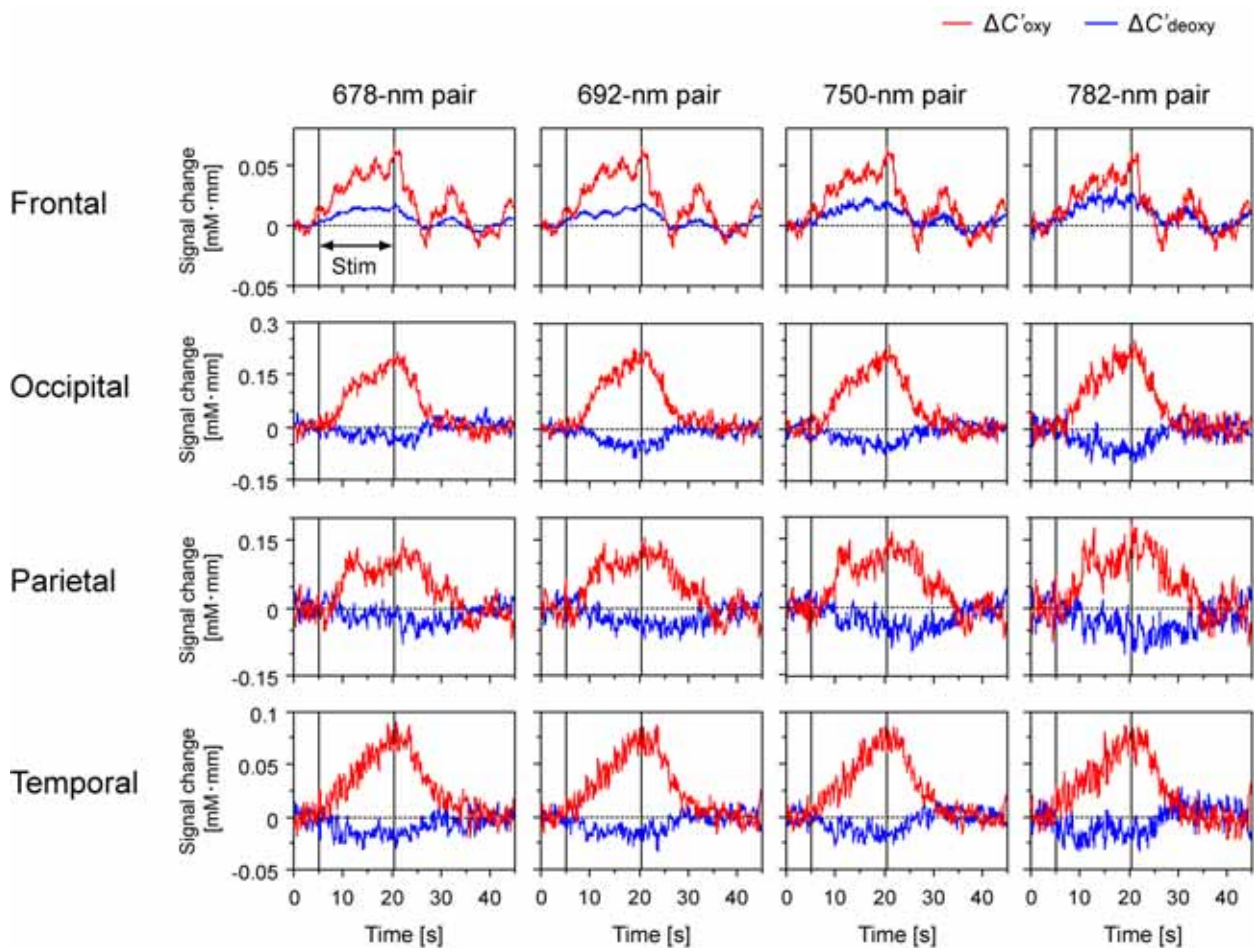


**Fig. 5.4** Block-averaged hemodynamics in each cortical area for each wavelength pair for a representative subject. All wavelength pairs were simultaneously measured in each area. In the ‘stim’ period, a stimulus or task was given to the subject.

**Table 5.2 Relative signal-to-noise ratios (S/Ns) for four areas for 782-nm pairing, calculated by dividing signal (amplitude of Hb signals in activation periods) by noise level (standard deviation during pre-activation period). They were normalized using  $\Delta C'_{oxy}$  data for frontal area.**

Hb signals	Area	Relative S/N (Mean $\pm$ S.E.)
$\Delta C'_{oxy}$	Frontal	1.00
	Occipital	$0.57 \pm 0.11$
	Parietal	$0.46 \pm 0.05$
	Temporal	$0.62 \pm 0.04$
$\Delta C'_{deoxy}$	Frontal	$0.64 \pm 0.04$
	Occipital	$0.31 \pm 0.13$
	Parietal	$0.20 \pm 0.08$
	Temporal	$0.37 \pm 0.10$

S.E.: standard error.

After low-pass 0.8-Hz filtering, the profiles obtained from the four wavelength-pairs were compared. The low-pass filtering eliminated the effects of high-frequency system noise. The correlation coefficients (Pearson's product-moment correlation coefficient) are listed in Table 5.3. Every comparison shows a significant positive correlation ( $p < 0.0001$ ) for all subjects, indicating that every wavelength pair measured almost the same cortical area.

The correlation coefficients for  $\Delta C'_{deoxy}$  for all areas except for the frontal area were relatively low because of the lower S/N in those areas. The mean S/Ns for  $\Delta C'_{deoxy}$  in the occipital, parietal, and temporal areas were about 31%, 20%, and 37%



relative to the S/N for  $\Delta C'_{oxy}$  in the frontal area, respectively (Table 6.1). The lower correlate coefficients for  $\Delta C'_{deoxy}$  may have resulted from the area dependence of the detected power (Fig. 5.2) and a lower S/N.

**Table 5.3 Correlation-coefficients of  $\Delta C'_{oxy}$  and  $\Delta C'_{deoxy}$  time-courses in wavelength-pairs comparison. Profiles after low-pass 0.8-Hz filtering were compared.**

### $\Delta C'_{oxy}$

Wavelength-pairs comparison	Frontal (Mean±S.E.)	Occipital (Mean±S.E.)	Parietal (Mean±S.E.)	Temporal (Mean±S.E.)
678-830 / 692-830	0.998 ± 0.001	0.934 ± 0.028	0.967 ± 0.021	0.983 ± 0.013
678-830 / 750-830	0.998 ± 0.001	0.937 ± 0.029	0.959 ± 0.029	0.986 ± 0.004
678-830 / 782-830	0.989 ± 0.003	0.909 ± 0.031	0.891 ± 0.045	0.977 ± 0.006
692-830 / 750-830	0.998 ± 0.001	0.918 ± 0.039	0.948 ± 0.038	0.985 ± 0.004
692-830 / 782-830	0.992 ± 0.002	0.902 ± 0.042	0.884 ± 0.049	0.981 ± 0.006
750-830 / 782-830	0.993 ± 0.002	0.909 ± 0.031	0.887 ± 0.050	0.980 ± 0.005

### $\Delta C'_{deoxy}$

Wavelength-pairs comparison	Frontal (Mean±S.E.)	Occipital (Mean±S.E.)	Parietal (Mean±S.E.)	Temporal (Mean±S.E.)
678-830 / 692-830	0.979 ± 0.014	0.803 ± 0.081	0.730 ± 0.091	0.795 ± 0.075
678-830 / 750-830	0.978 ± 0.006	0.824 ± 0.058	0.810 ± 0.070	0.782 ± 0.088
678-830 / 782-830	0.970 ± 0.013	0.782 ± 0.059	0.575 ± 0.058	0.760 ± 0.090
692-830 / 750-830	0.972 ± 0.019	0.845 ± 0.052	0.760 ± 0.070	0.779 ± 0.101
692-830 / 782-830	0.970 ± 0.017	0.825 ± 0.047	0.598 ± 0.084	0.829 ± 0.054
750-830 / 782-830	0.981 ± 0.008	0.824 ± 0.049	0.641 ± 0.076	0.801 ± 0.076

S.E.: standard error.

### 5.3.3 Activation-signal amplitude

The activation-signal amplitudes normalized using the data for the 782-nm pairing are shown in Fig. 5.5. The amplitudes were lower for the shorter wavelengths in most cases. An analysis of variance (ANOVA) (wavelength-pairs  $\times$  areas) indicated significant effect of wavelength pairs for  $\Delta C'_{\text{deoxy}}$  ( $F(3,40) = 3.65$ ,  $p < 0.05$ ) although no significant effect for  $\Delta C'_{\text{oxy}}$  ( $F(3,48) = 0.97$ ,  $p > 0.1$ ) was found. According to eqs. (1-1)-(1-3), the NIRS signals ( $\Delta C'_{\text{oxy}}$  and  $\Delta C'_{\text{deoxy}}$ ) do not depend on the wavelength pair, but it is possible that the activation-signal amplitudes were affected by a difference in optical path-lengths ( $Ls$ ) among the wavelengths.

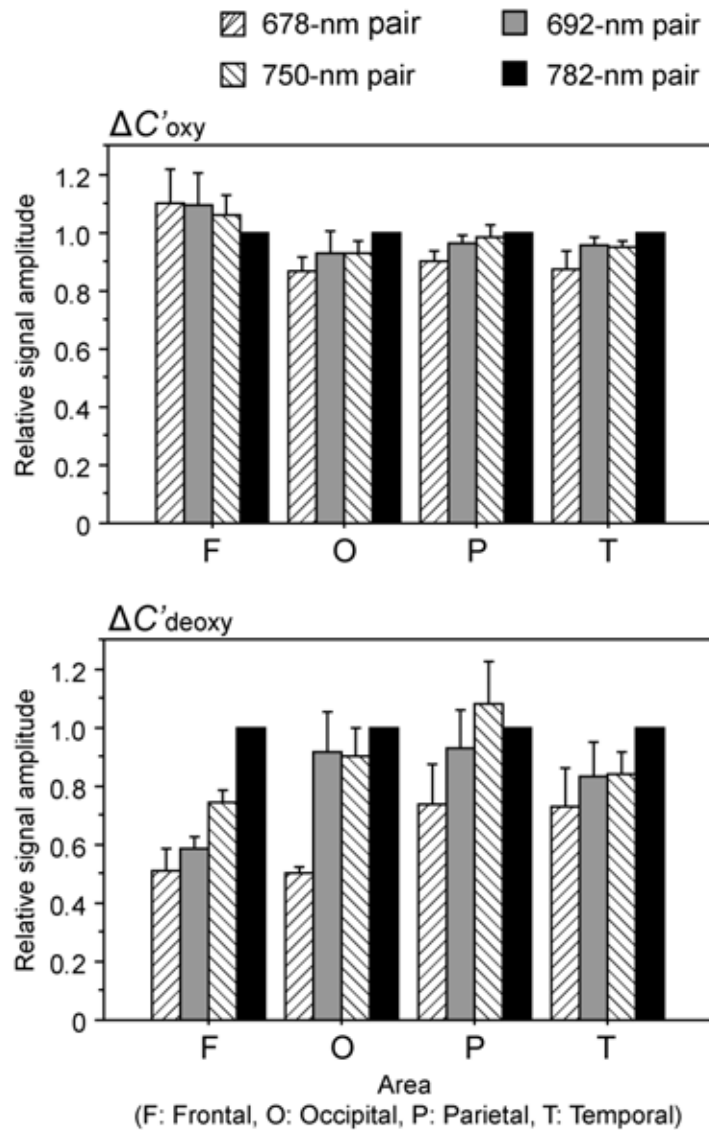


**Fig. 5.5** Relative mean signals in activation periods, normalized using data in 782-nm pairing. Each sample was intra-subject averaged data from 6 s after onset of stimulation to end of stimulation. Error bars indicate standard error.

Although the path-length ( $L$ ) should be the same for different wavelengths according to eqs.(1-1)-(1-3), it changes depending on the optical properties of the biological tissue.  $L$  was defined as the partial path-length, which is the average

path-length of light traveling through a focal region of absorber changes.<sup>92</sup> To estimate the wavelength dependence of the activation-signal amplitude, the relative path-length ( $L'$ ) was calculated for each wavelength, on the assumption that the path-lengths of 782 and 830 nm are the same:

$$L'(\lambda 1) = \frac{\Delta A_{(\lambda 1)}}{\epsilon_{\text{oxy}}(\lambda 1) \times \Delta C'_{\text{oxy}(782, 830)} + \epsilon_{\text{deoxy}}(\lambda 1) \times \Delta C'_{\text{deoxy}(782, 830)}}, \quad (5-3)$$

where the concentration changes for the 782-nm pairing were used as the standard changes ( $\Delta C'_{\text{oxy}(782, 830)}$  and  $\Delta C'_{\text{deoxy}(782, 830)}$ ) for every wavelength in order to isolate the difference in amplitude of  $\Delta C'_{\text{oxy}}$  and  $\Delta C'_{\text{deoxy}}$  for the 678-, 692-, and 750-nm pairings due to the variance in optical path-length ( $L$ ) from that for the 782-nm pairing. Recent reports suggest that the partial path-length is more appropriate than the differential path-length, for compensating for the difference in NIRS sensitivity.<sup>33, 34</sup>

The relative path-lengths ( $L'$ ) calculated for each area are shown in Fig. 5.6. The average path-lengths for 678, 692, and 750 nm were shorter than those for 782 and 830 nm although there were large inter-subject variances. These results indicate that the variances in the signal amplitude might be explained by the effect of the varying path-lengths. The large variances for 678, 692, and 750 nm would

greatly affect the  $\Delta C'_{\text{deoxy}}$  because shorter wavelengths have a higher absorption coefficient in deoxy-Hb.

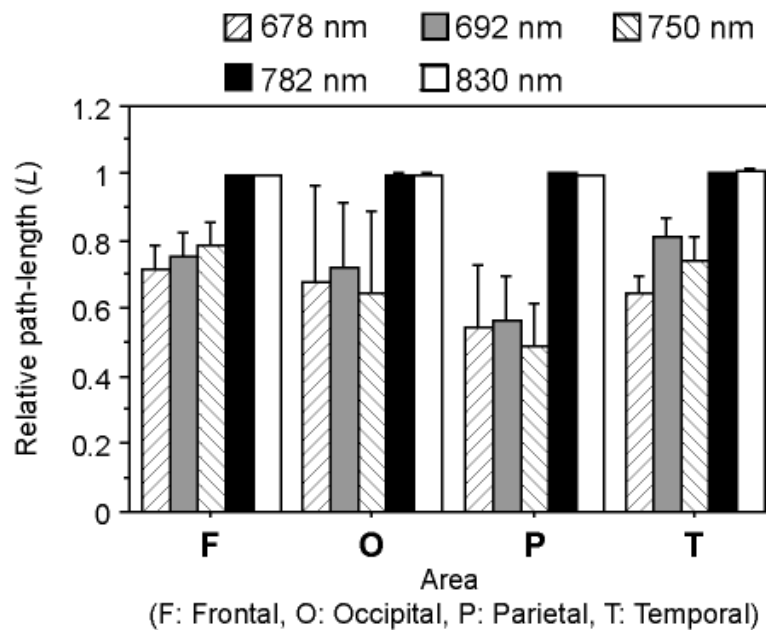


**Fig. 5.6** Relative optical path-length ( $L$ ) calculated for each block for each subject and area and then averaged for each area. Error bars indicate standard error.

The wavelength dependence of the optical path-length might raise concern about the cross talk effect.<sup>35</sup> Although the optimal wavelength pair, which actually resulted in the minimum cross talk, could not be determined since the  $L$ 's were calculated on the assumption that the path-lengths of 782 and 830 nm are the same, it is important that the direction of the signal (positive or negative) was consistent among the wavelength-pairs in each hemoglobin and subject. This suggests that the

wavelength dependence of cross talk was small enough not to cause a different activation pattern, and that the signal amplitude can be corrected using the relative path-length when the signal amplitudes in the 782-nm pair are fixed as the standard.

#### *5.3.4 Wavelength-dependence of spatial sensitivity*

The wavelength dependence of the optical path-length also suggests that the measurement area differs among wavelengths. Significantly, the relative path-lengths were (1) the partial path-length in the activation area and (2) the calculated path-length when the concentration change for the 782-nm pair was fixed as the standard. It was not possible to determine whether each optical path passed through the same tissue because the optical path depends on absorption and scattering not only in the cerebral cortex but also in the skin, muscle, skull, and so on. However, the similar shape time-courses shown in Fig. 5.4 and Table 5.2 demonstrate that every wavelength could be used to measure the same area and that differences in the signal amplitude are due to differences in the partial path-length.

To estimate the spatial distribution of the optical path at these wavelengths, an additional measurement for the occipital cortex was conducted with three

different S-D distances of 20, 30, and 40 mm (Fig. 5.7). In general, the amplitude of the activation Hb-signal was smaller at shorter S-D distances due to a shorter optical path-length in the activation area. It is therefore expected that the difference in spatial distribution of the optical path will be reflected in the inclinations of the amplitude of the activation signal (the change in signal amplitudes depends on the S-D distances).

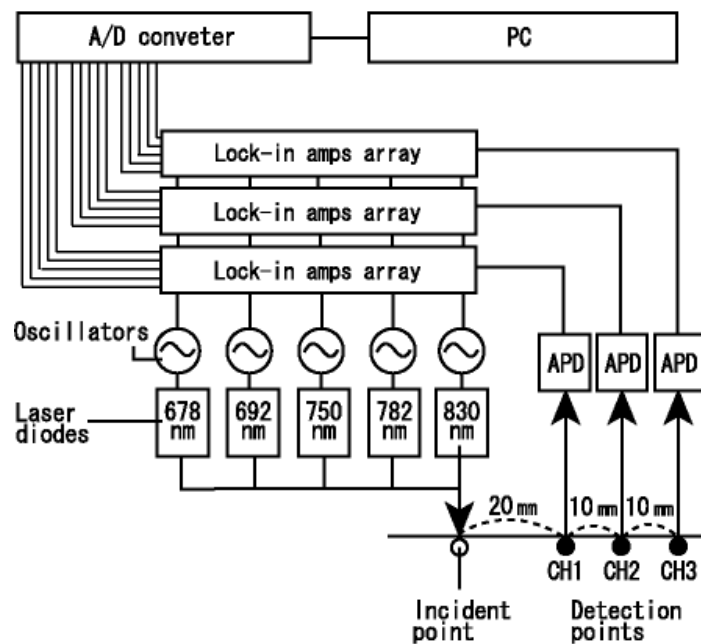


**Fig. 5.7 Schematic setup for simultaneous measurements with five wavelengths.**

**PC: personal computer, APD: avalanche photodiode.**

The differences in activation-signal amplitudes depending on the S-D distance among the four wavelength pairs were examined. The activation-signal

amplitude was defined as the average values during the activation period; these are plotted in fig. 5.8. The larger activation-signal amplitudes were obtained at the channels with larger S-D distances for every wavelength pair. Concerning the wavelength dependence, the inclinations of activation-signal amplitude according to S-D distance appeared to be the same for the wavelength 692, 750, and 782 nm, but slightly different for 678 nm. These results suggest that the difference in spatial distributions of optical paths is negligible when using the wavelength 692, 750, and 782 nm pairing with 830 nm.

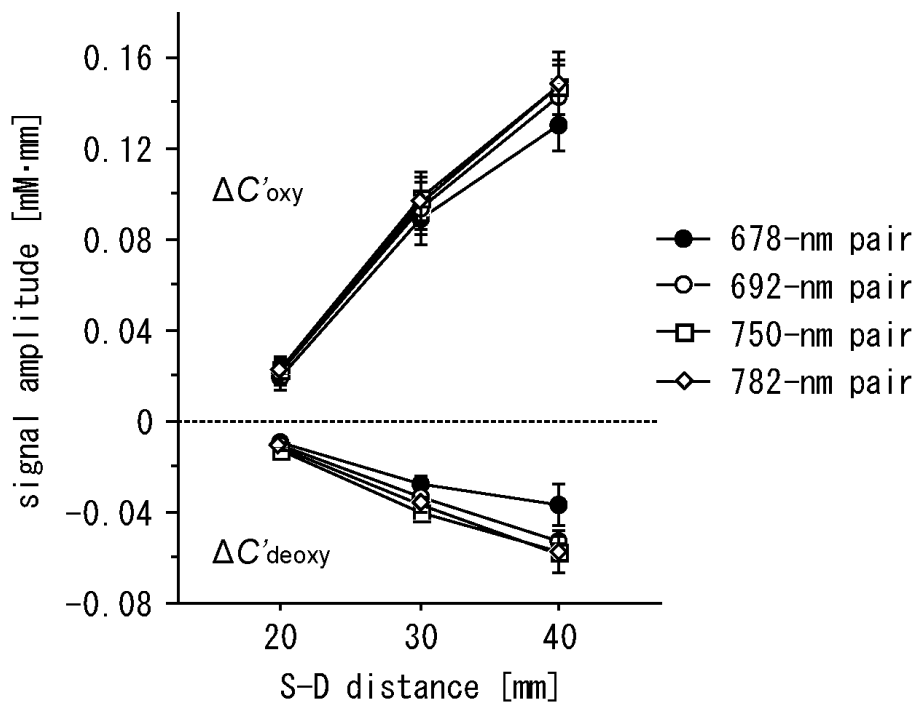


**Fig. 5.8** Amplitudes of activation signals (averages in stimulation period with 7-s delay).



### 5.3.5 Noise levels in $\Delta C'_{oxy}$ and $\Delta C'_{deoxy}$

The noise levels normalized by the noise amplitude in the 782-nm pairing are shown in Fig. 5.9 for the four wavelength pairs and four areas. The wavelength pairs using 678, 692, and 750 nm generally produced less noise for both  $\Delta C'_{oxy}$  and  $\Delta C'_{deoxy}$  in every area. An ANOVA (wavelength-pairs  $\times$  areas) was used to test the dependence of the wavelength pairs on noise in Hb signals. It showed a significant main effect of wavelength pairs ( $\Delta C'_{oxy}$ :  $F(3, 48) = 3.36$ ,  $p < 0.05$ ,  $\Delta C'_{deoxy}$ :  $F(3, 48) = 21.90$ ,  $p < 0.0001$ ). Post-hoc tests (Fisher's PLSD) revealed differences between the 678-nm pairing and the 782-nm pairing ( $\Delta C'_{oxy}$ :  $p < 0.01$ ,  $\Delta C'_{deoxy}$ :  $p < 0.01$ ) and between the 692-nm pairing and 782-nm pairing ( $\Delta C'_{oxy}$ :  $p < 0.05$ ,  $\Delta C'_{deoxy}$ :  $p < 0.01$ ). Although a significant main effect of area was shown in the ANOVA ( $\Delta C'_{oxy}$ :  $F(3, 48) = 17.00$ ,  $p < 0.001$ ,  $\Delta C'_{deoxy}$ :  $F(3, 48) = 2.80$ ,  $p < 0.05$ ), the interaction between wavelength pair and area was not significant. These results suggest that the noise levels in the 678- and 692-nm pairings were lower than those in the 782-nm pairing regardless of area and subject. The dependence of the noise level on the area was probably due to the difference in transparency between areas, as previously mentioned.

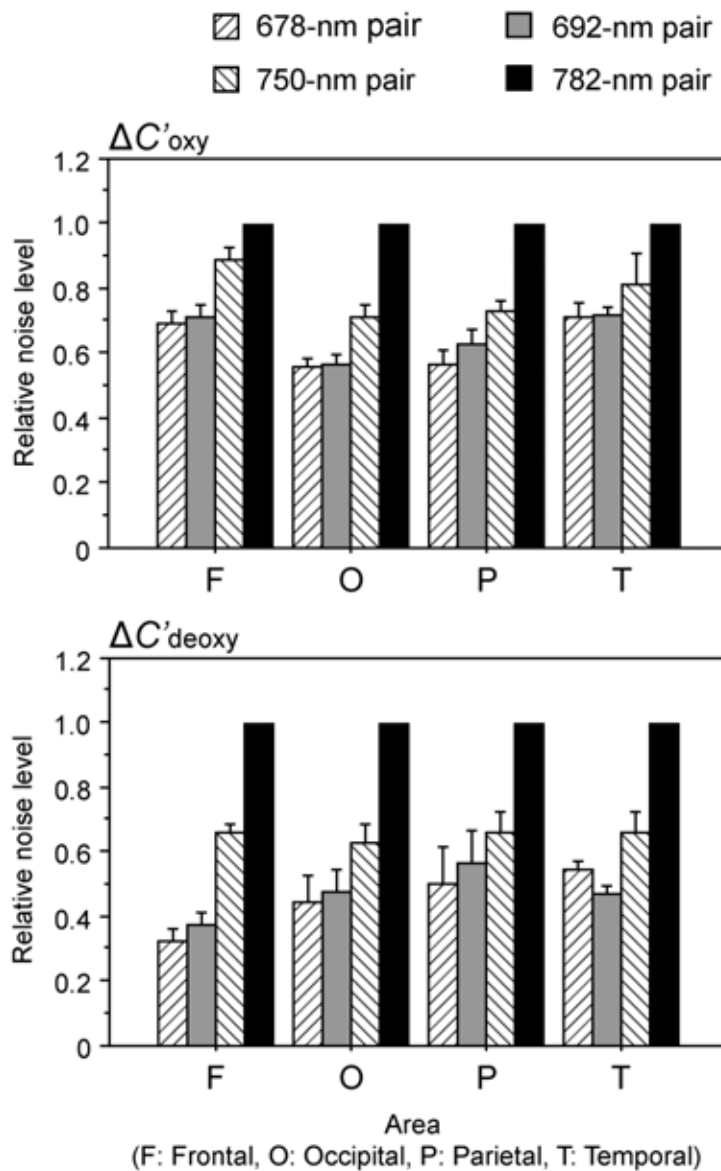


**Fig. 5.9** Relative noise level of  $\Delta C'_{oxy}$  and  $\Delta C'_{deoxy}$ . Noise level was standard deviation in rest period, normalized by standard deviation in 782-nm pairing. Levels were calculated for each subject, then averaged among subjects. Error bars indicate standard error.

The experimentally obtained noise levels corresponded to those derived from theory (eqs. (5-1) and (5-2)), as shown in Fig. 5.10. The experimental and theoretical noise levels showed significantly high correlation coefficients ( $\Delta C'_{oxy}$ : 0.99,  $p < 0.0001$ ,

$\Delta C'_{\text{deoxy}}$ : 0.99,  $p < 0.0001$ ), indicating that the noise levels were properly assessed.

Consequently, these results suggest that using a shorter wavelength reduces noise levels in most OT measurements.

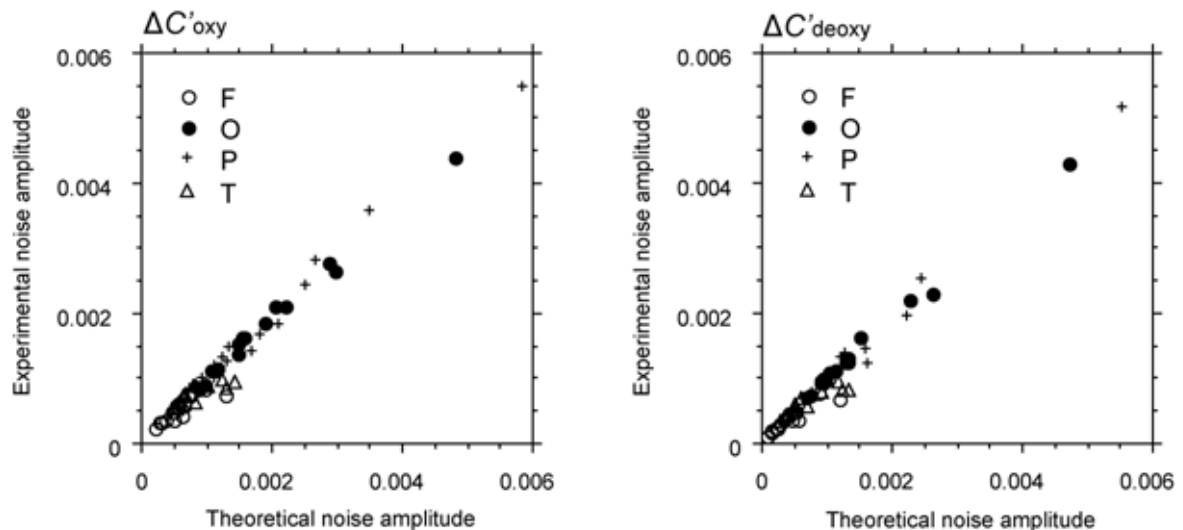


**Fig. 5.10** Scattering diagram of theoretical noise amplitude (horizontal axis) and experimental noise amplitude (vertical axis). F: frontal area, O: occipital area, P: parietal area, and T: temporal area.

### 5.3.6 Signal-to-noise ratio

The relative S/N levels normalized using those in the 780-nm pairing are shown in Fig. 5.11. In most areas, using 678 or 692 nm with 830 nm produced the highest S/N. An ANOVA (wavelength-pairs  $\times$  areas) revealed a significant main effect of wavelength pairs both for  $\Delta C'_{\text{oxy}}$  ( $F(3,48) = 21.90$ ,  $p < 0.001$ ) and for ( $\Delta C'_{\text{deoxy}}$  ( $F(3,40) = 6.27$ ,  $p < 0.005$ ). For  $\Delta C'_{\text{oxy}}$ , post-hoc tests (Fisher's PLSD) indicated a

difference for every comparison ( $p < 0.005$ ) except for that between the 678-nm pairing and the 692-nm pairing, suggesting that the most sensitive measurement is achieved using the 678- or the 692-nm pairing. In contrast, post-hoc tests (Fisher's PLSD) for  $\Delta C'_{\text{deoxy}}$  revealed a difference between the 678-nm pairing and the 692-nm pairing ( $p < 0.05$ ). A difference for every comparison ( $p < 0.05$ ) except for that between the 678- and the 750-nm pairing was demonstrated in this analysis. Therefore, it can be concluded that the 692-nm pairing provides the highest S/N for  $\Delta C'_{\text{deoxy}}$  measurements in this system.

The S/Ns for the 692-nm pairing for  $\Delta C'_{\text{oxy}}$  and  $\Delta C'_{\text{deoxy}}$  were approximately 1.52 and 1.63 times higher than those for the 782-nm pairing. Thus, the 692-nm pairing provided the highest S/N for both  $\Delta C'_{\text{oxy}}$  and  $\Delta C'_{\text{deoxy}}$  in the present system although the error-propagation law predicts a higher S/N when using shorter wavelength such as 678 nm. This suggests that the optimal wavelength cannot be determined only by the wavelength (absorption-coefficient of hemoglobin species)—the optical properties of the measurement area must be considered. Note that the optimal wavelength also depends on the system properties, such as the irradiated light intensity and detection device. These results demonstrate the practicality of using around 690 nm to improve OT measurements for brain functional study.

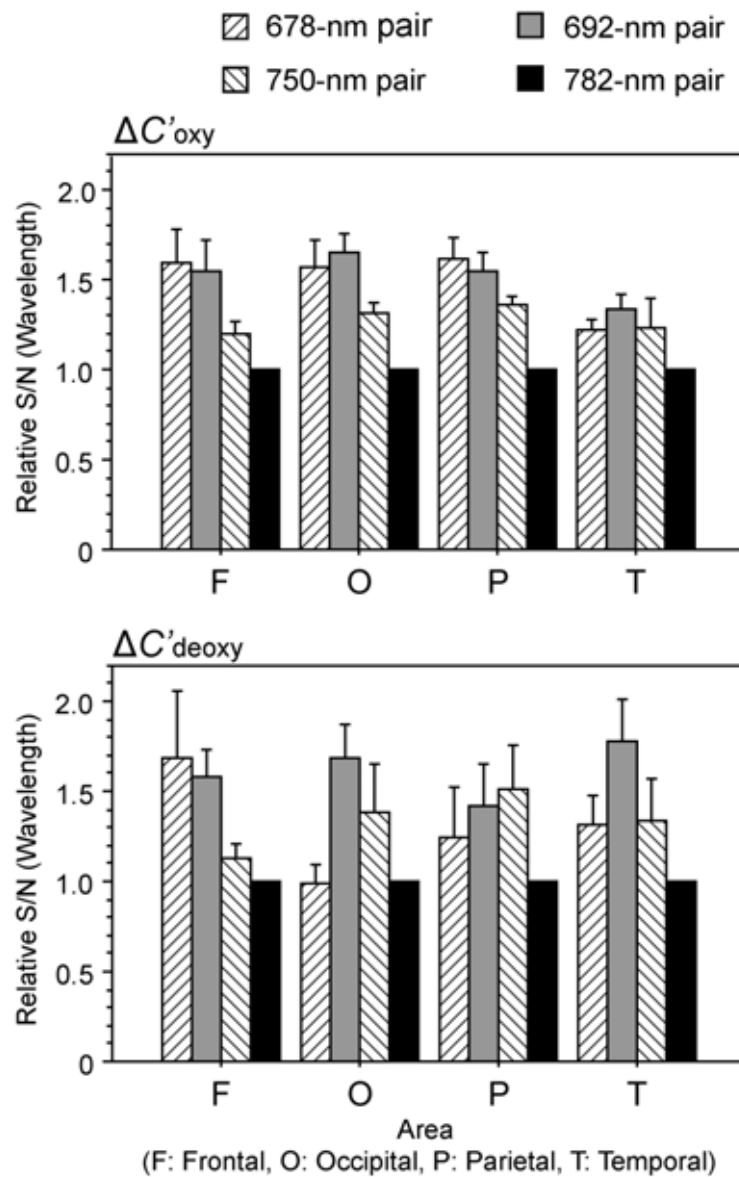


**Fig. 5.11** Relative signal-to-noise ratio for wavelength pairs, normalized using data in 782-nm pairing. Error bars indicate standard error.

## 5.4 Conclusion

This study examined the practicality of wavelength selection for reducing the system-related noise. Wavelength selection, which is one of the system-related factors, is concerned with the optical properties of the head (random factor 2: interaction noise between the system and a subject) in relation to the measurement algorithm. One light wavelength should be shorter than the conventional wavelength (780 nm) used in the theoretical estimation of system-related factors (measurement algorithm), but the wavelength range should be limited based on the actual optical properties of subject's head. Therefore, the possible wavelengths of 678, 692, 750, and 782 nm are examined for pairing with the wavelength of 830 nm in the practical NIRS measurements of activation signals in four different cortical areas among four subjects.

Noise levels in  $\Delta C'_{oxy}$  and  $\Delta C'_{deoxy}$  decreased when using wavelengths shorter than 782 nm, as predicted by the error-propagation law, and the S/N was improved in most cases. Although it has been suggested that activation-signal amplitudes are affected by a difference in the optical path-lengths, the  $\Delta C'_{oxy}$  and  $\Delta C'_{deoxy}$  time courses measured using all wavelength pairs agreed well in each cortical area. This suggests that this wavelength range can be used to measure the same cortical area.

The 692-nm pairing generally provided the highest S/N both for oxy- and deoxy-Hb in this system. Although the detected power of the transparent light at 678 and 692 nm did weaken in most cases, the effects of the absorption coefficients surpassed those of the decreasing transparent light on noise reduction for measurements of  $\Delta C'_{\text{oxy}}$  and  $\Delta C'_{\text{deoxy}}$ . Consequently, a wavelength of approximately 690 nm is a more optimal choice than that of approximately 780 nm for pairing with 830 nm in order to reduce the system-related noise in practical approaches. This in turn will help in achieving a higher S/N in the measurement of  $\Delta C'_{\text{oxy}}$  and  $\Delta C'_{\text{deoxy}}$  induced by cortical activity.

## 6. Conclusion

### 6.1 Conclusions

This study aims at improving the existing OT system—wherein the signals may be affected by a number of random factors—to a more useful and practical complete imaging method for human brain functions. The activation signals that were measured using the conventional OT method were examined in order to evaluate the tolerance of the random factors under the present conditions. Some solutions to reduce the fluctuations in the activation signals caused by some random factors were also studied.

First, the reproducibility of the activation signals measured by OT was examined to evaluate the tolerance of the random factors and to explore the tolerant characteristics of the activation signals. In chapter 2, the within-subject reproducibility of the activation signals was examined during the imaging of sensorimotor activations by a finger-tapping task. The within-subject comparison of the activation signals, which was evaluated by conducting two sessions six months apart for each subject, showed a consistent fundamental pattern involving a positive



$\Delta C'_{\text{oxy}}$  and a negative  $\Delta C'_{\text{deoxy}}$  for the activation signals. The high reproducibility of the temporal and spatial information of the activation signals was particularly emphasized; however, the signal amplitudes were not consistent between the two sessions. These results suggest that the time course of temporal information is particularly useful in detecting activation signals with tolerant characteristics for random factors. Moreover, the high reproducibility of the spatial information (location of the activation area) indicated the efficacy of the 10–20 system in determining the locations of probe positions within the same subject. In chapter 3, the reproducibility (generality) and variability of activation patterns such as a positive  $\Delta C'_{\text{oxy}}$  and a negative  $\Delta C'_{\text{deoxy}}$  were studied in 31 subjects by applying the same paradigm as described in chapter 2. Here, a positive  $\Delta C'_{\text{oxy}}$  was observed in 90% of the subjects with similar location of the activation center, thereby suggesting that a positive  $\Delta C'_{\text{oxy}}$  is the most useful parameter for detecting activation signals and that the 10–20 system is useful in determining the locations of probe positions even in different subjects. However, atypical activation patterns observed in the remaining 10% subjects were due to fluctuations caused by some random factors.

Second, possible solutions for some random factors causing fluctuations in activation signals were examined. The study of chapter 4 examined a solution to reduce the fluctuation from the background functions, such as the attention level of

subjects. In this study, a dichotic listening task that controlled the subjects' attention was used at every stage to detect an intact activation signal from the targeted cognitive process of the speech recognition. The results showing localized activation signal, which was consistent with a previous cognitive study, demonstrated the significance of a devising-task paradigm for reducing the fluctuation from background functions in OT measurements. In chapter 5, a study that examines the practical relevance of wavelength selection in reducing the system-related noise of activation signals is reported. Although optimal wavelength pairs can be proposed on the basis of theoretical estimations, the wavelength range should be limited based on the actual optical properties of the subject's head. The study conducted the measurements with the possible wavelengths of 678, 692, 750, and 782 nm, for pairing with the wavelength of 830 nm, to identify the optimal wavelengths for practical measurements. The evaluations for the activation signals and noise levels in four cortical areas in four subjects demonstrated that the 692 and 830 nm pair produced the highest common S/N.

## 6.2 Prospects

From these findings above, I propose a future direction of improving the OT system in order to render it more useful and effective (Fig. 6.1).

First, a support system for some diagnostics is suggested based on the finding of high reproducibility in temporal information within subject as described in chapter 2 (Fig. 6.1 , Japan-patent pending: Application No. 2004-174925). This system accumulates the OT data by subject and displaying the longitudinal change in the temporal information within subject. Though the effectiveness for any diagnosis has been unclear, the temporal information should have important information representing the subjects' state.

Second, a probe cap with tape measures can be developed according to the evidence that the 10-20 system is useful to determine the locations of probe positions on the head as suggested in chapter 2 and 3 (Fig. 6.1 , Japan-patent pending: Application No. 2002-363370). This probe cap enables us to determine the accurate positions relative to some biological marks, such as inion and nasion, which is used in the 10-20 system.

Thirdly, I developed a more convenient stimulation system to perform a variety of task-paradigms or stimulation-paradigms using visual, auditory, and

tactile stimulation (Fig. 6.1 , Japan-patent pending: Application No. 2005-240551). This is characterized by the easy method to develop task-paradigms by using a list and a table without computer programs. It will help users not being engaged in research but in clinical or industrial fields, and will contribute to the expansion of OT in various fields.

Fourthly, the new system equipped with laser diodes at 690 nm paired with 830 nm has been on the market (Fig.6.1 , ETG-4000, Hitachi Medical Corporation, Japan), because the practicality of using 690 nm rather than 780 nm was confirmed in the study described in chapter 5. In addition, the method to select proper wavelengths depending on the head position (Japan-patent pending: Application No.2002-198282; US-patent: US 6,907,279 B2), and the method to set the optimum proportion in the light power of the two wavelengths (Japan-patent pending: Application No. 2003-373891), according to the findings in chapter 5. They should be useful to achieve more sensitivity for Hb signals by optimizing parameters by the head part, but it is difficult to practice them due to some reasons, such as device performance and production cost.

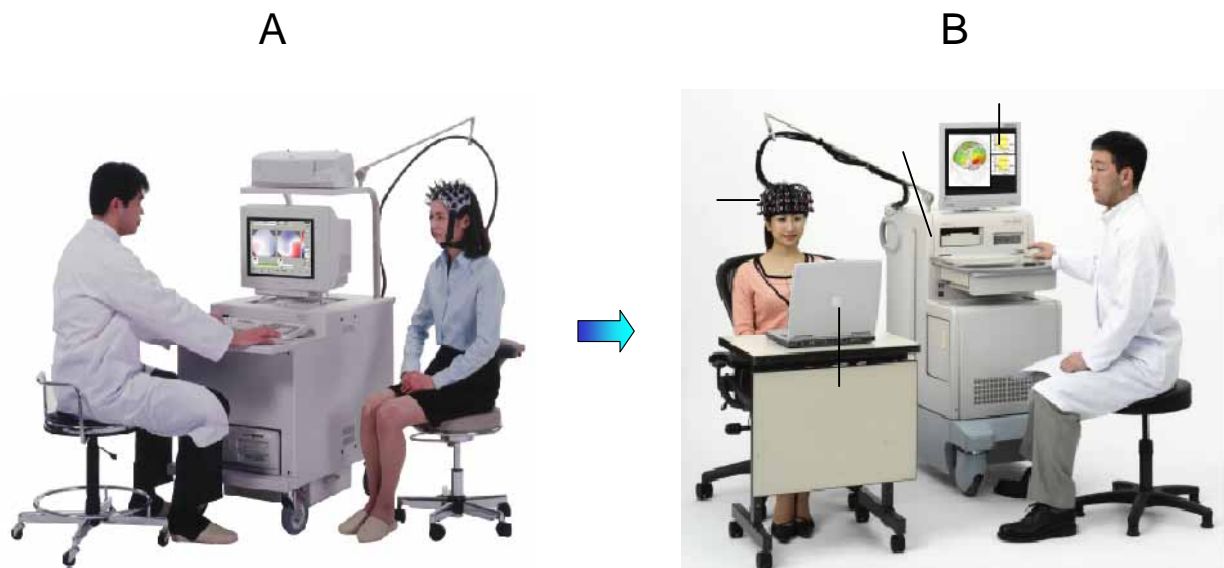


**Fig. 6.1** Rough sketch of a novel approach for improving the OT system. **A:** conventional OT measurement, **B:** OT measurement as proposed in this chapter. The photographs have been provided by Hitachi Medical Corporation.

This thesis examined the activation signals measured in the conventional OT measurement and explore some solutions to reduce the fluctuations caused by random factors. It is no more than an initial step for OT to be a more useful and practical complete imaging method for human brain functions. Even if the potential of the OT technique is exploited to its fullest, it may still fail to compete with fMRI as an imaging modality. However, I would emphasize the unique advantages of OT to other modalities, for example, its complete noninvasiveness, its ease of use and less constraints for the subject, its ability to measure two different signals ( $\Delta C'_{oxy}$  and  $\Delta C'_{oxy}$ ), suggesting that these are strong assets of this technique. I will seek and

realize a new application, which administers to human and society, while I continue to improve the OT system itself.

Finally, two concrete technical issues, that should be solved urgently, are described here.

(1) A standard method for signal processing and statistical analysis is demanded.

The analytical methods tolerable for some random factors have been developed in some laboratories,<sup>93</sup> including the findings described in this thesis. These methods should be shared on a common platform for signal processing and statistical analysis. Our group has started the collaborate project to develop the platform software for signal processing and statistical analysis in OT (OT Signal-processing Platform: OSP).

(2) To identify the probe positions on the anatomical image without MRI

measurement is a desirable technique in OT. A group of National Food Research Institute (Tsukuba, Japan) examined the cranio-cerebral correlation using MRI via the 10-20 system, and normalized cortical projection points of the 10-20 system to the standard coordinates of the brain with their probabilistic distribution.<sup>65</sup> Based on their study, the method for corresponding the spatial information of OT to the anatomical information of the brain is also been developing in the collaboration project for OSP.

## Acknowledgements

I would like to thank all of the people involved in my thesis for their invaluable helps and encouragements.

First, I would like to gratefully acknowledge the polite supervision of Dr. Eiji Okada during this work. I also thank Dr. Kazuo Tanishita, Dr. Yutaka Tomita, and Dr. Masaaki Ikehara for their review and useful suggestion.

Next, I thank the entire team of the Advanced Research Laboratory, Hitachi, Ltd. I was very happy and proud to be a part of the work team. I am especially grateful to Dr. Atsushi Maki and Dr. Hideaki Koizumi for their employing me as a researcher in the year 2000 and for their gentle and accurate directions. I could not continue my study without their kindness. I also thank Dr. Nobuyuki Osakabe for his encouragement. In addition, I would like to thank Dr. Masashi Kiguchi and Dr. Naoki Tanaka for their technical advices of great worth. I also thank Ms. Yukari Yamamoto, Dr. Tsuyoshi Yamamoto, Mr. Noboru Moriya for their technical assistances. Further, I would like to express my deepest gratitude to my best friends as colleagues, Mr. Takusige Katura, Dr. Akiko Obata, and Mr. Ryosuke Takahashi for their help and encouragement when it was most required.

I thank the people who have taught me general foundations of research: my undergraduate teachers at International Christian University (Dr. Atsuko Mukai and Dr. David W. Rackham), and my graduate teacher at the University of Tokyo (Dr. Kuniyoshi L. Sakai). I would like to especially thank Dr. David W. Rackham without whom this thesis would not exist. I have also benefited from many discussions with my senior, Dr. Hiroki C. Tanabe, and my friends in graduate school, Dr. Fumitaka Homae, Dr. Ryuichiro Hashimoto, and Mr. Tatsuya Takeuchi.

Finally, I want to express my hearty thanks to my wife, Miyuki, for her understanding, patience, and encouragement. My daughter, Yuika, also supremely relieved me when I was distressed. In addition, I thank Miyuki's parents, Mr. and Mrs. Kitajima, for their understanding and valuable help. Further, I wish to thank my parents, Shinsaku and Atsuko, my brother, Kazuhide, and my sister, Ai. They believed me and supported me all the time.



## References

1. A. Villringer, "Physiological changes during brain activation," in *Functional MRI*, C. T. W. Moonen and P. A. Bandettini, eds. (Springer, Berlin, 1999), pp. 3-13.
2. R. Cooper, Osselton, J.W., Shaw, J.C., *EEG Techonology -3rd ed.*, 3rd ed. (Butterworth&Co.Ltd., London, UK, 1980).
3. D. Cohen, "Magnetoencephalography: detection of the brain's electrical activity with a superconducting magnetometer," *Science* **175**(22), 664-666 (1972).
4. S. Kuhou, Kuriki, S., "MEG no hassei to nou-kinou," in *Nou-jiki kagaku -SQUID keisoku to igaku ouyou-*, H. Hara, Kuriki, S., ed. (Ohm-sha, Tokyo, Japan, 1997), pp. 126-139.
5. C. T. W. Moonen, Bandettini, P.A. (Eds.), *Functional MRI* (Springer, Berlin, Germany, 1999).
6. S. Ogawa, T. M. Lee, A. R. Kay, and D. W. Tank, "Brain magnetic resonance imaging with contrast dependent on blood oxygenation," *Proc Natl Acad Sci U S A* **87**(24), 9868-9872 (1990).
7. S. Ogawa, T. M. Lee, A. S. Nayak, and P. Glynn, "Oxygenation-sensitive contrast in magnetic resonance image of rodent brain at high magnetic fields," *Magn Reson Med* **14**(1), 68-78 (1990).
8. H. Koizumi, Y. Yamashita, A. Maki, T. Yamamoto, Y. Ito, H. Itagaki, and R. P. Kennan, "Higher-order brain function analysis by trans-cranial dynamic near-infrared spectroscopy imaging," *J Biomed Opt* **4**(4), 403-413 (1999).
9. A. Maki, Y. Yamashita, Y. Ito, E. Watanabe, Y. Mayanagi, and H. Koizumi, "Spatial and temporal analysis of human motor activity using noninvasive NIR topography," *Med Phys* **22**(12), 1997-2005 (1995).
10. K. Cheng, R. A. Waggoner, and K. Tanaka, "Human ocular dominance columns as revealed by high-field functional magnetic resonance imaging," *Neuron* **32**(2), 359-374 (2001).
11. Y. Yamashita, A. Maki, Y. Ito, E. Watanabe, H. Mayanagi, and H. Koizumi, "Noninvasive near-infrared topography of human brain activity using intensity modulation spectroscopy," *Opt Eng* **35**, 1046-1099 (1996).
12. A. Maki, Y. Yamashita, E. Watanabe, and H. Koizumi, "Visualizing human motor activity by using non-invasive optical topography," *Front Med Biol Eng*

- 7(4), 285-297 (1996).
13. P. T. Fox and M. E. Raichle, "Focal physiological uncoupling of cerebral blood flow and oxidative metabolism during somatosensory stimulation in human subjects," *Proc Natl Acad Sci U S A* **83**(4), 1140-1144 (1986).
  14. Y. Ito, R. P. Kennan, E. Watanabe, and H. Koizumi, "Assessment of heating effects in skin during continuous wave near infrared spectroscopy," *J Biomed Opt* **5**(4), 383-390 (2000).
  15. G. Taga, K. Asakawa, A. Maki, Y. Konishi, and H. Koizumi, "Brain imaging in awake infants by near-infrared optical topography," *Proc Natl Acad Sci U S A* **100**(19), 10722-10727 (2003).
  16. M. Pena, A. Maki, D. Kovacic, G. Dehaene-Lambertz, H. Koizumi, F. Bouquet, and J. Mehler, "Sounds and silence: an optical topography study of language recognition at birth," *Proc Natl Acad Sci U S A* **100**(20), 11702-11705 (2003).
  17. I. Miyai, H. C. Tanabe, I. Sase, H. Eda, I. Oda, I. Konishi, Y. Tsunazawa, T. Suzuki, T. Yanagida, and K. Kubota, "Cortical mapping of gait in humans: a near-infrared spectroscopic topography study," *Neuroimage* **14**(5), 1186-1192 (2001).
  18. M. Okamoto, H. Dan, K. Shimizu, K. Takeo, T. Amita, I. Oda, I. Konishi, K. Sakamoto, S. Isobe, T. Suzuki, K. Kohyama, and I. Dan, "Multimodal assessment of cortical activation during apple peeling by NIRS and fMRI," *Neuroimage* **21**(4), 1275-1288 (2004).
  19. M. Suzuki, I. Miyai, T. Ono, I. Oda, I. Konishi, T. Kochiyama, and K. Kubota, "Prefrontal and premotor cortices are involved in adapting walking and running speed on the treadmill: an optical imaging study," *Neuroimage* **23**(3), 1020-1026 (2004).
  20. F. F. Jobsis, "Noninvasive, infrared monitoring of cerebral and myocardial oxygen sufficiency and circulatory parameters," *Science* **198**(4323), 1264-1267 (1977).
  21. D. T. Delpy, M. C. Cope, E. B. Cady, J. S. Wyatt, P. A. Hamilton, P. L. Hope, S. Wray, and E. O. Reynolds, "Cerebral monitoring in newborn infants by magnetic resonance and near infrared spectroscopy," *Scand J Clin Lab Invest Suppl* **188**, 9-17 (1987).
  22. M. Cope and D. T. Delpy, "System for long-term measurement of cerebral Blood flow and tissue oxygenation on newborn infants by infra-red transillumination pathlength," *Med. Biol. Eng. Comput.* **26**, 289-294 (1988).
  23. S. Wray, M. Cope, D. T. Delpy, J. S. Wyatt, and E. O. Reynolds, "Characterization of the near infrared absorption spectra of cytochrome aa3 and haemoglobin for the non-invasive monitoring of cerebral oxygenation," *Biochim Biophys Acta* **933**(1), 184-192 (1988).

24. J. S. Wyatt, M. Cope, D. T. Delpy, C. E. Richardson, A. D. Edwards, S. Wray, and E. O. Reynolds, "Quantitation of cerebral blood volume in human infants by near-infrared spectroscopy," *J Appl Physiol* **68**(3), 1086-1091 (1990).
25. F. F. Jobsis-VanderVliet, C. A. Piantadosi, A. L. Sylvania, S. K. Lucas, and H. H. Keizer, "Near-infrared monitoring of cerebral oxygen sufficiency. I. Spectra of cytochrome c oxidase," *Neurol Res* **10**(1), 7-17 (1988).
26. B. Chance, Z. Zhuang, C. UnAh, C. Alter, and L. Lipton, "Cognition-activated low-frequency modulation of light absorption in human brain," *Proc Natl Acad Sci U S A* **90**(8), 3770-3774 (1993).
27. Y. Hoshi and M. Tamura, "Dynamic multichannel near-infrared optical imaging of human brain activity," *J Appl Physiol* **75**(4), 1842-1846 (1993).
28. Y. Hoshi and M. Tamura, "Detection of dynamic changes in cerebral oxygenation coupled to neuronal function during mental work in man," *Neurosci Lett* **150**(1), 5-8 (1993).
29. T. Kato, A. Kamei, S. Takashima, and T. Ozaki, "Human visual cortical function during photic stimulation monitoring by means of near-infrared spectroscopy," *J Cereb Blood Flow Metab* **13**(3), 516-520 (1993).
30. A. Villringer, J. Planck, C. Hock, L. Schleinkofer, and U. Dirnagl, "Near infrared spectroscopy (NIRS): a new tool to study hemodynamic changes during activation of brain function in human adults," *Neurosci Lett* **154**(1-2), 101-104 (1993).
31. D. T. Delpy, M. Cope, P. van der Zee, S. Arridge, S. Wray, and J. Wyatt, "Estimation of optical pathlength through tissue from direct time of flight measurement," *Phys Med Biol* **33**(12), 1433-1442 (1988).
32. D. T. Delpy, S. R. Arridge, M. Cope, D. Edwards, E. O. Reynolds, C. E. Richardson, S. Wray, J. Wyatt, and P. van der Zee, "Quantitation of pathlength in optical spectroscopy," *Adv Exp Med Biol* **248**, 41-46 (1989).
33. E. Okada and D. T. Delpy, "Near-infrared light propagation in an adult head model. I. Modeling of low-level scattering in the cerebrospinal fluid layer," *Appl Opt* **42**(16), 2906-2914 (2003).
34. E. Okada and D. T. Delpy, "Near-infrared light propagation in an adult head model. II. Effect of superficial tissue thickness on the sensitivity of the near-infrared spectroscopy signal," *Appl Opt* **42**(16), 2915-2922 (2003).
35. K. Uludag, M. Kohl, J. Steinbrink, H. Obrig, and A. Villringer, "Cross talk in the Lambert-Beer calculation for near-infrared wavelengths estimated by Monte Carlo simulations," *J Biomed Opt* **7**(1), 51-59 (2002).
36. K. Uludag, J. Steinbrink, A. Villringer, and H. Obrig, "Separability and cross talk: optimizing dual wavelength combinations for near-infrared spectroscopy of the adult head," *Neuroimage* **22**(2), 583-589 (2004).

37. N. C. Bruce, "Experimental study of the effect of absorbing and transmitting inclusions in highly scattering media," *Appl Opt* **33**(28), 6692-6698 (1994).
38. T. Yamamoto, A. Maki, Y. Yamashita, Y. Tanikawa, Y. Yamada, and H. Koizumi, "Noninvasive brain function measurement system: optical topography," *Proc. SPIE Int. Soc. Opt. Eng.* **4250**, 339-350 (2001).
39. Y. Yamashita, A. Maki, and H. Koizumi, "Measurement system for noninvasive dynamic optical topography," *J Biomed Opt* **4**(4), 414-417 (1999).
40. Y. Yamashita, A. Maki, and H. Koizumi, "Near-infrared topographic measurement system: imaging of absorbers localized in a scattering medium," *Rev Sci Instrum* **67**, 730-732 (1996).
41. T. Yamamoto, A. Maki, T. Kadoya, Y. Tanikawa, Y. Yamada, E. Okada, and H. Koizumi, "Arranging optical fibres for the spatial resolution improvement of topographical images," *Phys Med Biol* **47**(18), 3429-3440 (2002).
42. A. Maki, Yamashita, Y., Ito, Y., Watanabe, E., Koizumi, H., "Spatial and temporal analysis of human motor activity using non-invasive optical topography," in *OSA Trends in Optics and Photonics on Advanced in Optical Imaging and Photon Migration*, R. R. a. F. Alfano, J.G., ed. (Optical Society of America, Washington, DC, 1996), pp. 357-362.
43. M. Firbank, Hiraoka, M., Delpy, D.T., "Development of a stable and reproducible tissue equivalent phantom for use in infrared spectroscopy and imaging," *Proceeding of SPIE* **1888**, 264-270 (1993).
44. I. Loubinoux, C. Carel, F. Alary, K. Boulanouar, G. Viillard, C. Manelfe, O. Rascol, P. Celsis, and F. Chollet, "Within-session and between-session reproducibility of cerebral sensorimotor activation: a test--retest effect evidenced with functional magnetic resonance imaging," *J Cereb Blood Flow Metab* **21**(5), 592-607 (2001).
45. A. Arieli, A. Sterkin, A. Grinvald, and A. Aertsen, "Dynamics of ongoing activity: explanation of the large variability in evoked cortical responses," *Science* **273**(5283), 1868-1871 (1996).
46. J. Neumann, G. Lohmann, S. Zysset, and D. Y. von Cramon, "Within-subject variability of BOLD response dynamics," *Neuroimage* **19**(3), 784-796 (2003).
47. H. Obrig, C. Hirth, J. G. Junge-Hulsing, C. Doge, T. Wolf, U. Dirnagl, and A. Villringer, "Cerebral oxygenation changes in response to motor stimulation," *J Appl Physiol* **81**(3), 1174-1183 (1996).
48. H. Obrig, R. Wenzel, M. Kohl, S. Horst, P. Wobst, J. Steinbrink, F. Thomas, and A. Villringer, "Near-infrared spectroscopy: does it function in functional activation studies of the adult brain?" *Int J Psychophysiol* **35**(2-3), 125-142 (2000).
49. U. Dirnagl, L. Edvinsson, and A. Villringer, "Measuring cerebral blood flow

- and metabolism," in *Cerebral blood flow and metabolism*, L. Edvinsson and D. N. Krause, eds. (Lippincott Williams & Wilkins, Philadelphia, 2002), pp. 371-383.
50. A. Seiyama, J. Seki, H. C. Tanabe, I. Sase, A. Takatsuki, S. Miyauchi, H. Eda, S. Hayashi, T. Imaruoka, T. Iwakura, and T. Yanagida, "Circulatory basis of fMRI signals: relationship between changes in the hemodynamic parameters and BOLD signal intensity," *Neuroimage* **21**(4), 1204-1214 (2004).
  51. A. Shmuel, E. Yacoub, J. Pfeuffer, P. F. Van de Moortele, G. Adriany, X. Hu, and K. Ugurbil, "Sustained negative BOLD, blood flow and oxygen consumption response and its coupling to the positive response in the human brain," *Neuron* **36**(6), 1195-1210 (2002).
  52. C. E. Stark and L. R. Squire, "When zero is not zero: the problem of ambiguous baseline conditions in fMRI," *Proc Natl Acad Sci U S A* **98**(22), 12760-12766 (2001).
  53. M. E. Raichle, A. M. MacLeod, A. Z. Snyder, W. J. Powers, D. A. Gusnard, and G. L. Shulman, "A default mode of brain function," *Proc Natl Acad Sci U S A* **98**(2), 676-682 (2001).
  54. J. Rowe, K. Friston, R. Frackowiak, and R. Passingham, "Attention to action: specific modulation of corticocortical interactions in humans," *Neuroimage* **17**(2), 988-998 (2002).
  55. H. Obrig, M. Neufang, R. Wenzel, M. Kohl, J. Steinbrink, K. Einhaupl, and A. Villringer, "Spontaneous low frequency oscillations of cerebral hemodynamics and metabolism in human adults," *Neuroimage* **12**(6), 623-639 (2000).
  56. G. Taga, Y. Konishi, A. Maki, T. Tachibana, M. Fujiwara, and H. Koizumi, "Spontaneous oscillation of oxy- and deoxy- hemoglobin changes with a phase difference throughout the occipital cortex of newborn infants observed using non-invasive optical topography," *Neurosci Lett* **282**(1-2), 101-104 (2000).
  57. T. Katura, Tanaka, N., Obata, A., Sato, H., Maki, A., "Information transfer of spontaneous fluctuations in cerebral hemodynamics and cardiovascular dynamics," presented at the 11th Annual Meeting of the Organization of Human Brain Mapping, Tronto, Canada, 2005.
  58. W. F. Cheong, S. A. Prah, and A. J. Welch, "A review of the optical properties of biomedical tissues," *IEEE Journal of Quantum Electronics* **26**(12), 2166-2185 (1990).
  59. S. G. Kim, J. Ashe, A. P. Georgopoulos, H. Merkle, J. M. Ellermann, R. S. Menon, S. Ogawa, and K. Ugurbil, "Functional imaging of human motor cortex at high magnetic field," *J Neurophysiol* **69**(1), 297-302 (1993).
  60. S. M. Rao, J. R. Binder, P. A. Bandettini, T. A. Hammeke, F. Z. Yetkin, A. Jesmanowicz, L. M. Lisk, G. L. Morris, W. M. Mueller, and L. D. Estkowski,

- "Functional magnetic resonance imaging of complex human movements," *Neurology* **43**(11), 2311-2318 (1993).
61. S. T. Grafton, R. P. Woods, J. C. Mazziotta, and M. E. Phelps, "Somatotopic mapping of the primary motor cortex in humans: activation studies with cerebral blood flow and positron emission tomography," *J Neurophysiol* **66**(3), 735-743 (1991).
  62. P. E. Roland, B. Larsen, N. A. Lassen, and E. Skinhoj, "Supplementary motor area and other cortical areas in organization of voluntary movements in man," *J Neurophysiol* **43**(1), 118-136 (1980).
  63. W. S. Jasper, Sr., "Urinary symptoms in the elderly male," *Med Times* **86**(1), 20-26 (1958).
  64. G. H. Klem, H. O. Luders, H. H. Jasper, and C. Elger, "The ten-twenty electrode system of the International Federation. The International Federation of Clinical Neurophysiology," *Electroencephalogr Clin Neurophysiol Suppl* **52**, 3-6 (1999).
  65. M. Okamoto, H. Dan, K. Sakamoto, K. Takeo, K. Shimizu, S. Kohno, I. Oda, S. Isobe, T. Suzuki, K. Kohyama, and I. Dan, "Three-dimensional probabilistic anatomical cranio-cerebral correlation via the international 10-20 system oriented for transcranial functional brain mapping," *Neuroimage* **21**(1), 99-111 (2004).
  66. H. Steinmetz, G. Furst, and B. U. Meyer, "Craniocerebral topography within the international 10-20 system," *Electroencephalogr Clin Neurophysiol* **72**(6), 499-506 (1989).
  67. V. L. Towle, J. Bolanos, D. Suarez, K. Tan, R. Grzeszczuk, D. N. Levin, R. Cakmur, S. A. Frank, and J. P. Spire, "The spatial location of EEG electrodes: locating the best-fitting sphere relative to cortical anatomy," *Electroencephalogr Clin Neurophysiol* **86**(1), 1-6 (1993).
  68. B. M. Mazoyer, N. Tzourio, V. Frak, A. Syrota, N. Murayama, O. Levrier, G. Salamon, S. Dehaene, L. Cohen, and J. Mehler, "The cortical representation of speech," *Journal of Cognitive Neuroscience* **5**(4), 467-479 (1993).
  69. C. Carel, I. Loubinoux, K. Boulanouar, C. Manelfe, O. Rascol, P. Celsis, and F. Chollet, "Neural substrate for the effects of passive training on sensorimotor cortical representation: a study with functional magnetic resonance imaging in healthy subjects," *J Cereb Blood Flow Metab* **20**(3), 478-484 (2000).
  70. L. M. Carey, D. F. Abbott, G. F. Egan, H. J. Tochon-Danguy, and G. A. Donnan, "The functional neuroanatomy and long-term reproducibility of brain activation associated with a simple finger tapping task in older healthy volunteers: a serial PET study," *Neuroimage* **11**(2), 124-144 (2000).
  71. T. Yamamoto, E. Okada, F. Kawaguchi, A. Maki, Y. Yamada, and H. Koizumi,

- "Optical fiber arrangement of optical topography for spatial resolution improvement," *Proc. SPIE Int. Soc. Opt. Eng.* **4955**, 487-496 (2003).
72. T. Suto, M. Fukuda, M. Ito, T. Uehara, and M. Mikuni, "Multichannel near-infrared spectroscopy in depression and schizophrenia: cognitive brain activation study," *Biol Psychiatry* **55**(5), 501-511 (2004).
  73. M. A. Franceschini, S. Fantini, J. H. Thompson, J. P. Culver, and D. A. Boas, "Hemodynamic evoked response of the sensorimotor cortex measured noninvasively with near-infrared optical imaging," *Psychophysiology* **40**(4), 548-560 (2003).
  74. V. Toronov, M. A. Franceschini, M. Filiaci, S. Fantini, M. Wolf, A. Michalos, and E. Gratton, "Near-infrared study of fluctuations in cerebral hemodynamics during rest and motor stimulation: temporal analysis and spatial mapping," *Med Phys* **27**(4), 801-815 (2000).
  75. A. Kleinschmidt, H. Obrig, M. Requardt, K. D. Merboldt, U. Dirnagl, A. Villringer, and J. Frahm, "Simultaneous recording of cerebral blood oxygenation changes during human brain activation by magnetic resonance imaging and near-infrared spectroscopy," *J Cereb Blood Flow Metab* **16**(5), 817-826 (1996).
  76. J. Pujol, A. Lopez-Sala, J. Deus, N. Cardoner, N. Sebastian-Galles, G. Conesa, and A. Capdevila, "The lateral asymmetry of the human brain studied by volumetric magnetic resonance imaging," *Neuroimage* **17**(2), 670-679 (2002).
  77. D. A. Boas, T. Gaudette, G. Strangman, X. Cheng, J. J. Marota, and J. B. Mandeville, "The accuracy of near infrared spectroscopy and imaging during focal changes in cerebral hemodynamics," *Neuroimage* **13**(1), 76-90 (2001).
  78. T. Yamamoto and T. Kato, "Paradoxical correlation between signal in functional magnetic resonance imaging and deoxygenated haemoglobin content in capillaries: a new theoretical explanation," *Phys Med Biol* **47**(7), 1121-1141 (2002).
  79. E. Watanabe, A. Maki, F. Kawaguchi, K. Takashiro, Y. Yamashita, H. Koizumi, and Y. Mayanagi, "Non-invasive assessment of language dominance with near-infrared spectroscopic mapping," *Neurosci Lett* **256**(1), 49-52 (1998).
  80. Y. Minagawa-Kawai, K. Mori, I. Furuya, R. Hayashi, and Y. Sato, "Assessing cerebral representations of short and long vowel categories by NIRS," *Neuroreport* **13**(5), 581-584 (2002).
  81. R. P. Kennan, D. Kim, A. Maki, H. Koizumi, and R. T. Constable, "Non-invasive assessment of language lateralization by transcranial near infrared optical topography and functional MRI," *Hum Brain Mapp* **16**(3), 183-189 (2002).

82. T. Paus, S. Marrett, K. J. Worsley, and A. C. Evans, "Extraretinal modulation of cerebral blood flow in the human visual cortex: implications for saccadic suppression," *J Neurophysiol* **74**(5), 2179-2183 (1995).
83. S. C. Cramer, S. P. Finklestein, J. D. Schaechter, G. Bush, and B. R. Rosen, "Activation of distinct motor cortex regions during ipsilateral and contralateral finger movements," *J Neurophysiol* **81**(1), 383-387 (1999).
84. R. Kawashima, P. E. Roland, and B. T. O'Sullivan, "Fields in human motor areas involved in preparation for reaching, actual reaching, and visuomotor learning: a positron emission tomography study," *J Neurosci* **14**(6), 3462-3474 (1994).
85. R. C. Oldfield, "The assessment and analysis of handedness: the Edinburgh inventory," *Neuropsychologia* **9**(1), 97-113 (1971).
86. J. Talairach and P. Tournoux, *Co-planar stereotaxic atlas of the human brain* (Thieme Medical Publishers, Inc., New York, 1988).
87. E. Watanabe, Y. Yamashita, A. Maki, Y. Ito, and H. Koizumi, "Non-invasive functional mapping with multi-channel near infra-red spectroscopic topography in humans," *Neurosci Lett* **205**(1), 41-44 (1996).
88. K. Sakai and Y. Miyashita, "Memory and imagery in the temporal lobe," *Curr Opin Neurobiol* **3**(2), 166-170 (1993).
89. Y. Yamashita, A. Maki, and H. Koizumi, "Wavelength dependence of the precision of noninvasive optical measurement of oxy-, deoxy-, and total-hemoglobin concentration," *Med Phys* **28**(6), 1108-1114 (2001).
90. G. Strangman, M. A. Franceschini, and D. A. Boas, "Factors affecting the accuracy of near-infrared spectroscopy concentration calculations for focal changes in oxygenation parameters," *Neuroimage* **18**(4), 865-879 (2003).
91. K. Takahashi, S. Ogata, Y. Atsumi, R. Yamamoto, S. Shiotsuka, A. Maki, Y. Yamashita, T. Yamamoto, H. Koizumi, H. Hirasawa, and M. Igawa, "Activation of the visual cortex imaged by 24-channel near-infrared spectroscopy," *J Biomed Opt* **5**(1), 93-96 (2000).
92. M. Hiraoka, M. Firbank, M. Essenpreis, M. Cope, S. R. Arridge, P. van der Zee, and D. T. Delpy, "A Monte Carlo investigation of optical pathlength in inhomogeneous tissue and its application to near-infrared spectroscopy," *Phys Med Biol* **38**(12), 1859-1876 (1993).
93. M. L. Schroeter, M. M. Bucheler, K. Muller, K. Uludag, H. Obrig, G. Lohmann, M. Tittgemeyer, A. Villringer, and D. Y. von Cramon, "Towards a standard analysis for functional near-infrared imaging," *Neuroimage* **21**(1), 283-290 (2004).



## Publication List

### 1. Original papers related to this doctoral dissertation

- (1) Sato, H., Takeuchi, T., and Sakai, K.L., 1999. Temporal cortex activation during speech recognition: An optical topography study, *Cognition* Vol.73, No. 3, pp. B55-B66.
- (2) Sato, H., Kiguchi, M., Kawaguchi, F., and Maki, A., 2004. Practicality of Wavelength Selection to Improve Signal-to-Noise Ratio in Near-infrared Spectroscopy, *NeuroImage* Vol.21, No. 4, pp.1554-1562.
- (3) Sato, H., Fuchino, Y., Kiguchi, M., Katura, T., Maki, A., Yoro, T., and Koizumi, H., 2005. Inter-subject variability of NIRS signals during sensorimotor cortex activation, *Journal of Biomedical Optics* Vol. 10, No. 4, 044001.
- (4) Sato, H., Kiguchi, M., Maki, A., Fuchino, Y., Obata, A., Yoro, T., and Koizumi, H., 2006. Within-subject reproducibility of NIRS signals in sensorimotor activation after six months, *Journal of Biomedical Optics* Vol. 11, No. 1 (in press).
- (5) Sato, H., Kiguchi, M., and Maki, A., Wavelength-Dependence of Effective Pathlength Factor in Non-Invasive Optical Measurements of Human Brain Functions, *Japanese Journal of Applied Physics* (accepted for publication).

### 2. Other articles

- (1) Koizumi, H., Yamamoto, T., Maki, A., Yamashita, Y., Sato, H., Kawaguchi, H., and Ichikawa, N., 2003. Optical topography: practical problems and new applications, *Applied Optics* Vol.42, No.16, pp.3054-3062.
- (2) Obata, A., Morimoto, K., Sato, H., Maki, A., and Koizumi, H., 2003. Acute effects of alcohol on hemodynamic changes during visual stimulation assessed using 24-channel near-infrared spectroscopy, *Psychiatry Research: Neuroimaging* Vol.123, No.2, pp.145–152.
- (3) Koizumi, H., Maki, A., Yamamoto, T., Sato, H., Yamamoto, Y., and Kawaguchi, H., 2005. Non-invasive brain-function imaging by optical topography, *Trend in Analytical Chemistry* Vol.24, No.2, pp.147-156.
- (4) Obata, A., Morimoto, K., Sato, H., Takeshita, T., Kawaguchi, H., Koizumi, H., and Maki, A., 2005. Effects of alcohol on hemodynamic and cardiovascular reaction in different genotypes, *Psychiatry Research: Neuroimaging* Vol.139, No.1, pp.65–72.

- (5) Sato, H., Maki, A., 2005. Hikari ni yoru noukinou imeijingu: Hikari topogurafi, *Ninchi Kagaku*, Vol. 12, No. 3, pp.296-307.
- (6) Katura, T., Tanaka, N., Obata, A., Sato, H., Maki, A., Quantitative evaluation of interrelations between spontaneous low-frequency oscillations in cerebral hemodynamics and systemic cardiovascular dynamics, *NeuroImage* (accepted for publication).
- (7) Sato, H., Tanaka, N., Uchida, M., Hirabayashi, Y., Kanai, M., Ashida, T., Konishi, I., Tsubokura, H., Konishi, Y., Maki, A., Wavelet analysis for detecting body-movement artifacts in optical topography signals, *NeuroImage* (submitted).